UNIWERSYTET ŚLĄSKI
W KATOWICACH

WYDZIAŁ NAUK ŚCISŁYCH I TECHNICZNYCH

INSTYTUT FIZYKI IM. AUGUSTA CHEŁKOWSKIEGO

PRACA DOKTORSKA:

Mechanizmy odpowiadające za poprawę fizycznej stabilności amorficznych farmaceutyków po zastosowaniu krzemionkowych materiałów nanoporowatych

mgr inż. Daniel Kramarczyk

PROMOTOR PRACY:
Dr hab. inż. Justyna Knapik-Kowalczuk, Prof. UŚ

KATOWICE 2024

SPIS TREŚCI:

1. WSTĘP

Stałe postacie leków, takie jak tabletki, kapsułki, drażetki i peletki, są zdecydowanie najczęściej stosowaną formą leków na świecie[1]. Szacuje się, że stanowią one ponad 80% wszystkich przyjmowanych farmaceutyków. Istnieje wiele powodów, dla których stałe postacie leków są tak popularne. Do ich głównych zalet należą: (i) łatwość oraz komfort przyjmowania leków w takiej postaci przez pacjentów, (ii) bezpieczeństwo wynikające z dokładnego dawkowania leku w postaci stałej oraz (iii) wysoka stabilność fizyczna materiału leczniczego w takiej postaci[2]. W zdecydowanej większości produktów leczniczych o stałej postaci stosuje się substancje leczniczo-czynne w formie krystalicznej. Ta z kolei – forma krystaliczna farmaceutyku – często charakteryzuje się niską biodostępnością wynikającą ze słabej rozpuszczalnością w wodzie[3,4]. Zgodnie z zestawieniem 200 najczęściej sprzedawanych leków doustnych w UE oraz USA aż 39.7% substancji leczniczych jest praktycznie nierozpuszczalnych w wodzie[1]. Co ciekawe, kolejne 33.8% farmaceutyków również wykazuje problem niskiej rozpuszczalności w wodzie. Substancje te należą do grup leków o bardzo trudnej (5.3%), trudnej (13.2%) oraz słabej rozpuszczalności (15.3%). Spośród całej opisywanej grupy 200 najczęściej stosowanych leków jedynie 26.5% substancji leczniczych można nazwać rozpuszczalnymi. Przy czym bardzo dobrze rozpuszcza się jedynie 3.2%. Graficzna prezentacja przywoływanych danych statystycznych została przedstawiona na Rysunku 1, a definicje terminów opisujących stopień rozpuszczalność wyjaśniono w opisie do tego rysunku.

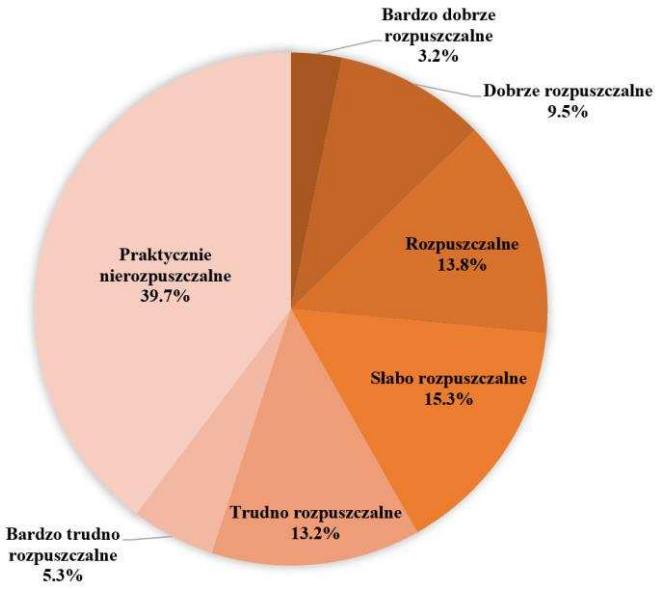

Rysunek 1. Zestawienie 200 najczęściej sprzedawanych leków doustnych w UE oraz USA względem ich rozpuszczalności w wodzie. Przyjęte definicje rozpuszczalności: praktycznie nierozpuszczalne (<0.1 mg/mL); bardzo trudno rozpuszczalne (0.1 – 1 mg/mL); trudno rozpuszczalne (1 – 10 mg/mL); słabo rozpuszczalne (10 – 33 mg/mL); rozpuszczalne (33 – 100 mg/mL); dobrze rozpuszczalne (100 – 1000 mg/mL); bardzo dobrze rozpuszczalne (> 1000 mg/mL)[1].

Niestety przywołane statystyki ujawniają jedynie czubek góry lodowej problemu współczesnej farmacji. Niska rozpuszczalność w wodzie obecnie stosowanych substancji leczniczych nie jest tak zatrważająca jak predykcje przyszłości. Szacuje się, że 75% związków o dużym leczniczym potencjale będących obecnie w fazie badań i rozwoju ma problem z rozpuszczalnością w wodzie[5]. Natomiast aż 90% nowych związków chemicznych będących potencjalnymi kandydatami na substancje lecznicze, zostanie odrzucona w trakcie procesu badawczo rozwojowego tylko i wyłącznie z powodu wspomnianej niskiej rozpuszczalności[6,7].

Ważność opisywanego problemu słabej rozpuszczalności w wodzie materiałów leczniczych sprawiła, że obecnie wiele grup badawczych z całego świata skupia się na poszukiwaniu nowatorskich metod pozwalających rozwiązać ten problem[3,4,8]. Jedną z takich metod jest konwersja krystalicznej substancji leczniczej do jej amorficznej, tj. bezpostaciowej, formy[9,10]. Amorficzny materiał, w związku z brakiem dalekozasięgowego uporządkowania molekularnego charakterystycznego dla krystalicznych materiałów, charakteryzuje się wyższą energią wewnętrzną przez co lepiej się rozpuszcza[11,12]. Niestety, amorficzne materiały również posiadają pewne ograniczenia. Główną wadą takich materiałów jest ich ograniczona fizyczna stabilność[13–15]. Substancje te dążąc do oddania nadmiaru posiadanej energii wewnętrznej mogą w trakcie przechowywania, lub procesu ich produkcji rekrystalizować, czyli powracać do swojej pierwotnej formy[16]. Ponieważ powrót do stanu wyjściowego, tzn. takiego o niższej energii wewnętrznej, spowoduje utratę unikalnych właściwości wynikających z nieuporządkowania, istotne jest (i) znalezienie głównych przyczyn odpowiedzialnych za wspomnianą rekrystalizację oraz (ii) poszukiwanie skutecznych sposobów jej zapobiegania.

Uważa się, że dynamika molekularna materiału amorficznego jest kluczowym czynnikiem odpowiedzialnym za jego rekrystalizację[17,18]. Dlatego najpopularniejsze metody poprawy fizycznej stabilności amorficznych leków bazują na spowolnieniu ruchliwości jego cząsteczek[19]. W tym celu najczęściej stosowane są polimerowe dodatki charakteryzujące się wysoką wartością temperatury przejścia szklistego (T_g)[20–23]. Jeśli temperatura przejścia szklistego dodatku (T_{gEXC}) jest wyższa od temperatury przejścia szklistego substancji leczniczej (T_{gAPI}) to można spodziewać się, że ich mieszanina będzie charakteryzować się wartością przejścia szklistego z jednej strony niższą od T_{gEXC}, a z drugiej strony wyższą od T_{gAPI}. W takiej sytuacji dochodzi do spowolnienia dynamiki molekularnej leku (odzwierciedlonej poprzez wzrost wartości jego temperatury przejścia szklistego) nazywanego efektem antyplastyfikacyjnym wywieranym przez substancje pomocniczą na substancję leczniczą[24,25]. Spowolnienie dynamiki molekularnej leku w formie amorficznej nie jest jedynym powodem, który może przyczynić się do poprawy jego fizycznej stabilności. Innymi czynnikami

mogącymi wpłynąć na rekrystalizację bezpostaciowej substancji leczniczej są między cząsteczkowe oddziaływania pomiędzy lekiem a substancją stabilizującą, zawady steryczne wywierane przez stabilizator lub też obecność więcej niż jednego izomeru substancji leczniczej w systemie (np. obecność różnych tautomerów)[26,27]. Oczywistym jest, że w większości wypadków mechanizm stabilizacyjny ma charaktery hybrydowy.

Przeprowadzone przeze mnie badania, będące podstawą niniejszej rozprawy doktorskiej koncentrowały się na dwóch głównych wątkach. Z jednej strony, w trakcie mojej pracy badawczej, skupiałem się na stabilizacji amorficznych substancji leczniczych poprzez konkretny typ materiału stabilizującego – nanoporowaty materiał krzemionkowy (NMK). Chciałem ocenić jego efektywność w hamowaniu rekrystalizacji różnego rodzaju amorficznych farmaceutyków (pomagającej normalizować stężenie lipidów we krwi symwastatyny, działającego przeciwbólowo i przeciwzapalnie celecoxibu oraz stosowanego w leczeniu schizofrenii i różnych form zaburzeń afektywnych aripiprazolu). Rysunek 2 zestawia wzory strukturalne badanych materiałów leczniczych. Drugim ważnym wątkiem moich badań było określenie mechanizmów molekularnych odpowiedzialnych za obserwowaną zmianę fizycznej stabilności badanych leków pod wpływem zastosowanego NMK.

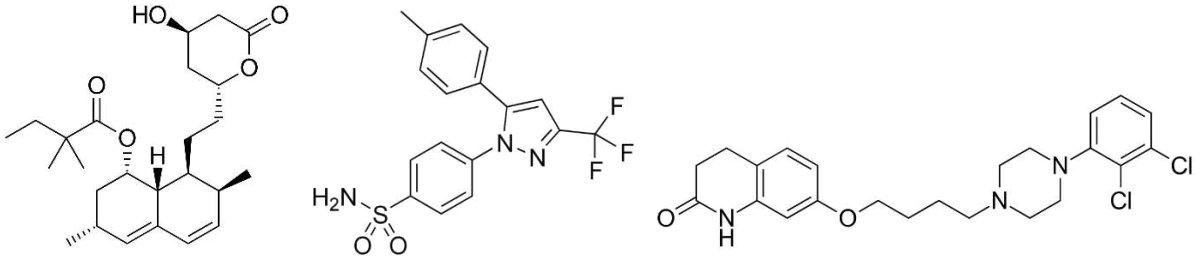

Symwastatyna Celekoksyb Aripiprazol

Rysunek 2 Porównanie wzorów strukturalnych badanych w ramach pracy doktorskiej materiałów leczniczych.

Wybór NMK jako stabilizatorów oczywiście nie był przypadkowy. W ostatnich latach dużą uwagę poświęcono nanonauce i nanotechnologii[28,29]. Materiały nanostrukturalne, takie jak układy na bazie krzemionki lub szkielety metaloorganiczne, są obecnie wykorzystywane w prawie wszystkich dziedzinach nauki[30,31]. Od 2001 roku, kiedy po raz pierwszy zaproponowano mezoporowaty materiał MCM-41 jako nośnik leku, systemy nanoporowate stały się szeroko stosowane w przemyśle farmaceutycznym[32]. Obecnie w tej dziedzinie NMK są głównie wykorzystywane do kontrolowania uwalniania leków, dostarczania aktywnego składnika farmaceutycznego do leczonego obszaru ciała, a także do produkcji metastabilnych odmian polimorficznych farmaceutyków[33–36]. Niestety nadal stanowią one jedną z najrzadziej stosowanych grup materiałów do hamowania rekrystalizacji amorficznych substancji

leczniczych. Dlatego uważam, że pełne poznanie ich możliwości stabilizacyjnych wpłynie na zwiększenie częstotliwości używania nanoporowatych materiałów krzemionkowych w roli stabilizatorów amorficznych farmaceutyków.

Rezultaty prowadzonych badań zostały opublikowane, jako ciąg trzech tematycznie spójnych artykułów, w prestiżowych czasopismach naukowych Pharmaceutics, European Journal of Pharmaceutical Sciences oraz Molecular Pharmaceutics, których współczynniki oddziaływania (IF) wynoszą odpowiednio 4.9, 4.3 oraz 4.5:

A1: J. Knapik-Kowalczuk, D. Kramarczyk, K. Chmiel, J. Romanova, K. Kawakami, M. Paluch, *Importance of Mesoporous Silica Particle Size in the Stabilization of Amorphous Pharmaceuticals— The Case of Simvastatin*. **2020** Pharmaceutics, 12, 384.

A2: D. Kramarczyk*, J. Knapik-Kowalczuk, W. Smolka, M. Ferreira Monteiro, L. Tajber, M. Paluch, *Inhibition of celecoxib crystallization by mesoporous silica – Molecular dynamics studies leading to the discovery of the stabilization origin*. **2022** European Journal of Pharmaceutical Sciences 171, 106132.

A3 D. Kramarczyk*, J. Knapik-Kowalczuk, J. Klimontko, M. Kurek, R. Jachowicz, M. Paluch, *Tuning the Physical State of Aripiprazole by Mesoporous Silica*. **2024** Mol. Pharmaceutics 21, 5, 2315–2326.

Treść wyżej wymienionych publikacji naukowych, które stanowią podstawę rozprawy doktorskiej, można znaleźć w rozdziale 3.

Poza problematyką pracy doktorskiej pozostaje 10 współautorskich artykułów naukowych, które nie zostały włączone do rozprawy, ale świadczą o mojej aktywności naukowej:

B1: J. Pyteraf, W. Jamróz, M. Kurek, J. Szafraniec-Szczęsny, D. Kramarczyk, K. Jurkiewicz, J. Knapik-Kowalczuk, J. Tarasiuk, S. Wroński, M. Paluch, R. Jachowicz, *How to Obtain the Maximum Properties Flexibility of 3D Printed Ketoprofen Tablets Using Only One Drug-Loaded Filament?* **2021** Molecules 26 (11), 3106.

B2: J. Szafraniec-Szczesny, A. Antosik-Rogóz, M. Kurek, K. Gawlak, A. Górska, S. Peralta, J. Knapik-Kowalczuk, D. Kramarczyk, M. Paluch, R. Jachowicz, *How Does the Addition of Kollidon® VA64 Inhibit the Recrystallization and Improve Ezetimibe Dissolution from Amorphous Solid Dispersions?* **2021** Pharmaceutics 13 (2), 147.

B3: J. Knapik-Kowalczuk, D. Kramarczyk, K. Jurkiewicz, K. Chmiel, M. Paluch, *Ternary Eutectic Ezetimibe–Simvastatin–Fenofibrate System and the Physical Stability of Its Amorphous Form*. **2021** Molecular pharmaceutics 18 (9), 3588-3600.

B4: M. Rams-Baron, D. Kramarczyk, J. Knapik-Kowalczuk, B. Hachula, A. Kocot, M. Paluch, *Broadband-dielectric-spectroscopy study of molecular dynamics in a mixture of itraconazole and glycerol in glassy, smectic-A, and isotropic phases*. **2021** Physical Review E 104 (3), 034702.

B5: T. Tranová, J. Pyteraf, M. Kurek, W. Jamróz, W. Brniak, D. Spálovská, J. Loskot, K. Jurkiewicz, J. Grelska, D. Kramarczyk, J. Mužíková, M. Paluch, R. Jachowicz, *Fused Deposition Modeling as a Possible Approach for the Preparation of Orodispersible Tablets*. **2022** Pharmaceuticals 15 (1), 69.

B6: M. Rams-Baron, M. Musiał, D. Kramarczyk, M. Paluch, *Insight from high-pressure dielectric studies into molecular dynamics of the itraconazole-glycerol mixture in smectic and isotropic phases*. **2022** The Journal of Chemical Physics 156 (15), 154501.

B7: K Łucak, D Kramarczyk, O Janus, S Pawlus, *How differences in the molecular structure of monohydroxy alcohols affect the tendency to crystallization*. **2022** The European Physical Journal E 45 (8), 1-5.

B8: J. Pyteraf, W. Jamróz, M. Kurek, U. Bąk, J. Loskot, D. Kramarczyk, M. Paluch, R. Jachowicz, *Preparation and advanced characterization of highly drug-loaded, 3D printed orodispersible tablets containing fluconazole*. **2022** International Journal of Pharmaceutics, 122444.

B9: J. Knapik-Kowalczuk, D. Kramarczyk, R. Jachowicz, M. Paluch, *Effect of shear strain on the supercooled itraconazole*. **2023** Journal of Pharmaceutical Sciences 112 (6) 1644-1652.

B10: K. Łucak, A. Szeremeta, R. Wrzalik, J. Grelska, K. Jurkiewicz, N. Soszka, B. Hachuła, D. Kramarczyk, K. Grzybowska, B. Yao, K. Kamiński, S. Pawlus, *Experimental and Computational Approach to Studying Supramolecular Structures in Propanol and Its Halogen Derivatives*. **2023** The Journal of Physical Chemistry B 127 (42), 9102-9110

Rezultaty moich badań były również prezentowane na poniżej wymienionych międzynarodowych konferencjach naukowych:

- *3rd International Conference of Contemporary Pharmacy Challenges* (2024) Kraków, Polska;
- *International Conference on Science and Technology of Pharmaceutical Glass* (2023), Tsukuba, Japonia;
- *2nd International Conference on Contemporary Pharmaceutical Challenges* (2021) Dortmund, Niemcy.

Przeprowadzone na potrzeby niniejszej pracy doktorskiej badania finansowane były w ramach programu SYMFONIA 3 Narodowego Centrum Nauki pt. *Wpływ procesów fizycznych oraz substancji pomocniczych na charakterystykę właściwości substancji leczniczych trudno rozpuszczalnych w wodzie* o numerze UMO-2015/16/W/NZ7/00404 oraz OPUS 16 Narodowego Centrum Nauki pt. *Badanie właściwości polimerowych matryc z substancjami leczniczymi otrzymanych techniką druku 3D* otrzymanego na podstawie decyzji numer: DEC-2018/31/B/ST8/01327.

2. OMÓWIENIE ARTYKUŁÓW NAUKOWYCH

2.1. Otrzymywanie oraz charakterystyka czystych amorficznych form badanych farmaceutyków – symwastatyna, celekoksyb, aripiprazol

Główną motywacją podjętych badań była chęć poprawy fizycznej stabilności łatwo rekrystalizujących amorficznych farmaceutyków poprzez zastosowanie NMK oraz zrozumienie mechanizmów za to odpowiedzialnych. W tym celu głównie skoncentrowano się na badaniu wpływu krzemionkowego materiału na zmianę tendencji do rekrystalizacji substancji leczniczych. Aby jednak móc ocenić efektywność NMK w stabilizacji amorficznych farmaceutyków niezbędne było przygotowanie oraz scharakteryzowanie ich czystych form. Jako metodę amorfizacji wybrano witryfikację, polegającą na szybkim przechłodzeniu uprzednio stopionego krystalicznego materiału. Temperaturę topnienia badanych krystalicznych farmaceutyków (tj. symwastatyny, celekoksybu oraz aripiprazolu), jak również temperaturę przejścia szklistego ich amorficznych odpowiedników wyznaczono przy pomocy skaningowej kalorymetrii różnicującej (DSC – ang. *Differerential Scaning Calorymetry*). Termogramy DSC wyjściowych, tj. krystalicznych, materiałów (symwastatyny, celekoksybu oraz aripiprazolu) przedstawiono odpowiednio w publikacjach stanowiących podstawę niniejszej rozprawy doktorskiej na rysunkach: [A1 / Rysunek 6 / panel a], [A2 / Rysunek 1], oraz [A3 / Rysunek 1 / panel a], a także zestawiono razem na poniżej przedstawionym Rysunku 3 – panel a. Wyznaczone na podstawie termogramów temperatury topienia (T_m) badanych farmaceutyków wynoszą: $T_{m\ SVT}$ = 413 K; $T_{m\ CEL}$ = 434 K oraz $T_{m1\ ARP}$ = 420 K, $T_{m2\ ARP}$ = 413 K, $T_{m3\ ARP}$ = 410 K, oraz $T_{m4\ ARP}$ = 406 K. Po stopieniu oraz szybkim przechłodzeniu (wewnątrz DSC z prędkością chłodzenia równą 20 K/min) możliwe było uzyskanie formy szklistej w przypadku wszystkich trzech badanych farmaceutyków. Podczas procesu chłodzenia nie zarejestrowano ich rekrystalizcji. Otrzymane szkła zostały ponownie podgrzane, a ich termogramy zaprezentowano w publikacjach na rysunkach: [A1 / Rysunek 6 / panel b], [A2 / Rysunek 3], oraz [A3 / Rysunek 1 / panel a] odpowiednio dla symwastatyny, celekoksybu oraz aripiprazoku oraz zestawiono razem na poniżej przedstawionym Rysunku 3 – panel b. Wyznaczone na podstawie termogramów, otrzymanych z prędkością grzania (*HR*) równą 10 K/min, temperatury przejścia szklistego (T_g) badanych farmaceutyków wynoszą: $T_{g\ SVT}$ = 305 K; $T_{g\ CEL}$ = 331 K oraz $T_{g\ ARP}$ = 307 K.

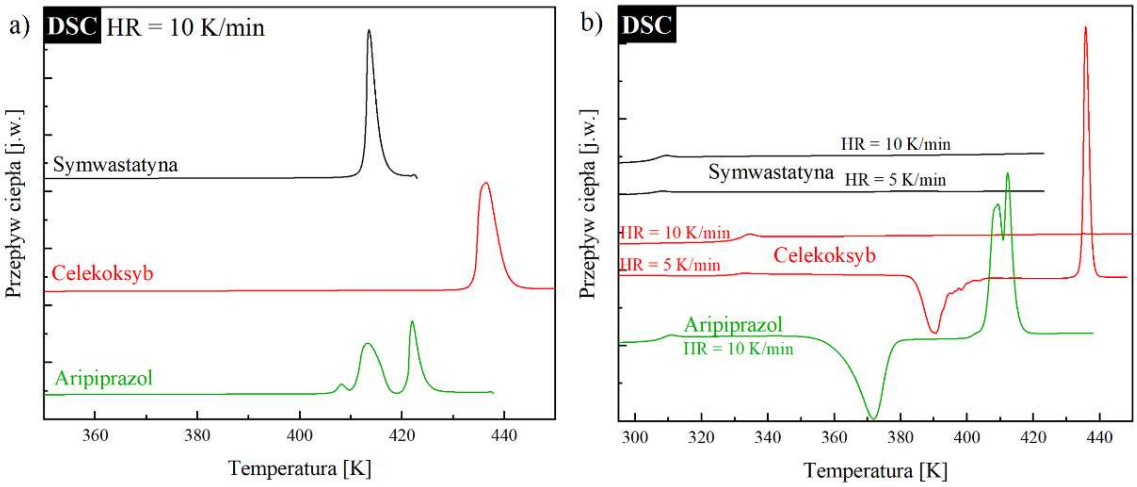

Rysunek 3. Termogramy DSC (a) krystalicznych oraz (b) amorficznych form badanych leków. Kolor czarny odpowiada termogramom symwastatyny, kolorem czerwonym oznaczono termogramy DSC celekoksybu, natomiast kolor zielony odpowiada aripiprazolowi.

Po uzyskaniu oraz termicznej charakterystyce czystej amorficznej formy badanych leków, każdy z materiałów poddano eksperymentom mającym na celu ocenę ich tendencji do rekrystalizacji.

Ponieważ, w przypadku symwastatyny, podczas nieizotermicznych badań kalorymetrycznych przeprowadzonych zarówno z tempem grzania HR = 10 K/min jak i HR = 5 K/min (patrz Rysunek 3 panel b) nie zarejestrowano rekrystalizacji z cieczy przechłodzonej, fizyczną stabilność tego farmaceutyku badano także w warunkach izotermicznych w T = 363 K. Eksperymenty te wykonywano zarówno przy pomocy DSC [A1 / Rysunek 1] jak i szerokopasmowej spektroskopii dielektrycznej (BDS – ang. *Broadband Dielectric Spectroscopy*) [A1 / Rysunek 3]. Otrzymane wyniki wykazały, że przechłodzona symwastatyna rekrystalizuje w trakcie jej przechowywania w warunkach izotermicznych. Analiza otrzymanych wyników, przeprowadzona przy pomocy modelu Avramova, pozwoliła w pełni scharakteryzować kinetykę izotermicznej rekrystalizacji badanej substancji leczniczej, co przyczyniło się do oceny jej fizycznej stabilności. Zestawienie parametrów izotermicznej kinetyki krystalizacji otrzymanych poprzez dopasowanie modelu Avramova do danych eksperymentalnych przedstawiono w [A1 / Tabela 2] oraz [A1 / Tabela 3].

Fizyczną stabilność amorficznej formy czystego celekoksybu wstępnie oceniano na podstawie nieizotermicznych badań kalorymetrycznych przeprowadzonych zarówno z tempem grzania HR = 10 K/min jak i HR = 5 K/min (Rysunek 3 panel b). Badania te wykazały, że amorficzny celekosyb wykazuje tendencję do rekrystalizacji z cieczy przechłodzonej (T_c = 385 K) podczas podgrzewania go z tempem 5 K/min. Wynik ten dowodzi, że amorficzny

celekoksyb ma większą tendencję do rekrystalizacji w porównaniu do, wcześniej opisywanej, symwastatyny. W celu dokładniejszej oceny fizycznej stabilności celekoksybu w obszarze cieczy przechłodzonej, przeprowadzono izotermiczne badania dielektrycznych tego materiału w T = 363 K [A2 / Rysunek 5]. Badania te wykazały, że celekoksyb przechowywany w temperaturze równej 363 K w pełni powraca do swojej pierwotnej, tj. krystalicznej, formy już po 6. godzinach od jego amorfizacji.

Najłatwiej rekrystalizującym materiałem spośród badanych amorficznych farmaceutyków jest aripiprazol. Endotermiczny proces odzwierciedlający rekrystalizację tej substancji zarejestrowano już podczas jej podgrzewania z prędkością równą 10 K/min w trakcie nieizotermicznych badań kalorymetrycznych (patrz Rysunek 3 panel b oraz [A3 / Rysunek 1 / panel a]). Początek procesu rekrystalizacji odpowiada T_c = 357 K. Rekrystalizację aripiprazolu zauważono również podczas badań dielektrycznych prowadzonych w nieizotermicznych warunkach [A3 / Rysunek 2 / panel a]. Celem tych eksperymentów było scharakteryzowanie dynamiki molekularnej czystych amorficznych substancjach leczniczych, w tym właśnie aripiprazolu.

Badania dynamiki molekularnej przeprowadzane przy pomocy BDS stanowiły ostatni etap charakterystyki czystych badanych farmaceutyków. Ich istotność była ogromna, gdyż uważa się, że to właśnie dynamika molekularna materiału amorficznego odgrywa kluczową rolę w jego fizycznej stabilności[37,38]. BDS dzięki badaniu efektów związanych z oddziaływaniem zewnętrznego zmiennego pola elektrycznego z badanym materiałem, umożliwia obserwowanie występujących w nim procesów relaksacyjnych w szerokim zakresie częstotliwości oraz temperatur. Otrzymane widma dielektryczne symwastatyny badanej w temperaturach z zakresu: (a) od 302 do 362 K (odpowiadającym cieczy przechłodzonej) oraz (b) od 173 do 293 K (odpowiadającym szkle) zaprezentowano odpowiednio na [A1 / Rysunek 8 / panel a] oraz [A1 / Rysunek 10 / panel a]. Analizując widma strat dielektrycznych *ε"(f)* zauważono, że symwastatyna posiada trzy procesy relaksacyjne. Poza, dobrze widoczną w $T > T_g$, relaksacją strukturalną (α), odzwierciedlającą kooperatywne ruchy całych molekuł, symwastatyna ujawnia również dwa drugorzędowe procesy relaksacyjne. Procesom tym przypisuje się pochodzenie wewnątrz molekularne. Drugorzędowe procesy relaksacyjne symwastatyny są dobrze widoczne na widmach dielektrycznych zarejestrowanych w $T < T_g$ i zostały oznaczone przy pomocy greckich liter β i γ.

Artykuł A2, koncentrujący się na badaniu wpływu NMK na fizyczną stabilność amorficznego celekoksybu, nie przedstawia dynamiki molekularnej tego czystego amorficznego farmaceutyku, a jedynie odnosi się do danych wcześniej opublikowanych[39–41].

Na podstawie danych literaturowych zauważyć można, że dynamika molekularna celekoksybu jest bardziej złożona od dynamiki molekularnej symwastatyny, gdyż, poza relaksacją strukturalną celekoksyb ujawnia aż trzy drugorzędowe procesy relaksacyjne (β, γ oraz δ). Być może właśnie dzięki bardziej złożonej wewnętrznej ruchliwości molekularnej celekoksyb, w porównaniu do symwastatyny, wykazuje większą tendencję do rekrystalizacji.

Dynamika molekularna najłatwiej rekrystalizującego spośród badanych amorficznych farmaceutyków – aripiprazolu – została przedstawiona w A3. Badania dielektryczne wykonane w szerokim zakresie częstotliwości oraz T [A3 / Rysunek 3] wykazały, że na widmach strat dielektrycznych aripiprazolu, podobnie jak symwastatyny, poza α-relaksacja zarejestrowano dwa drugorzędowe procesy relaksacyjne (β oraz γ). W A3 wykazano jednak, że pochodzenie β-relaksacji aripiprazolu jest inne niż β-relaksacji symwastatyny. W przypadku aripiprazolu, bazując na modelu *coupling* (CM), relaksacji tej przypisano między molekularne pochodzenie wynikające z lokalnego ruchu całej molekuły [A3 / Rysunek 3 / panel b]. Natomiast, β – proces w symwastatynie związany jest z wewnątrz molekularną relaksacją pochodzącą od ruchu angażującego tylko fragment całej molekuły [A1 / Rysunek 11]. Oczywiście różnica w pochodzeniu jednego z drugorzędowych relaksacji porównywanych farmaceutyków może mieć wpływ na zauważalnie wyższą fizyczną stabilność symwastatyny w porównaniu do aripiprazolu. Nie należy jednak wykluczać obecności jeszcze innych czynników przyczyniających się do łatwiejszej rekrystalizacji aripiprazolu. Warto nadmienić, że aripiprazol jest znany ze swojej wyjątkowej struktury pozwalającej molekule łatwo zmieniać konformację. Opisywana giętkość molekuły aripiprazolu sprawiła, że materiał ten jest w stanie tworzyć wiele odmian polimorficznych. Substancja ta, tuż po ROY'u, zajmuje drugie miejsce wśród materiałów posiadających największą ilość znanych odmian polimorficznych. Możliwość rekrystalizacji amorficznej formy aripiprazolu do wielu różnych odmian polimorficznych jest prawdopodobnie jednym z dominujących czynników wpływających na fakt, że farmaceutyk ten, w porównaniu z innymi badanymi materiałami leczniczymi, wykazuje najniższą stabilność fizyczną.

2.2. Wpływ wielkości cząstek NMK na fizyczną stabilność amorficznej symwastatyny

Poszukując efektywnego stabilizatora amorficznej formy symwastatyny wybrano dwa – różniące się głównie wielkością cząstek – komercyjnie dostępne nanoporowate materiały krzemionkowe. Średnia wielkość cząstek pierwszego z zastosowanych stabilizatorów krzemionkowych, tj. Syloidu 244FP, waha się między 2.5 – 3.7 μm, natomiast drugiego – Syloidu 3050 – wynosi 59 μm. Pozostałe parametry użytych NMK tj. średnica porów, objętość

porów oraz obszar powierzchni przedstawiono w [A1 / Tabela 1]. Przygotowanie układów binarnych składających się z symwastatyny oraz NMK w postaci albo Syloidu 244FP lub Syloidu 3050 zostało opisane w [A1 / Rozdział 2 / Podrozdział 2.2]. Aby ocenić wpływ Syloidu 244FP oraz Syloidu 3050 na fizyczną stabilność amorficznej formy symwastatyny układy binarne poddano izotermicznym (T = 363 K) badaniom kalorymetrycznym oraz dielektrycznym. Badania te były wykonywane w sposób analogiczny do eksperymentów mających na celu scharakteryzowanie tendencji do rekrystalizacji czystej amorficznej formy symwastatyny. Otrzymane wyniki zestawiono razem na [A1 / Rysunek 1 / panel a] oraz [A1 / Rysunek 3 / panel a i b]. Analizę otrzymanych wyników zaprezentowano na [A1 / Rysunek 1 / panel b], [A1 / Rysunek 2], [A1 / Rysunek 3 / panel c], [A1 / Rysunek 4], oraz [A1 / Rysunek 5]. Jak można zauważyć znacznie lepszą efektywność w hamowaniu rekrystalizacji amorficznej formy symwastatyny przechowywanej T = 363 K wykazuje NMK charakteryzujący się mniejszą wielkością cząstek tj. Syloid 244FP. Warto podkreślić, że przeprowadzone nieizotermiczne badania kalorymetryczne oraz dielektryczne dowiodły, że żaden z zastosowanych stabilizatorów nie wpłynął w znaczący sposób na temperaturę topienia symwastatyny [A1 / Rysunek 6 / panel a], temperaturę przejścia szklistego tego materiału [A1 / Rysunek 6 / panel b], oraz jego dynamikę molekularną ($\tau_\alpha(T)$, $\tau_\beta(T)$ oraz $\tau_\gamma(T)$) [A1 / Rysunek 11]. W konsekwencji, żaden ze znanych mechanizmów stabilizacyjnych nie jest w stanie wyjaśnić obserwowanej różnicy w hamowaniu rekrystalizacji symwastatyny poprzez zastosowane NMK. Jak wykazano kluczowym parametrem odpowiedzialnym za hamowanie rekrystalizacji symwastatyny poprzez zastosowane NMK jest wielkość ich cząstek. Stosując tą samą ilość cząstek o mniejszym rozmiarze zwiększa się ilość zawad sterycznych („przeszkód") blokujących propagację wzrostu kryształu symwastatyny. W takiej sytuacji amorficzny materiał leczniczy jest w pewnym sensie zamknięty w wielu mniejszych obszarach, co skutecznie utrudnia jego powrót do formy wyjściowej, tj. krystalicznej. Opisywane wolne przestrzenie między rozproszonymi w amorficznym materiale leczniczym cząstkami NMK uwidoczniono metodą mikroskopii optycznej [A1 / Rysunek 13]. Rysunek 4 oraz [A1 / Rysunek 12] przedstawiają wizualizację opisywanego efektu.

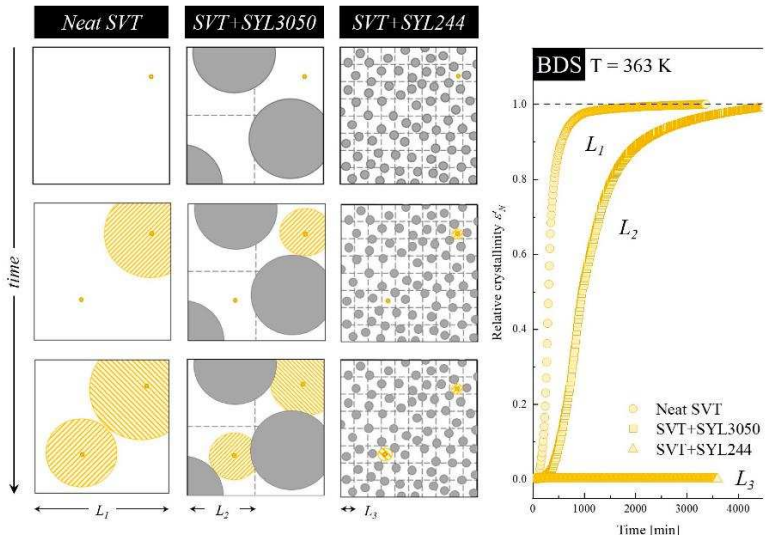

Rysunek 4. Zestawienie kinetycznych krzywych procesu rekrystalizacji czystej symwastatyny (kółka), symwastatyny + 9% Syloidu 3050 (kwadraty) i symwastatyny + Syloidu 244 (trójkąty), które uzyskano na podstawie izotermicznych badań dielektrycznych opisanych w A1, wraz ze schematycznym wyjaśnieniem mechanizmu stabilizacji. Żółte punkty, żółte wzorzyste pola i szare wypełnione pola reprezentują odpowiednio zarodki nukleacji symwastatyny, kryształy symwastatyny oraz cząstki NMK.

2.3. Mechanizmy odpowiedzialne za stabilizację amorficznej formy celekoksybu po zastosowaniu NMK

Korzystając z uzyskanej w A1 wiedzy, że NMK charakteryzujący się mniejszym rozmiarem cząstek efektywniej stabilizuje amorficzny materiał niż NMK o większych cząstkach, do hamowania rekrystalizacji celekoksybu zastosowano Syloid 244FP. W A2 skoncentrowano się na ocenie wpływu różnej koncentracji tego NMK na fizyczną stabilność badanego leku. Metoda przygotowania różnych koncentracji binarnych układów celekoksyb + Syloid 244FP była analogiczna do tej zastosowanej w przypadku binarnych układów symwastatyna + NMK. Dokładny opis metody przygotowania przedstawiono w [A2 / Rozdział 2 / Podrozdział 2.1]. W założeniu większa ilość cząstek o takim samym rozmiarze również powinna spowolnić propagację wzrostu kryształu amorficznego materiału poprzez wzrost ilości zawad sterycznych.

Przeprowadzone nieizotermiczne badania kalorymetryczne [A2 / Rysunek 3] oraz dielektryczne [A2 / Rysunek 5] dowiodły, że podobnie jak w przypadku symwastatyny, Syloid 244FP nie wpływa znacząco na temperaturę przejścia szklistego oraz temperaturową zależność czasów relaksacji strukturalnej ($\tau_\alpha(T)$) stabilizowanego farmaceutyku. Ponieważ czysty amorficzny celekoksib wykazuje większą tendencję do rekrystalziacji w porównaniu do czystej amorficznej symwastatyny 9-cio procentowy dodatek masowy Syloidu 244FP nie był w stanie tak efektywnie zahamować rekrystalizacji amorficznego celekoksybu jak miało to miejsce w

przypadku symwastatyny. Proces rekrystalizacji amorficznej formy celekoksybu zarejestrowano podczas jego podgrzewania w trakcie nieizotermicznych badań dielektrycznych układów zawierających w składzie 9, 18 oraz 27% Syloidu 244FP. Aby dokładnie ocenić wpływ koncentracji zastosowanego NMK na zmianę tendencji do rekrystalizacji amorficznej formy celekoksybu przeprowadzone zostały izotermiczne (T = 363 K) pomiary dielektryczne wszystkich badanych układów [A2 / Rysunek 9]. Zestawienie oraz analizę uzyskanych wyników przedstawiono na [A1 / Rysunek 10]. Jak widać, dokładnie tak jak zakładano, wraz ze zwiększeniem ilości cząstek NMK wydłuża się czas rekrystalizacji amorficznej formy celekoksybu z binarnych układów lek + NMK. Efekt ten wynika ze wzrostu ilości zawad sterycznych wywieranych na farmaceutyk przez materiał krzemionkowy, co w efekcie rejestrowane jest jako hamowanie propagacji wzrostu kryształu. Warto podkreślić, że wraz ze wzrostem ilości cząstek NMK, zwiększa się również frakcja celekoksybu, która pozostaje niewykrystalizowana – fizycznie stabilna pomimo zakończonej rekrystalizacji. Obecność niewykrystalizowanej frakcji amorficznej leku w układach zawierających krzemionkowy materiał, związana jest z oddziaływaniem części cząsteczek farmaceutyku z powierzchnią NMK. Taki mechanizm stabilizacji amorficznego leku występuje, jeśli siła oddziaływania między cząsteczkami leku jest słabsza od oddziaływania cząsteczek leku z powierzchnia krzemionki. W takiej sytuacji proces rekrystalizacji jest mniej korzystny energetycznie dla molekuł farmaceutyku w porównaniu do procesu ich adsorpcji na powierzchni NMK.

W A2 zaprezentowano również, że bazując zarówno na danych kalorymetrycznych [A2 / Rysunek 4], jak i danych dielektrycznych [A2 / Rysunek 10, panel b] możliwe jest wyznaczenie stężenia NMK gwarantującego wysoką fizyczną stabilność dodanego do niego amorficznego leku. Koncentracja ta odpowiada takiej ilości cząsteczek leku, które oddziałując z powierzchnią NMK tworzą jedno-molekularną warstwę. Poniżej zamieszczony Rysunek 5. przedstawia opisywany wpływ różnej koncentracji Syloidu 244FP na proces rekrystalizacji dodanego do niego amorficznego celekoksybu.

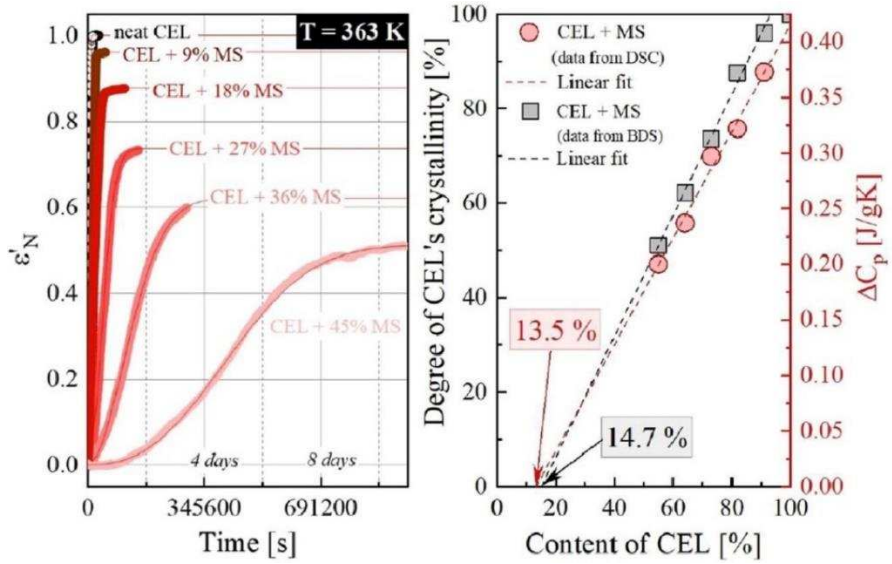

Rysunek 5. Lewy panel: zestawienie kinetycznych krzywych procesu rekrystalizacji czystego celekoksybu (puste koła – dane z Ref. [41], pełne koła – dane z A2] i jego mieszanin z 9, 18, 27, 36 i 45% Syloidu 244FP prowadzonego w temperaturze 363 K. Prawy panel: porównanie zależności stężenia od stopnia krystaliczności celekoksybu, który uzyskano po izotermicznych badaniach dielektrycznych oraz zależności stężenia celekoksybu od wartości jego ΔC_p.

2.4. Modyfikacja tendencji do rekrystalizacji amorficznego aripiprazolu przy pomocy NMK

Ostatni artykuł – A3 – należący do cyklu prezentowanych publikacji stanowiących podstawę niniejszej rozprawy doktorskiej koncentruje się na amorficznym aripiprazolu oraz modyfikacji jego tendencji do rekrystalizacji po zastosowaniu NMK w postaci Syloidu 244FP. Metoda przygotowywania binarnych układów lek + krzemionkowy stabilizator była analogiczna do tej użytej w przypadku pozostałych badanych farmaceutyków (symwastatyny oraz celekoksybu) i została opisana w [A3 / Rozdział 2 / Podrozdział 2.2.]. Przeprowadzone w pracy A3 eksperymenty wykazały, że na podstawie wyboru typu oraz koncentracji samego stabilizatora trudno jednoznacznie przewidzieć, jak wpłynie on na zmianę fizycznej stabilności amorficznego leku. Zgodnie z obserwowanymi w przypadku celekoksybu (patrz sekcja 2.3.) mechanizmami blokującymi rekrystalizację tego leku przy pomocy NMK można by wnioskować, że tendencja do rekrystalizacji amorficznej formy aripiprazolu będzie się zmieniać w podobny sposób. Tymczasem przedstawione w A3 wyniki badań jasno pokazały, że w stabilizacji amorficznych materiałów przy pomocy NMK równie ważną rolę co sam stabilizator odgrywa także stabilizowana substancja.

Przedstawione na [A3 / Rysunek 4 / panel a] termogramy DSC binarnych układów aripiprazol + Syloid 244FP pokazały, że tendencja do rekrystalizacji badanej substancji leczniczej wzrasta wraz ze wzrostem ilości Syloidu 244FP przy zastosowaniu niewielkich (< 30%) koncentracji krzemionkowego materiału. Trend ten się zmienia tzn. fizyczna stabilność

amorficznego aripiprazolu się poprawia wraz ze wzrostem ilości Syloidu 244FP w układzie, gdy stężenie NMK >30%. Opisywany efekt potwierdziły również nieizotermiczne badania dielektryczne układów binarnych składających się z amorficznego aripiprazolu i Syloidu 244FP, które przedstawiono na [A3 / Rysunek 6 / panel a-c]. Zestawienie, wyznaczonych na ich podstawie temperaturowych zależności $\Delta\varepsilon''$, zostało zaprezentowane na [A3 / Rysunek 6 / panel d].

Nieizotermiczne badania kalorymetryczne przeprowadzone na materiałach poddanych uprzedniemu wygrzewaniu przez 0, 4 oraz 20 godzin w T = 313 K [A3 / Rysunek 8], a także badania strukturalne tych układów przeprowadzone przy pomocy dyfrakcji rentgenowskiej (XRD – ang. *X-Ray Diffraction*) [A3 / Rysunek 9 / panel a-c] wykazały, że w zależności od ilości zastosowanego NMK koncentracja polimorficznych odmian, do których amorficzny aripiprazol rekrystalizuje, ulega zmianie. Fakt ten wskazuje, że różny stopień ograniczeń sterycznych wywierane przez cząsteczki Syloidu 244FP na cząsteczki amorficznego aripiprazolu wpływa na tworzenie się zarodków krystalizacji różnych odmian polimorficznych tego leku. W efekcie sterując ilością krzemionkowego materiału można otrzymywać krystaliczny aripiprazol o różnych właściwościach.

Zarówno badania kalorymetryczne [A3 / Rysunek 4 / panel a] jak i dielektryczne [A3 / Rysunek 6 / panel a, b oraz d] wykazały, że równocześnie do powyżej opisywanego efektu zmiany tendencji do rekrystalizacji amorficznego aripiprazolu, wraz ze wzrostem stężenia NMK w układzie aripiprazol + Syloid 244FP zauważyć można wzrost niezrekrystalizowanej frakcji leku. Efekt ten jest bardzo podobny do tego opisywanego w przypadku celekoksybu w sekcji 2.3. i wynika z działania identycznego mechanizmu stabilizującego amorficzny farmaceutyk tj. oddziaływania molekuł aripiprazolu z powierzchnią NMK.

Na koniec tej sekcji warto dodać, że zastosowany materiał krzemionkowy, bez względu na użytą koncentrację, nie wpływa znacząco ani na T_g, ani na $\tau_\alpha(T)$, $\tau_\beta(T)$ i $\tau_\gamma(T)$ amorficznego aripiprazolu (podobnie jak w przypadku symwastatyny oraz celekoksybu). Fakt ten wyklucza, że modyfikacja dynamiki molekularnej odgrywała kluczową rolę w zmianie fizycznej stabilności amorficznej formy aripiprazolu po zastosowaniu Syloidu 244FP.

3. WYKAZ ARTYKUŁÓW STANOWIĄCYCH PODSTAWĘ ROZPRAWY DOKTORSKIEJ WRAZ Z OŚWIADCZENIAMI WSPÓŁAUTORÓW

3.1. A1 – J. Knapik-Kowalczuk, D. Kramarczyk, K. Chmiel, J. Romanova, K. Kawakami, M. Paluch, *Importance of Mesoporous Silica Particle Size in the Stabilization of Amorphous Pharmaceuticals— The Case of Simvastatin*. **2020** Pharmaceutics, 12, 384.

Impact Factor czasopisma z roku opublikowania pracy: 5.4.
Liczba punktów ministerialnych MNiSW czasopisma z roku opublikowania pracy: 100 pkt.
DOI: 10.3390/pharmaceutics12040384.

Udział pierwszego autora w poniżej załączonym artykule polegał na wykonaniu pomiarów dielektrycznych, analizie wszystkich otrzymanych wyników oraz pracach nad powstawaniem manuskryptu. Wkład pozostałych współautorów, w formie oświadczeń, zamieszczono na końcu artykułu.

pharmaceutics

MDPI

Article

Importance of Mesoporous Silica Particle Size in the Stabilization of Amorphous Pharmaceuticals—The Case of Simvastatin

Justyna Knapik-Kowalczuk [1,2,*], Daniel Kramarczyk [1], Krzysztof Chmiel [1], Jana Romanova [2,3], Kohsaku Kawakami [2] and Marian Paluch [1]

1 Faculty of Science and Technology, Institute of Physics, University of Silesia, SMCEBI, 75 Pułku Piechoty 1a, 41-500 Chorzów, Poland
2 International Center for Materials Nanoarchitectonics, National Institute for Materials Science, Tsukuba, Ibaraki 305-0044, Japan
3 Department of Physical Chemistry, Faculty of Chemical Technology, University of Pardubice, Studentská 573, 532 10 Pardubice, Czech Republic
* Correspondence: justyna.knapik-kowalczuk@us.edu.pl

Received: 27 March 2020; Accepted: 14 April 2020; Published: 22 April 2020

Abstract: In this paper, the role of mesoporous silica (MS) particle size in the stabilization of amorphous simvastatin (SVT) is revealed. For inhibiting recrystallization of the supercooled drug, the two MS materials (Syloid® XDP 3050 and Syloid® 244 FP) were employed. The crystallization tendency of SVT alone and in mixture with the MS materials was investigated by Differential Scanning Calorimetry (DSC) and Broadband Dielectric Spectroscopy (BDS). Neither confinement of the SVT molecules inside the MS pores nor molecular interactions between functional groups of the SVT molecules and the surface of the stabilizing excipient could explain the observed stabilization effect. The stabilization effect might be correlated with diffusion length of the SVT molecules in the MS materials that depended on the particle size. Moreover, MS materials possessing different particle sizes could offer free spaces with different sizes, which might influence crystal growth of SVT. All of these factors must be considered when mesoporous materials are used for stabilizing pharmaceutical glasses.

Keywords: simvastatin; amorphous pharmaceuticals; mesoporous silica; stabilization; recrystallization

1. Introduction

The poor aqueous solubility of active pharmaceutical ingredients (APIs) is one of the most challenging issues of modern pharmacy [1–3]. Currently, over 40% of marketed immediate-release oral dosage forms contain poorly soluble drugs [4,5]. One of the most efficient methods that can improve solubility of poorly soluble drugs is amorphization [6–8]. It has been many times reported that the transformation into amorphous form significantly increased the solubility of drug molecules in comparison with their crystalline counterparts [8,9]. These benefits, however, come at a risk. The high internal energy of amorphous solids, which, on the one hand, is the reason for their high solubility, on the other hand, makes amorphous materials thermodynamically unstable [10–14]. Thus, currently, much effort is being made to (i) investigate physical stability of amorphous form of pharmaceuticals [15–17], (ii) find effective methods leading to their stabilization [18–20], and (iii) discover the molecular mechanisms responsible for the observed recrystallization inhibition [16,21–25].

As has been recently proven, one of the very effective inhibitors for recrystallization of the amorphous APIs during the time of their storage, transportation, or manufacturing are mesoporous silica (MS) materials [17,26–28]. It is worth highlighting that MS materials seem to be ideal excipients for drug formulation. This is because they might very effectively stabilize amorphous APIs and

they can also very effectively enhance their bioavailability [29]. A great example of a drug in which bioavailability has been effectively enhanced after preparation MS based formulation is fenofibrate [30]. In choosing an appropriate MS for drug formulation, it is important to check its degradability. This is mainly because the approved pharmaceutical products must not accumulate in the human body since it can lead to unpredictable side-effects [31]. It has been proven that various biodegradable MSs are characterized by different speeds of biodegradability. This is a huge advantage of MS, since it results in the possibility of tuning the material to the selected drug according to the targeted applications [32].

Usually, the improvement of an amorphous drug's physical stability by MS is explained by one of two mechanisms: (i) confinement of the API molecules inside the MS pores or (ii) molecular interactions between functional groups of the API molecules and the surface of the stabilizing excipient [28,33,34]. It is worth noting that, in the case of the former mechanism, it is possible to reach even an eternal stabilization effect [35]. Such a situation might occur only when the pore diameter of the employed MS is smaller than the critical crystal nuclei of the API, as well as if all API molecules are incorporated inside the pores. When the drug molecules are present outside the MS pores, the stabilization is usually explained by the second mechanism [36,37]. MS materials can inhibit the recrystallization of disordered APIs through interactions between the functional groups of the drug molecules and those on the MS surface; this is mainly due to their large specific surface area, which is often larger than 300 m^2/g [38]. It has to be pointed out that this stabilization mechanism has one limitation—it works only when amount of the MS is enough to host a few layers of API molecules. In other words, if the number of drug molecules exceeds the amount of drug that can be "immobilized" on the MS surface, this mechanism cannot work for the inhibition of drug recrystallization. To accurately determine the loading capacity of a drug on MS surface, one can employ the method found by Hempel et al. (2019), which is an extension of the principle proposed by Mellaertes et al. (2017) [39,40]. This method is based on quantification of the API fraction that has not been immobilized by the MS surface through the detection of a glass transition temperature by Differential Scanning Calorimetry (DSC).

In both stabilization mechanisms mentioned above, pores size, pore-volume, and surface area of MS play crucial roles. Consequently, one can find plenty of information on how these parameters affect the physical stability of amorphous APIs [41–43]. Little is known, however, about how the physical stability of amorphous APIs is influenced by the particle size of MS. Thus, the main aim of this article was to investigate the effect of the particle size of MS on the physical stability of amorphous API. As a model drug, we chose simvastatin (SVT)—a commonly prescribed lipid-lowering medication. This pharmaceutical is characterized by excellent permeability but exhibits poor, solubility-limited, bioavailability (5%) [44]. Therefore, there is a need to improve the solubility of this compound. Two MS materials with a brand name of Syloid® 244 FP (SYL244) and Syloid® 3050 XDP (SYL3050) have been employed for stabilizing amorphous state of SVT. These materials are characterized by nearly the same pore size, pore-volume, and surface area (see Table 1) [45,46] but differ in particle size. SYL3050 has an order of magnitude bigger particles than SYL244. To examine the tendency toward recrystallization of SVT mixed with MS materials, time-dependent isothermal crystallization experiments were performed utilizing two different experimental techniques: Differential Scanning Calorimetry (DSC) and Broadband Dielectric Spectroscopy (BDS). The principles of BDS are comprehensively reviewed in the book edited by Kremer and Schönhals (2003) [47]. The utilization of this experimental technique to study molecular mobility and crystallization phenomena in pharmaceutical systems are explained in detail in Grzybowska et al. [48] as well as in the books edited by Rams-Baron and Descamps [49,50]. The principles of DSC have been discussed in detail in Watson et al. (1964) [51] and Höhne et al. (2003) [52]. The use of DSC in the investigation of the isothermal cold crystallization of amorphous APIs has been briefly presented in Szklarz et al. and Kolodziejczyk et al. [13,53]. Since all performed experiments showed that particle size had a significant impact on the physical stability of supercooled SVT, we tried to find the molecular mechanism responsible for the observed recrystallization inhibition.

Table 1. Surface chemistry characterization of SYL244 and SYL3050 [47,48].

MS Name:	BATCH/LOS:	Surface Area (m^2/g)	Average Particle Size (μm)	Pore Diameter (nm)	Pore Volume (mL/g)
SYL244	1000320678	314	2.5–3.7	23	1.6
SYL3050	1000298877	320	59	22.9	1.7

2. Materials and Methods

2.1. Materials

Simvastatin (SVT) with purity higher than 99.3% and molecular mass M_w = 418.6 g/mol was purchased from Polpharma (Starogard Gdański, Poland). This pharmaceutical is described chemically as Butanoic acid, 2,2-dimethyl-(1S,3R,7S,8S,8aR)-1,2,3,7,8,8a-hexahydro-3,7-dimethyl-8-[2-[(2R,4R)-tetrahydro-4-hydroxy-6-oxo-2H-pyran-2-yl]ethyl]-1-naphthalenyl ester. Syloid® XDP 3050 (SYL3050) and Syloid® 244 FP (SYL244), with the detailed specification presented in Table 1, were received as a gift from Grace GmbH & CO. KG (Worms, Germany). All chemicals were used as received.

2.2. Sample Preparation

In order to obtain the binary mixtures containing simvastatin and 9, 18, 27, 36, 45, and 50 wt. % of SYL3050 or SYL244 the right amount of ingredients was weighed and mixed in mortars for about 10 min. Prior to each experiment, the simvastatin in the physical mixture was melted at 423 K and quenched. For DSC experiments the sample was vitrified in situ the machine (with the flow of N2 = 60 mL/min and cooling rate = 20 K/min), while for dielectric and microscopic experiments, the melting procedure takes place at the hot plate in air conditions. Melted material that was placed between the stainless-steel plates of the capacitor (for BDS) or glassy plates (for the optical microscope) was cooled by a cold cooper plate with a rate of ca. 60 K/min.

2.3. Differential Scanning Calorimetry (DSC)

Thermal properties of SVT alone and that with SYL244 or SYL3050 were examined by a Mettler–Toledo DSC 1 STAR^e System (Columbus, OH, USA) equipped with an HSS8 ceramic sensor and 120 thermocouples. The instrument was calibrated for temperature and enthalpy using indium and zinc standards. Melting point was determined as the onset temperature, whereas the glass transition temperature as the midpoint of the heat capacity increment. The samples were measured in an aluminum crucible (40 μL). During non-isothermal experiments, heating rate of 10 K/min was employed. Each non-isothermal experiment was repeated three times, while isothermal experiments were repeated twice.

2.4. Broadband Dielectric Spectroscopy (BDS)

Molecular dynamics of SVT alone and with SYL244 or SYL3050 was measured with a Novocontrol GMBH Alpha dielectric spectrometer (Montabaur, Germany). Dielectric spectra were registered in a broad frequency range from 10^{-1} Hz to 10^6 Hz. During the dielectric experiments the sample was heated from 173 K to 298 K with a step of 5 K and from 330 K to 362 K with a step of 2 K. The temperature was controlled by a Quattro temperature controller with temperature stability better than 0.1 K. The systems were measured in a parallel-plate cell made of stainless steel (diameter of 20 mm, and a 0.1 mm gap provided by silica spacer fibers).

2.5. Optical Microscope

Optical images of SVT alone and the mixtures with 9 wt. % of SYL3050 or 9 wt. % of SYL244 were captured using an Olympus BX51 polarized microscope (Olympus America Inc., Melville, NY, USA) equipped with an Olympus SC30 camera and a halogen source light. Optical images were collected using an Olympus Soft Imaging Solutions GmbH 5.1 (Münster, Germany) (analysis getIT software) at

UMPlanFI 10× objective and at 0.3 NA. All images were handled by Adobe Photoshop 12 software (Adobe Systems, San Jose, CA, USA).

3. Results and Discussion

3.1. Isothermal Crystallization Studies Performed by DSC

Isothermal crystallization of neat SVT and its mixture with 9 wt. % of SYL244 or SYL3050 was investigated using DSC at 363 K, which is higher than the glass transition temperature by 58 K. Figure 1a shows the representative results obtained during the time-dependent isothermal measurements. The DSC curves of neat SVT and system containing SVT and SYL3050 reveal the exothermic peak of isothermal crystallization. The temperatures for crystallization onset of neat SVT and that for the mixture with SYL3050 were nearly the same (there is ~6 min shift after MS inclusion). However, big difference was observed for the time required for complete crystallization. In the case of neat SVT, the recrystallization ended after 5 h, while the presence of SYL3050 extended this process to 8 h. Interestingly, the presence of the same amount of SYL244, which has a smaller particle size, inhibited crystallization. This result indicates that the particle size of MS might have a significant impact on the physical stability of the amorphous SVT.

Based on data obtained from DSC, one can estimate the relative degree of the sample crystallization (α_{DSC}) by utilizing the following formula:

$$\alpha_{DSC} = \frac{\int_{t_0}^{t} \frac{dH}{dt} dt}{\int_{t_0}^{t_\infty} \frac{dH}{dt} dt} \quad (1)$$

where dH/dt is the rate of heat evolution. t_0 and t_∞ represent the time at which crystallization begins and ends, respectively. The time evolutions of α_{DSC}, as determined from DSC experiments, are presented in Figure 1b. The kinetic curves were normalized by the maximal value of the α_{DSC}, which was registered when crystallization has ended. After the isothermal step of DSC experiments, the samples were cooled down and reheated to confirm the degree of crystallinity.

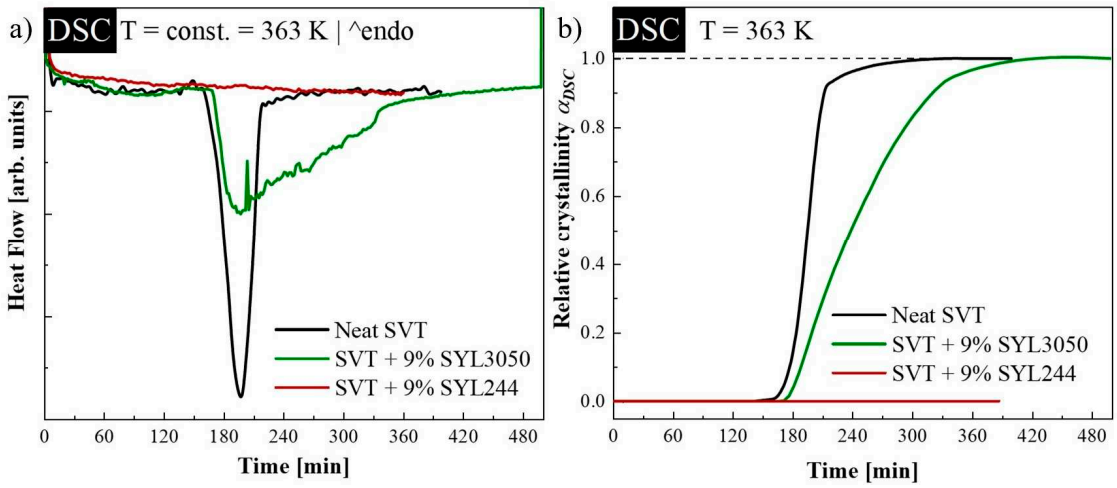

Figure 1. (**a**) Differential Scanning Calorimetry (DSC) traces of neat simvastatin (SVT) (black line), SVT + 9 wt. % of SYL3050 (green line), and SVT + 9 wt. % of SYL244 (red line) recorded during isothermal crystallization at 363 K (**b**) and corresponding relative crystallinity (α_{DSC}).

To properly describe the crystallization kinetics of the investigated samples under isothermal conditions, the Avramov model was employed [54]. In this approach, the dependence of α_{DSC}, together with its first derivative, is plotted versus *ln* t on the same axis. In coordinates α_{DSC} against *ln* t, the

inflection points in all cases appeared at $\alpha < 0.63$, and induction times have been determined as 8800 ± 100 s and 9150 ± 50 s for neat SVT and SVT + 9 wt. % of SYL3050, respectively. Finally, i.e., utilizing the value of t_0, the correct Avrami–Avramov plots have been constructed (see Figure 2). From this plot, one can obtain the value of the characteristic time of the crystallization process (τ_{cr}) as the time corresponds to $d(\alpha_{DSC})'/[d(ln(t - t_0))]$ peak maximum. The determined τ_{cr} for neat SVT and SVT + 9 wt. % of SYL3050 are equal to 55 ± 1 min and 107 ± 3 min, respectively. The change in τ_{cr} toward the larger value after addition of SYL3050 indicated improvement in physical stability of SVT in the presence of the MS. Of course, a much better stabilization effect has been reached after employment of the MS characterized by an order of magnitude smaller particle size than in case of SYL3050, what is reflected as lack of SVT re-crystallization.

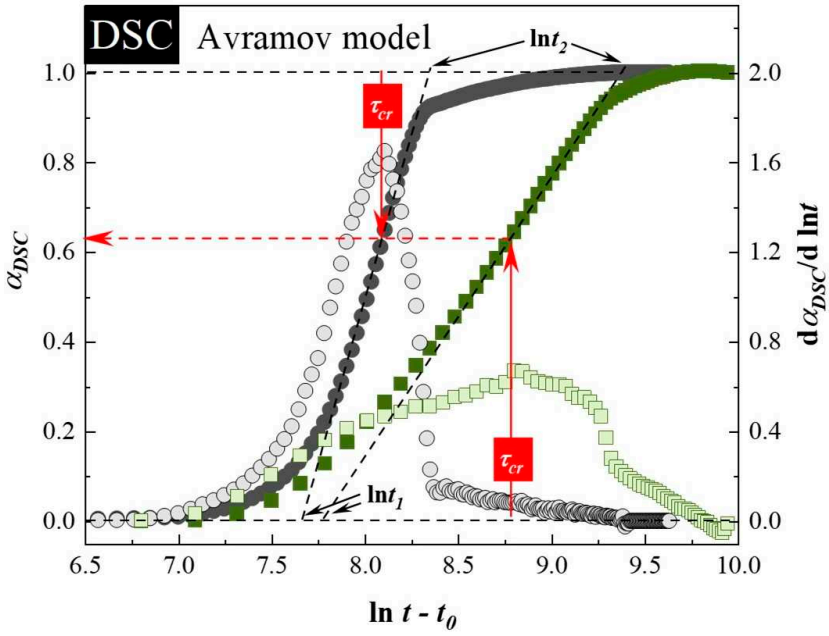

Figure 2. The Avrami–Avramov plot presenting a time evolution of relative crystallinity (α_{DSC}) (full symbols) and its first derivative toward the natural logarithm of the time (shadowed symbols) of neat SVT (grey circles) and SVT + 9 wt. % of SYL3050 (green squares).

Use of the Avramov model allows us to calculate another parameter, n, which is directly related to the nucleation dimensionality. Two methods are available to determine n. The first is based on employment the following equation:

$$n = \frac{(\alpha(t))'_{max}}{0.368} \quad (2)$$

where $(\alpha(t))'_{max}$ is a maximum value of the first derivative of the normalized degree of crystallization. The second approach of evaluation the Avramov parameter related to the nucleation dimensionality is based on drawing a tangent to the experimentally determined sigmoidal curve $\alpha_{DSC}(ln(t - t_0))$ at $t - t_0 = \tau_{cr}$ (see dashed lines in Figure 2). By determining the values of $ln\ t_1$ and $ln\ t_2$, which corresponds to the points of intersection of the tangent line with the horizontal straight lines, constructed at the limit values of α_{DSC}, i.e., at 0 and 1, it is possible to establish the n parameter from the following formula:

$$n = \frac{e}{\ln t_2 - \ln t_1} \quad (3)$$

The values of t_0, $ln\ t_1$, $ln\ t_2$, $(\alpha(t))'_{max}$, τ_{cr} as well as n calculated using both equations are collected in Table 2. As can be seen, regardless of the employed method for determination of n value, the dimensionality of crystallization of SVT was reduced when SYL3050 was added to the drug.

Table 2. Comparison of parameters estimated from Avramov model for kinetics of isothermal crystallization obtained from DSC measurements.

Sample:	t_0 (s)	τ_{cr} (min)	$ln\ t_1$	$ln\ t_2$	n (Equation (3))	$\alpha(t)'_{max}$	n (Equation (2))
neat SVT	8800 ± 100	55 ± 1	7.65 ± 0.02	8.361 ± 0.001	3.8 ± 0.1	1.57 ± 0.09	4.3 ± 0.2
SVT + SYL3050	9150 ± 50	107 ± 3	7.79 ± 0.04	9.33 ± 0.08	1.8 ± 0.1	0.73 ± 0.06	2.0 ± 0.2

3.2. Isothermal Crystallization Studies Performed by BDS

The second method employed to study the isothermal crystallization of neat SVT and its mixtures with MSs having two types of particle size was BDS. During the time-dependent dielectric experiments, the spectra of the complex dielectric permittivity $\varepsilon^*(\omega) = \varepsilon'(\omega) - i\varepsilon''(\omega)$ were investigated at specified time intervals of 300 s. By using dielectric spectroscopy, the crystallization process can be followed directly in both the real (ε') and imaginary (ε'') parts of the complex dielectric permittivity, reflected by a decrease of the static permittivity (ε_s) and reduction of the loss peak intensity with time, respectively [49]. For our purpose, the real part of complex dielectric permittivity was selected for further analysis. The representative frequency dependences of ε' measured during the time-dependent dielectric experiments performed at T = 363 K for SVT + 9 wt. % of SYL3050 as well as SVT + 9 wt. % of SYL244 are presented in Figure 3a,b. The neat SVT and that in the mixture with SYL3050 recrystallized as evidenced by the registered decrease in the static permittivity (ε_s). Lack of drop in the ε_s observed during identical measurements performed on the SVT + 9 wt. % of SYL244 system (Figure 3b) indicated that the MS with smaller particle size was a better stabilizer for the amorphous SVT. This investigation agrees with the finding made during the DSC study where the particle size of MS was the important parameter for stabilizing amorphous SVT. After the isothermal dielectric experiments, the neat SVT and its mixture with SYL3050 were subjected to the DSC measurement to confirm that crystallinity of both samples reached 100%.

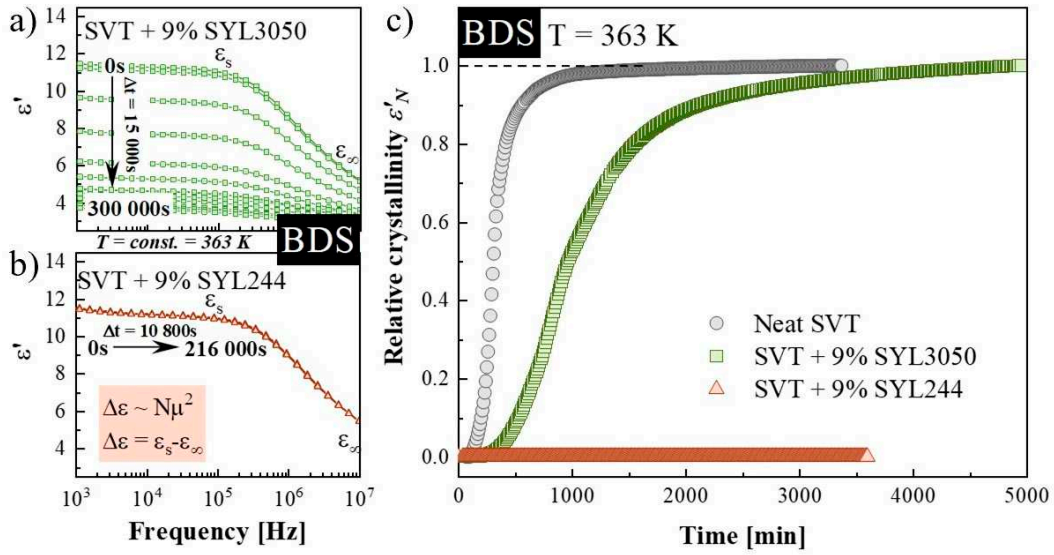

Figure 3. (**a**) Dielectric spectra of the real parts of the complex dielectric permittivity during an isothermal crystallization of SVT + 9 wt. % of SYL3050 performed at 363 K, (**b**) dielectric spectra of the real parts of the complex dielectric permittivity collected during the time-dependent isothermal experiment of SVT + 9 wt. % of SYL244 performed at 363 K, (**c**) normalized dielectric constants ε'_N as a function of time from crystallization processes occurring at 363 K.

Usually, the progress of crystallization is analyzed in terms of the normalized real permittivity (ε'_N) defined as follows [55–57]:

$$\varepsilon'_N(t) = \frac{\varepsilon'(0) - \varepsilon'(t)}{\varepsilon'(0) - \varepsilon'(\infty)} \quad (4)$$

where $\varepsilon'(0)$ is the initial static dielectric permittivity, $\varepsilon'(\infty)$ is the long-time limiting value, and $\varepsilon'(t)$ is the value at time t. The data normalized in this way and plotted versus time are shown in Figure 3c.

Crystallization of SVT in the mixture with 9 wt. % of SYL3050 is delayed in comparison to that of the neat SVT. The entire crystallization process of the neat SVT and that in the mixture with SYL3050 required ca. one day and three days, respectively, at 363 K. Analysis based on the Avramov model revealed that the inflection points have appeared at $\alpha < 0.63$, whereas the induction times have been determined as 13,600 ± 400 s and 29,750 ± 250 s for neat SVT and SVT + 9 wt. % of SYL3050, respectively. By utilizing the estimated values of t_0, the Avrami–Avramov plot for each sample was constructed (Figure 4). Determined from the $d(\alpha_{DSC})'/[d(ln\ t - t_0)]$ peak maximum, the characteristic time of the crystallization process (τ_{cr}) for neat SVT and that in the mixture with 9 wt. % of SYL3050 are equal to 201 ± 12 min and 737 ± 28 min, respectively.

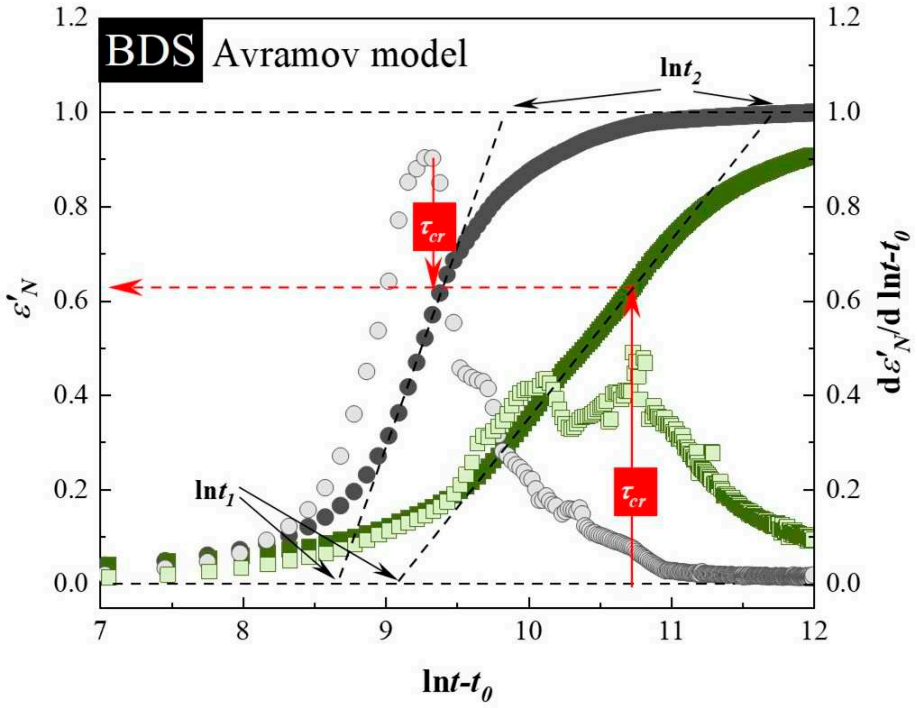

Figure 4. The Avrami–Avramov plot presenting a time evolution of normalized real permittivity (ε'_N) (full symbols) and its first derivative toward the natural logarithm of the time (shadowed symbols) of neat SVT (grey circles) and SVT + 9 wt. % of SYL3050 (green squares).

The n values together with other parameters were determined in the same manner as described in the previous section are summarized in Table 3. The n value for the SVT in the mixture with SYL3050 is smaller than that for the neat SVT, which agreed with the results obtained from the DSC study.

Table 3. Comparison of parameters estimated from Avramov model for kinetics of isothermal crystallization obtained from dielectric measurements.

Sample:	t_0 (s)	τ_{cr} (min)	ln*1*	ln*2*	*n* (Equation (3))	$\alpha(t)$max′	*n* (Equation (2))
neat SVT	13,600 ± 400	201 ± 12	8.71 ± 0.06	9.88 ± 0.02	2.34 ± 0.07	0.91 ± 0.01	2.48 ± 0.04
SVT + SYL3050	29,750 ± 250	737 ± 28	9.02 ± 0.08	11.67 ± 0.08	1.026 ± 0.003	0.488 ± 0.001	1.326 ± 0.001

It is worth highlighting that the crystallization kinetics of SVT was characterized by totally different parameter values for two different experimental techniques [58]. The recrystallization during the BDS measurement was much slower than that in the DSC study. For example, $t_{0\ BDS}$ for the SVT in the mixture was 3.25 times longer than $t_{0\ DSC}$. By employing the dielectric spectroscopy, one can also observe an increase in the value of τ_{cr} as well as decrease in the n parameter in comparison to the values determined from the DSC study. The described differences between crystallization kinetics of the same systems measured by different experimental techniques are natural and result from differences existing between the employed techniques. For example, samples used for the both techniques had totally different geometry (see inserts in Figure 5). The sample thickness for the BDS study was 0.1 mm, which was much thinner than that in the DSC measurement. The difference in the sample thickness results in different heat flow, which may influence the crystallization kinetics [58]. During the dielectric studies, samples were placed between stainless-steel electrodes, which inhibited their contact with air. A decrease in the specific surface area delays crystallization because nucleation is frequently initiated from the surface [59,60]. Also, in the case of DSC measurements, samples were heated and quenched at a rate of 20 K/min under a nitrogen atmosphere prior to the crystallization experiment, whereas those for BDS studies were melted in the air on a hot plate and quenched at a rate faster by four-times than that for the DSC study. Both the atmosphere and the cooling rate [61] influence the amorphous property. Dimension of crystal growth is also influenced by the sample geometry [59]. Thus, the smaller n values in the BDS study compared to those from the DSC study is natural observation. Nevertheless, it should be emphasized that, despite quantitative differences in the crystallization kinetics obtained by the two different experimental techniques, one can find qualitative similarities on effect of the presence of the MS material, that is, its stabilization effect against crystallization of SVT. Moreover, a more striking stabilization effect was observed for SYL244 relative to SLY3050 despite their almost equal surface area (~300 m^2/g), pore size (~20 nm), and pore volume (~1.65 mL/g). Therefore, it seems essential to find the reason for the observed differences in the stabilization of supercooled SVT. To achieve this goal, we were looking for the differences in the thermal properties and molecular dynamics of these compositions.

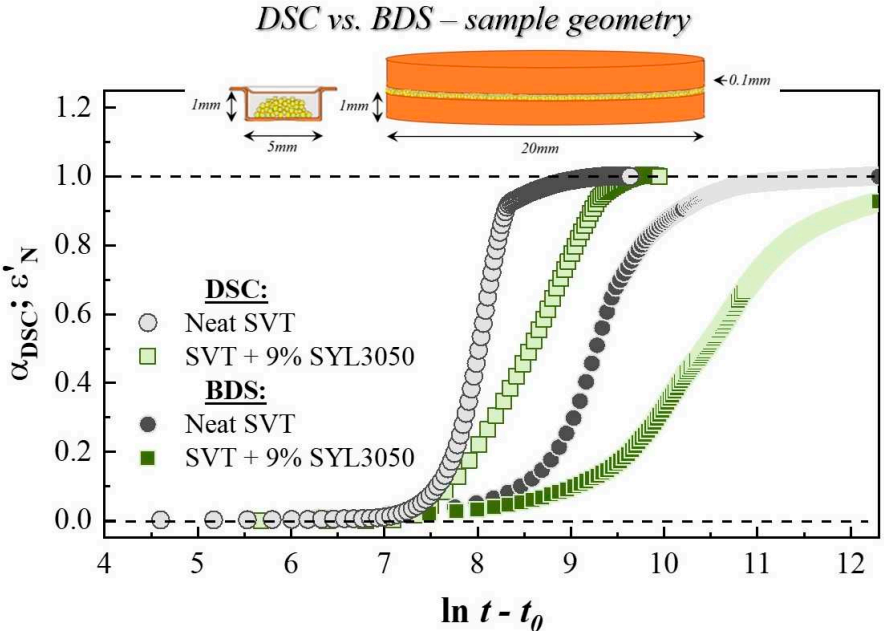

Figure 5. Comparison of the time evolutions of normalized real permittivity (ε'_N) and relative crystallinity (α_{DSC}) as well as its first derivatives toward the natural logarithm of the time of neat SVT (grey circles) and SVT + 9 wt. % of SYL3050 (green squares).

3.3. Loading Capacity of MSs for SVT

To investigate how the MS materials, possessing different particle sizes, influence the thermal properties of SVT, both physical mixtures (i.e., samples containing crystalline API) and quenched samples (i.e., samples containing amorphous API) have been investigated non-isothermally through DSC. Figure 6a presents the DSC thermograms obtained during the sample heating with a rate equal to 10 K/min. As can be seen, neither the melting temperature of SVT nor its glass transition has been significantly modified after the inclusion of MS materials. The melting temperature of neat SVT, determined as the onset of the registered melting endotherm, is equal to 413 K. Mixtures containing SVT and 9 wt. % of SYL244 or SYL3050 are characterized by T_m equal to 412 K. After the quenching of all samples, the reheating DSC curves were acquired. As can be seen in Figure 6b, the thermogram of each sample reveal one step-like thermal event corresponding to glass transition of SVT. The T_g midpoints of neat SVT, SVT + 9 wt. % of SYL244, and SVT + 9 wt. % of SYL3050 have the same value that is equal to 305 K, when heated at a rate 10 K/min.

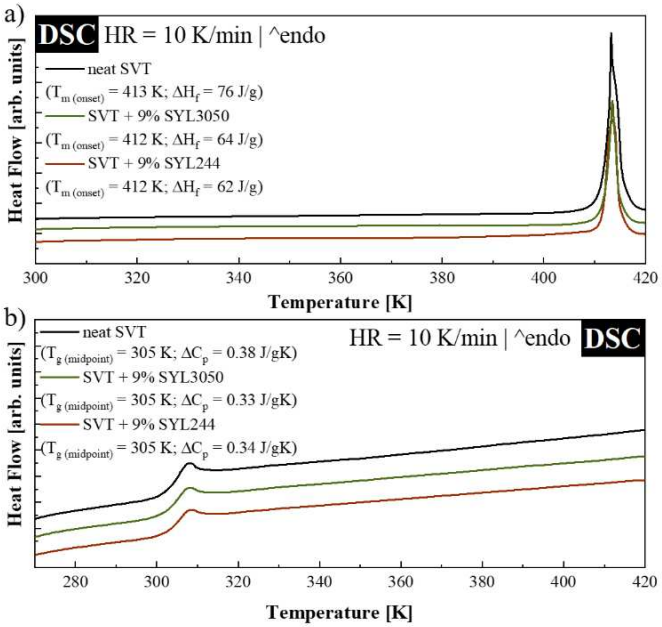

Figure 6. DSC thermograms of (**a**) crystalline and (**b**) amorphous SVT (grey lines), SVT + 9 wt. % of SYL3050 (green lines), and SVT + 9 wt. % of SYL244 (red lines).

After the inclusion of MS material to SVT, the value of its ΔC_p decreased. In the ideal case in which SVT molecules would not interact with the surface of MS, the value of ΔC_p of the mixture should have linear relationship with the amount of SVT. When, however, some interactions between the drug and surface of MS exist, the decrease of ΔC_p is larger than expected. Recently, Hempel et al. showed that by measuring the ΔC_p value of various concentrations of a system containing drug and MS material, it is possible to estimate the monomolecular loading capacity of the drug on the surface of MS [41]. A series of samples possessing various concentrations of MS and SVT have been prepared and investigated in the same manner. The concentration dependences of ΔC_p of SVT are presented in Figure 7.

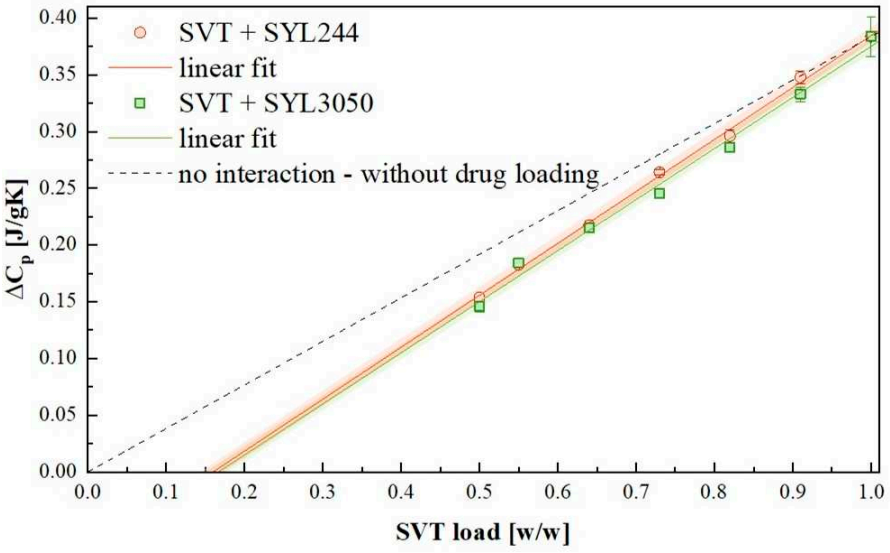

Figure 7. Linear extrapolation of the obtained ΔC_p as a function of drug load.

By extrapolating a straight line describing the concentration dependence of ΔC_p of both SVT + SYL244 and SVT + SYL3050 systems to zero, the monomolecular loading capacity values were determined. The amount of MS materials required to stabilize all SVT molecules on their surface was equal to 84.3 wt. % and 83.4 wt. % for SYL244 and SYL3050, respectively. Lack of significant discrepancies between these values proved that the employed MS materials interacted similarly with SVT. Therefore, considering these results, it is difficult to explain the dramatic difference in the stabilization effect of MS for the amorphous SVT by their loading capacities.

3.4. Effect of MS Materials on the Molecular Mobility of Supercooled SVT

Since no significant differences in loading capacities have been found between two MS materials, the following questions arise: Is the observed difference in SVT stabilization by MS materials possessing different particle size associated with some modifications in dynamics of the drug molecules? Is there any difference in the τ_α(T) of SVT when different MSs are employed? Or does the inhibition of the secondary relaxation processes play a crucial role? To answer these questions, molecular dynamics of the neat SVT and the systems containing SVT + 9 wt. % of SYL3050 and SVT + 9 wt. % of SYL244 were evaluated by means of BDS. Representative dielectric loss spectra, which were measured above the samples glass transition temperatures, are presented in Figure 8a,c,d. As can be seen at this temperature region, the spectra of all investigated samples exhibit two features—the dc-conductivity related to translational motions of ions and the structural (α) relaxation process associated with the cooperative rearrangement of the entire molecules. The α-relaxation mode always shifts toward higher frequencies with increasing temperature, indicating an increase in global mobility of the systems.

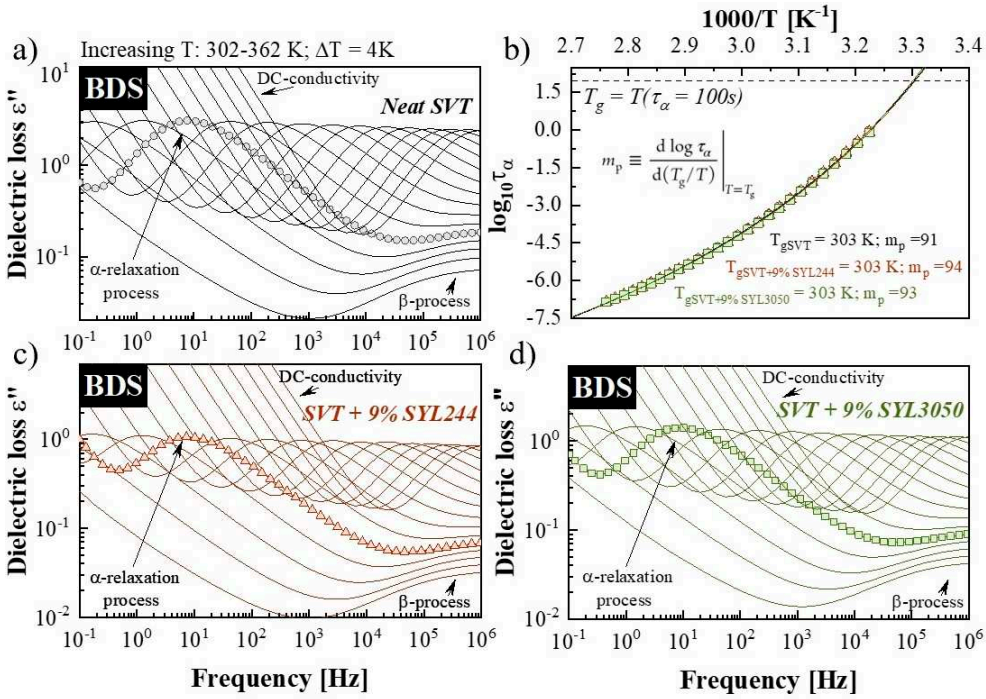

Figure 8. Dielectric loss spectra of (**a**) neat SVT, (**c**) SVT + 9 wt. % of SYL244, and (**d**) SVT + 9 wt. % of SYL3050 collected above their respective T_gs upon heating. In panel (**b**), activation plots are constructed for the tested compounds with gray circles, red triangles, and green squares referring to temperature dependences of α-relaxation times for neat SVT, SVT + 9 wt. % of SYL3050, and SVT + 9 wt. % of SYL244, respectively. The solid lines are the fitting results by the Vogel–Fulcher–Tammann (VFT) equation.

From the analysis of dielectric loss spectra registered at supercooled liquid state, the temperature dependences of structural relaxation time ($\tau_\alpha(T)$) of all investigated samples were determined (see Figure 8b). To obtain the value of τ_α at various temperature conditions, we fitted the experimental data by the Havriliak–Negami (HN) function. The empirical HN approach with the dc-conductivity term is given by the following formula [62]:

$$\varepsilon^*(\omega) = \varepsilon_\infty + \frac{\Delta\varepsilon}{[1 + (i\omega\tau_{HN})^a]^b} + \frac{\sigma_{dc}}{\varepsilon_0 i\omega} \quad (5)$$

where ε_∞ is the high-frequency limit permittivity, ε_0 denotes the permittivity of vacuum, $\Delta\varepsilon$ is dielectric strength, ω is equal to $2\pi f$, τ_{HN} is the HN relaxation time, and a and b represent symmetric and asymmetric broadening of the relaxation peak. Employing the fit parameters determined above, we finally calculated the values of τ_α as

$$\tau_\alpha = \tau_{max} = \tau_{HN}[\sin(\frac{\pi ab}{2+2b})]^{-\frac{1}{a}}[\sin(\frac{\pi ab}{2+2b})]^{\frac{1}{a}} \quad (6)$$

In the supercooled liquid region, the temperature evolution of τ_α usually shows non-Arrhenius behavior. Thus, to properly described $\tau_\alpha(T)$ dependences of neat SVT and its mixture with 9 wt. % of SYL244 or SYL3050 we employed the Vogel–Fulcher–Tammann (VFT) equation that is expressed as follows [63–65]:

$$\tau_\alpha = \tau_\infty \exp(\frac{DT_0}{T - T_0}) \quad (7)$$

where τ_∞, T_0, and B are fitting parameters. Parameter τ_∞ is a pre-exponential factor denoting the upper limit of temperature for τ_α, which is correlated to vibrational frequency (~10^{-11} to 10^{-14} s). T_0 is the Vogel temperature, which correspond to the state with infinite relaxation time, and D denotes deviation

from the Arrhenius model. Extrapolating the VFT fits to temperature at which τ_α = 100 s, the T_g values of all the samples have been estimated to be 303 K. The glass transition temperatures determined by this method are in good agreement with that obtained from calorimetric studies ($T_{gDSC\ \mathrm{HR}=10\ \mathrm{K/min}}$ = 305 K—see Figure 6). From the VFT fits, we also calculated the value of fragility parameter, m_p, for all investigated samples. This parameter is a measure of deviation the $\tau_\alpha(T)$ dependence from the Arrhenius behavior, and is defined as [66]

$$m_p = \left.\frac{d\log\tau_\alpha}{d(\frac{T_g}{T})}\right|_{T=T_g} \quad (8)$$

The typical values of the fragility parameter are between 50 and 100 [22,67,68]. The higher the fragility value, the more fragile the liquids. The m_p parameter is considered to help predict the physical stability of amorphous pharmaceuticals because it has been implied that strong materials are more stable than the fragile ones [61,69]. However, the addition of MS did not have much of an impact on m_p (Table 4); therefore, the difference in the crystallization behavior cannot be explained by the fragility. Thermodynamic parameters for each amorphous material are collected in Table 4. As can be seen, 9 wt. % of the used MS materials do not significantly modify the temperature evolution of τα of SVT, and consequently, no explanation of the observed stabilization has yet been found.

Table 4. Comparison of the obtained based on the dielectric data values of T_g, m_p and fitting parameters from the VFT for neat SVT, SVT + SYL3050, and SVT + SYL244.

Sample:	T_g (K)	log τ_∞	T_0 (K)	BT_0	m_p
SVT	303	−15.68 ± 0.13	244.01 ± 0.89	2386 ± 51	91
SVT + SYL3050	303	−15.23 ± 0.11	246.23 ± 0.77	2240 ± 42	93
SVT + SYL244	303	−15.18 ± 0.16	247.64 ±1.13	2183 ± 54	94

To check if the shape of the structural relaxation peak of SVT remains constant in the whole examined temperature range, as well as what impact on it have the employed MS excipients, a so-called master plot has been constructed for each sample (see Figure 9a–c). To obtain the master plot, dielectric spectra taken from 302 K to 350 K was shifted to superimpose on the reference spectrum at 314 K. The master plots show that the shape of the α-relaxation of SVT is invariant to the temperature changes, and the parameter β_{KWW} for all spectra is the same. The value of the β_{KWW} parameter of SVT, which describes the breadth of its structural relaxation loss peak, was determined by fitting the α-peak at a temperature T = 314 K through the one-side Fourier transform of the Kohlrausch−Williams−Watts (KWW) function [70]. This procedure gives a value of β_{KWW} equal to 0.60, 0.59 and 0.58 for neat SVT, SVT + 9 wt. % of SYL3050, and SVT + 9 wt. % of SYL244, respectively. It should be mentioned that the value of β_{KWW} may vary within the 0–1 range. This parameter approaches 1 if the α-relaxation peak is narrow and symmetric and corresponds to the Debye case; however, when its value is approaching 0, the structural relaxation process is broad and asymmetric [47]. The β_{KWW} might be correlated with crystallization tendency of amorphous materials [71]. It has been suggested that the physical stability of amorphous materials stored at similar relaxation times (τ_α) should decrease as β_{KWW} increases. Based on this assumption, the physical stability of SVT should not be improved after the addition of MS, although the difference in β_{KWW} is only marginal.

According to the recent study by Paluch et al., anticorrelation between the width of the α-loss peak and polarity of the molecule, van der Waals glass formers with a broad α-loss peak (i.e., a small value of β_{KWW}) should exhibit a low value of the dielectric strength ($\Delta\varepsilon_\alpha$) [72]. SVT with β_{KWW} = 0.6 and $\Delta\varepsilon_\alpha$ = 8.9 follows well this anticorrelation similarly to chloramphenicol (β_{KWW} = 0.8, $\Delta\varepsilon_\alpha$ = 55) [73], MD20 (β_{KWW} = 0.76, $\Delta\varepsilon_\alpha$ = 39) [74], azithromycin (β_{KWW} = 0.52, $\Delta\varepsilon_\alpha$ = 1.2), or roxithromycin (β_{KWW} = 0.62, $\Delta\varepsilon_\alpha$ = 1.6) [75] (see panel Figure 9d).

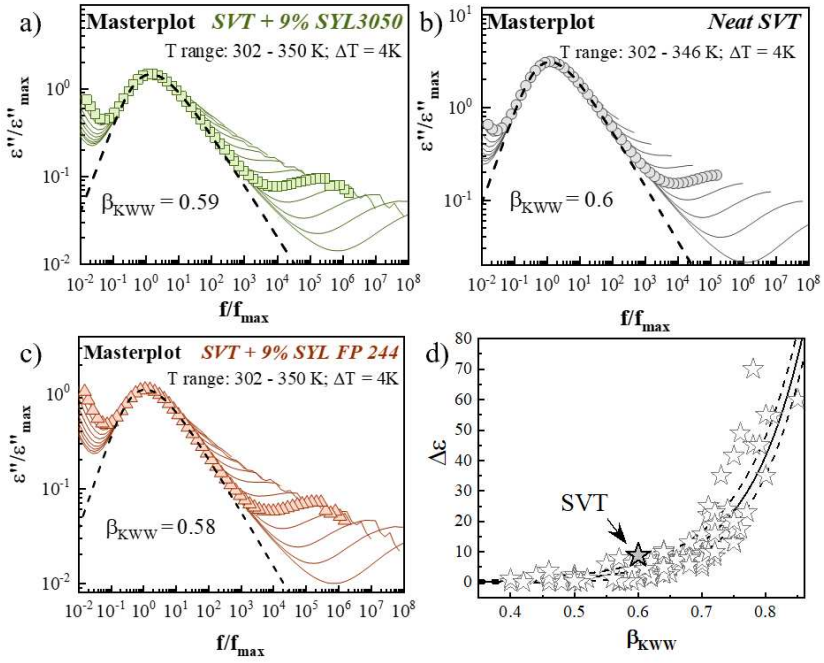

Figure 9. (**a**–**c**) The master plot dielectric loss spectra of SVT + 9 wt. % of SYL3050, neat SVT, and SVT + 9 wt. % of SYL244 formed by horizontal shifting of spectra to overlap the reference one. The dashed lines represent the KWW fit to the α-peak at 314 K with β_{KWW} = 0.6, 0.59, and 0.58 for neat SVT, SVT + 9 wt. % of SYL3050 and SVT + 9 wt. % of SYL244, respectively. (**d**) Dielectric strength $\Delta\varepsilon(T_g)$ as a function of the fractional exponent β_{KWW} in the Kohlrausch-Williams-Watts function, taken from the Reference [76].

3.5. Effect of MS Materials on the Molecular Mobility of Glassy SVT

In the glassy state, where the structural—α—relaxation becomes too slow to be experimentally observed, it is possible to monitor faster secondary relaxation processes associated with the local (inter- or intramolecular) motions [76]. It has been many times reported that this kind of motion might be responsible for the crystallization of amorphous materials. The best examples of APIs in which secondary relaxations play a crucial role in physical stability are celecoxib and sildenafil [77,78]. To investigate how the MSs materials affect the secondary relaxation of SVT, the dielectric spectra at temperatures 173–293 K have been measured utilizing BDS. Representative spectra for neat SVT, SVT + 9 wt. % of SYL244, and SVT + 9 wt. % of SYL3050 are shown in Figure 10a,c,d.

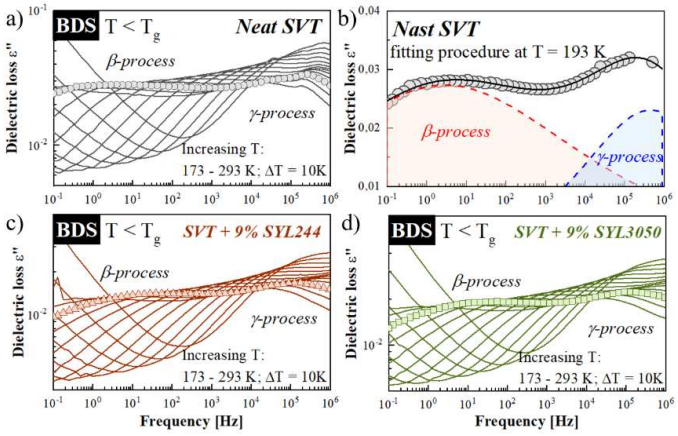

Figure 10. The dielectric loss spectra of (**a**) neat SVT, (**c**) SVT + 9 wt. % of SYL244, and (**d**) SVT + 9 wt. % of SYL3050 registered at temperatures below T_g. (**b**) Selected spectrum of neat SVT with two well-visible secondary relaxation processes β and γ.

Two secondary relaxations (β and γ) were observed for both the neat SVT and that in mixtures with SYL244 or SYL3050. Both modes move toward higher frequencies with increasing temperature, indicating an increase in molecular mobility. To determine the values of τ_β and τ_γ, the spectra of each sample have been fitted by two Cole−Cole (CC) functions. The example of the performed fitting procedure is presented in panel b of Figure 10. It is worth recalling that the CC function is a special case of the HN function (Equation (5)) in which the b parameter is fixed at 1. As Figure 11 presents, in the glassy state of SVT, both $\tau_\beta(T)$ and $\tau_\gamma(T)$ exhibit a linear dependence, and consequently can be well described by the Arrhenius equation:

$$\tau_\beta(T) = \tau_\infty \exp\left(\frac{E_a}{RT}\right) \quad (9)$$

where R is the gas constant, τ_∞ is the pre-exponential factor, and E_a is an activation energy. The obtained values of E_a are collected in Figure 11. However, this analysis revealed that the stabilization effect (exerted) by MS, especially SYL244, cannot be explained by the secondary relaxation as it does not modify the γ-relaxation and the fact that it barely changes the dynamics of β-process of SVT.

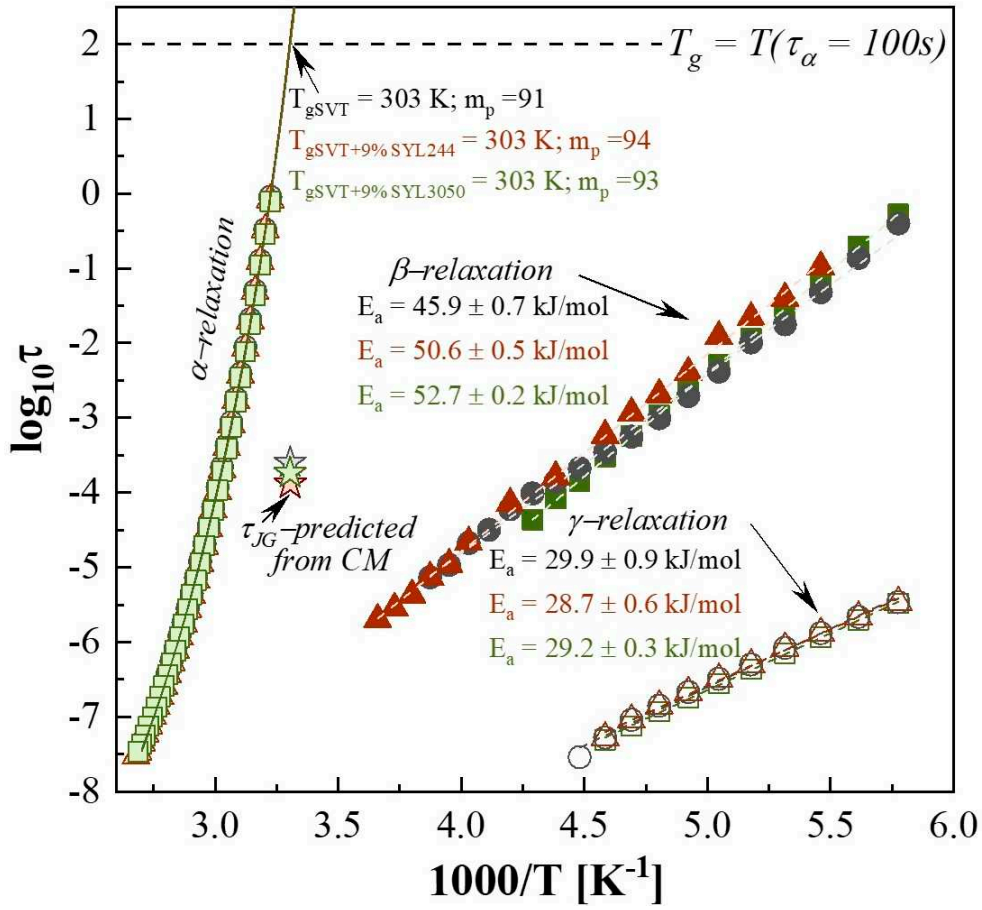

Figure 11. The relaxation map of neat SVT (gray points), SVT + 9 wt. % of SYL244 (red points), and SVT + 9 wt. % of SYL3050 (green points). The Vogel–Tammann–Fulcher (VTF) equation was applied to describe structural relaxation times, while the temperature dependences of secondary relaxation times were fitted to the Arrhenius equation.

3.6. Mechanism of SVT Stabilization with MS Materials

Crystallization of the SVT should be inhibited if it is strongly adsorbed on the surface of MS. In fact, the adsorbed SVT molecules did not exhibit even the glass transition behavior. However, it was obviously not enough to explain the stabilization mechanism. Extensive BDS and DSC analysis

revealed that many parameters to describe macroscopic thermodynamic and dynamic properties of the amorphous SVT remained almost the same after the addition of the MS materials. Moreover, despite significant difference in the stabilization effect between SYL244 and SLY3050, their influences on the amorphous properties of SVT was not obvious.

We have added only 9 wt. % of MS to observe the drastic stabilization effect of the amorphous SVT. To provide sufficient loading capacity for SVT, a much larger amount of MS material, ca. 84 wt. %, is required. Consequently, the only remaining difference to explain observed stabilization effect is the difference in the particle size of the MS.

Note that the stabilization effect was observed at 363 K, which is higher than the glass transition temperature by 60 K. Very high molecular mobility is expected for SVT at the experimental temperature for the crystallization study. A very small amount of stabilizers may influence the entirety of the materials because of the rapid diffusion of the SVT molecules. If the particle size is small, the exchange of the SVT molecules in the pores and those outside the particles should occur easily. If the particle size is large, the exchange may become difficult for the molecules located deep in the particles. This may explain the different stabilization effect of the two MS materials with different particle size.

The global crystallization observed through $X(t)$ (i.e., $\alpha_{DSC}(t)$ or $\varepsilon'_N(t)$) consists of nucleation and crystal growth. By a dimensional analysis of three-dimensional nucleation having the nucleation rate $N = L^{-3}t^{-1}$ and the linear crystal growth rate $V = Lt^{-1}$, one can describe the crystallization process using a characteristic time $t_0 = (NV^3)^{-1/4}$ and a characteristic size $\xi = (V/N)^{1/4}$. As explained by Descamps and Willart [79], the competition between the characteristic, natural length scale (ξ), and the real macroscopic size (L) of the system induces a change in the kinetic regime as discussed in references [79,80] and visualized in Figure 12.

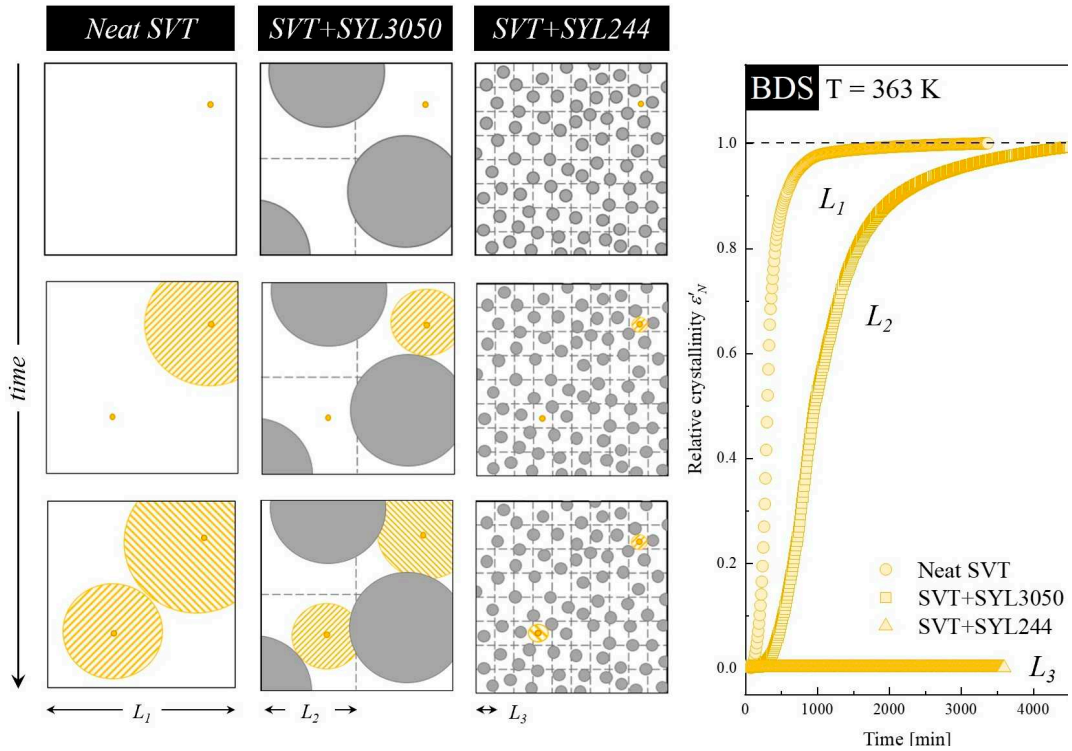

Figure 12. The time evolution of crystallinity of neat SVT (circles), SVT + 9 wt. % of SYL3050 (squares), and SVT + SYL244 (triangles), which were obtained from dielectric studies and described in Section 3.2, together with the schematic explanation of the stabilization mechanism by MS materials. Yellow dot, yellow patterned circles, and gray filled circles represent SVT nuclei, SVT crystals, and MS particles, respectively.

Particles of SYL244 (MS that is characterized by smaller particle size than SYL3050) may limit the real size of the drug (*L*) more effectively than large particles of SYL3050. On the other hand, particles of SYL3050 can form a restriction in SVT space that is absent when SVT is alone. Such a modification in the sample size can affect both the time scale of the crystallization process and the expression of the kinetic law itself. Consequently, a dramatic slowing down of the SVT kinetic is expected after the reduction of L that is realized by the employment of MS materials.

To verify the proposed hypothesis explaining the physical improvement of supercooled SVT after the inclusion MS materials, the optical microscopy was employed. The obtained optical images, with a scale bar equal to 50 μm are presented in Figure 13. Panels A–C present the row microscopic data, while panels D–E present improved images with adjustment of the contrast. As can be seen, the smaller the particle size, the more steric hindrance is generated (i.e., less free space for the sample crystal growth exists—compare the areas marked by the red circles in Figure 13E,F). It consequently leads to the reduction of drug connectivity and thereby loss of crystallization propagation pathways and an increase of the physical stability of SVT.

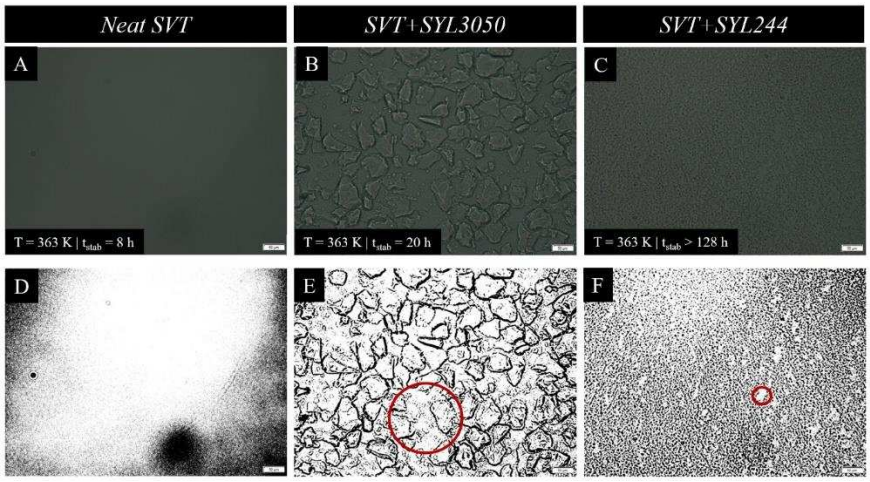

Figure 13. (**A**–**C**) The optical images, which were collected at 5× magnification, of neat SVT, SVT + 9 wt. % of SYL3050, and SVT + SYL244 (the scale bars are equal to 50 μm). (**D**–**F**) The images from panels A–C with artificial contrast (the red circles represent the representative free areas of the SVT alone and in mixture with MS).

4. Conclusions

In this paper, we investigated the effect of two MS materials (SYL244 and SYL3050) on the physical stability of supercooled SVT. These MS materials differ from each other only by the size of particles. SYL3050 possesses particles that are an order of magnitude larger than SYL244. To investigate the kinetics of crystallization of both SVT alone and in mixture with the MS, two experiments—DSC and BDS—were employed. Despite the differences in the obtained crystallization kinetics resulting from the use of different research techniques, one could have observed the same stabilization trends. Neat SVT begins to recrystallize faster, and its crystallization kinetic curve is much steeper than after the inclusion SYL3050. Furthermore, in the case of the MS having a smaller particle size, a lack of sample recrystallization was noted. To find a molecular mechanism responsible for the observed improvement of physical stability of SVT, we performed a series of calorimetric and dielectric studies. The obtained results showed that neither thermal properties nor molecular dynamics are significantly changing after inclusion to SVT the MS material. Consequently, none of the known stabilization mechanisms can explain the observed inhibition of SVT recrystallization. The particle size effect on the stabilization was likely to be explained by difference in exchange process between entrapped and bulk drug molecules. Moreover, reduction in size of the free space for crystal growth might be partially responsible for the different stabilization effect. These additional factors should be considered as well when mesoporous

materials are used for stabilizing pharmaceutical glasses in addition to the direct interaction between mesoporous materials and drug molecules.

Author Contributions: Conceptualization, J.K.-K. and M.P.; Funding acquisition, M.P.; Investigation, J.K.-K., D.K., K.C., J.R. and K.K.; Methodology, J.K.-K. and M.P.; Supervision, K.K. and M.P.; Validation, J.K.-K., K.C., J.R. and K.K.; Visualization, J.K.-K.; Writing—original draft, J.K.-K.; Writing—review and editing, K.K. and M.P. All authors have read and agreed to the published version of the manuscript.

Funding: This research was funded by the National Science Centre (Poland), Project No. 2015/16/W/NZ7/00404 (SYMFONIA 3).

Acknowledgments: The authors wish to express their thanks for the materials received as a gift from Grace GmbH & CO. KG (Worms, Germany).

Conflicts of Interest: The authors declare no conflict of interest.

References

1. Baird, J.A.; Taylor, L.S. Evaluation of amorphous solid dispersion properties using thermal analysis techniques. *Adv. Drug Deliv. Rev.* **2012**, *64*, 396–421. [CrossRef]
2. Liu, X.; Fahr, A. Drug delivery strategies for poorly water-soluble drugs. *Expert Opin. Drug Deliv.* **2007**, *4*, 403–416.
3. Williams, H.; Trevaskis, N.; Charman, S.; Shanker, R.; Charman, W.; Pouton, C.; Porter, C. Strategies to address low drug solubility in discovery and development. *Pharmacol. Rev.* **2013**, *65*, 315–499. [CrossRef] [PubMed]
4. Takagi, T.; Ramachandran, C.; Bermejo, M.; Yamashita, S.; Yu, L.X.; Amidon, G.L. A provisional biopharmaceutical classification of the top 200 oral drug products in the United States, Great Britain, Spain, and Japan. *Mol. Pharm.* **2006**, *3*, 631–643. [CrossRef] [PubMed]
5. Kalepu, S.; Nekkanti, V. Insoluble drug delivery strategies: Review of recent advances and business prospects. *Acta Pharm. Sin. B* **2016**, *5*, 442–453. [CrossRef]
6. Ozaki, S.; Kushida, I.; Yamashita, T.; Hasebe, T.; Shirai, O.; Kano, K. Evaluation of drug supersaturation by thermodynamic and kinetic approaches for the prediction of oral absorbability in amorphous pharmaceuticals. *J. Pharm. Sci.* **2012**, *101*, 4220–4230. [CrossRef]
7. Almeida E Sousa, L.; Reutzel-Edens, S.M.; Stephenson, G.A.; Taylor, L.S. Assessment of the amorphous "solubility" of a group of diverse drugs using new experimental and theoretical approaches. *Mol. Pharm.* **2015**, *12*, 484–495. [CrossRef]
8. Bogner, R.H.; Murdande, S.B.; Pikal, M.J.; Shanker, R.M. Solubility advantage of amorphous pharmaceuticals: II. application of quantitative thermodynamic relationships for prediction of solubility enhancement in structurally diverse insoluble pharmaceuticals. *Pharm. Res.* **2010**, *27*, 2704–2714.
9. Paradkar, A.R.; Chauhan, B.; Yamamura, S.; Pawar, A.P. Preparation and characterization of glassy celecoxib. *Drug Dev. Ind. Pharm.* **2003**, *29*, 739–744. [CrossRef]
10. Chmiel, K.; Knapik-Kowalczuk, J.; Jurkiewicz, K.; Sawicki, W.; Jachowicz, R.; Paluch, M. A New Method to Identify Physically Stable Concentration of Amorphous Solid Dispersions (I): Case of Flutamide + Kollidon VA64. *Mol. Pharm.* **2017**, *14*, 3370–3380. [CrossRef]
11. Kawakami, K. Modification of physicochemical characteristics of active pharmaceutical ingredients and application of supersaturatable dosage forms for improving bioavailability of poorly absorbed drugs. *Adv. Drug Deliv. Rev.* **2012**, *64*, 480–495. [CrossRef] [PubMed]
12. Lehmkemper, K.; Kyerematen, S.O.; Heinzerling, O.; Degenhardt, M.; Sadowski, G. Long-Term Physical Stability of PVP- and PVPVA-Amorphous Solid Dispersions. *Mol. Pharm.* **2017**, *14*, 157–171. [CrossRef] [PubMed]
13. Szklarz, G.; Adrjanowicz, K.; Knapik-Kowalczuk, J.; Jurkiewicz, K.; Paluch, M. Crystallization of supercooled fenofibrate studied at ambient and elevated pressures. *Phys. Chem. Chem. Phys.* **2017**, *19*, 9879–9888. [CrossRef] [PubMed]
14. Yoshioka, M.; Hancock, B.C.; Zografi, G. Crystallization of indomethacin from the amorphous state below and above its glass transition temperature. *J. Pharm. Sci.* **1994**, *83*, 1700–1705. [CrossRef]

15. Kawakami, K.; Harada, T.; Miura, K.; Yoshihashi, Y.; Yonemochi, E.; Terada, K.; Moriyama, H. Relationship between crystallization tendencies during cooling from melt and isothermal storage: Toward a general understanding of physical stability of pharmaceutical glasses. *Mol. Pharm.* **2014**, *11*, 1835–1843. [CrossRef]
16. Knapik, J.; Wojnarowska, Z.; Grzybowska, K.; Tajber, L.; Mesallati, H.; Paluch, K.J.; Paluch, M. Molecular Dynamics and Physical Stability of Amorphous Nimesulide Drug and Its Binary Drug-Polymer Systems. *Mol. Pharm.* **2016**, *13*, 1937–1946. [CrossRef]
17. Knapik-Kowalczuk, J.; Tu, W.; Chmiel, K.; Rams-Baron, M.; Paluch, M. Co-Stabilization of Amorphous Pharmaceuticals—The Case of Nifedipine and Nimodipine. *Mol. Pharm.* **2018**, *15*, 2455–2465. [CrossRef]
18. Kawakami, K. Ultraslow Cooling for the Stabilization of Pharmaceutical Glasses. *J. Phys. Chem. B* **2019**, *123*, 4996–5003. [CrossRef]
19. Grzybowska, K.; Chmiel, K.; Knapik-Kowalczuk, J.; Grzybowski, A.; Jurkiewicz, K.; Paluch, M. Molecular factors governing the liquid and glassy states recrystallization of celecoxib in binary mixtures with excipients of different molecular weights. *Mol. Pharm.* **2017**, *14*, 1154–1168. [CrossRef]
20. Knapik, J.; Wojnarowska, Z.; Grzybowska, K.; Jurkiewicz, K.; Tajber, L.; Paluch, M. Molecular dynamics and physical stability of coamorphous ezetimib and indapamide mixtures. *Mol. Pharm.* **2015**, *12*, 3610–3619. [CrossRef]
21. Knapik-Kowalczuk, J.; Wojnarowska, Z.; Rams-Baron, M.; Jurkiewicz, K.; Cielecka-Piontek, J.; Ngai, K.L.; Paluch, M. Atorvastatin as a Promising Crystallization Inhibitor of Amorphous Probucol: Dielectric Studies at Ambient and Elevated Pressure. *Mol. Pharm.* **2017**, *14*, 2670–2680. [CrossRef] [PubMed]
22. Grzybowska, K.; Paluch, M.; Grzybowski, A.; Wojnarowska, Z.; Hawelek, L.; Kolodziejczyk, K.; Ngai, K.L. Molecular dynamics and physical stability of amorphous anti-inflammatory drug: Celecoxib. *J. Phys. Chem. B* **2010**, *114*, 12792–12801. [CrossRef] [PubMed]
23. Priemel, P.A.; Laitinen, R.; Barthold, S.; Grohganz, H.; Lehto, V.P.; Rades, T.; Strachan, C.J. Inhibition of surface crystallisation of amorphous indomethacin particles in physical drug-polymer mixtures. *Int. J. Pharm.* **2013**, *456*, 301–306. [CrossRef] [PubMed]
24. Lehmkemper, K.; Kyerematen, S.O.; Degenhardt, M.; Sadowski, G. Influence of Low-Molecular-Weight Excipients on the Phase Behavior of PVPVA64 Amorphous Solid Dispersions. *Pharm. Res.* **2018**, *35*, 25. [CrossRef] [PubMed]
25. Shi, Q.; Moinuddin, S.M.; Cai, T. Advances in coamorphous drug delivery systems. *Acta Pharm. Sin. B* **2019**, *9*, 19–35. [CrossRef]
26. Azaı, T.; Tourné-Péteilh, C.; Aussenac, F.; Baccile, N.; Coelho, C.; Devoisselle, J.-M.; Babonneau, F. Solid-State NMR Study of Ibuprofen Confined in MCM-41 Material. *Chem. Mater.* **2006**, *18*, 6382–6390. [CrossRef]
27. Bahl, D.; Bogner, R.H. Amorphization of indomethacin by co-grinding with Neusilin US2: Amorphization kinetics, physical stability and mechanism. *Pharm. Res.* **2006**, *23*, 2317–2325. [CrossRef]
28. Andersson, J.; Rosenholm, J.; Areva, S.; Lindén, M. Influences of material characteristics on ibuprofen drug loading and release profiles from ordered micro- and mesoporous silica matrices. *Chem. Mater.* **2004**, *16*, 4160–4167. [CrossRef]
29. Bremmell, K.E.; Prestidge, C.A. Enhancing oral bioavailability of poorly soluble drugs with mesoporous silica based systems: Opportunities and challenges. *Drug Dev. Ind. Pharm.* **2019**, *45*, 349–358. [CrossRef]
30. Bukara, K.; Schueller, L.; Rosier, J.; Martens, M.A.; Daems, T.; Verheyden, L.; Eelen, S.; Van Speybroeck, M.; Libanati, C.; Martens, J.A.; et al. Ordered mesoporous silica to enhance the bioavailability of poorly water-soluble drugs: Proof of concept in man. *Eur. J. Pharm. Biopharm.* **2016**, *108*, 220–225. [CrossRef]
31. Cassano, D.; Mapanao, A.K.; Summa, M.; Vlamidis, Y.; Giannone, G.; Santi, M.; Guzzolino, E.; Pitto, L.; Poliseno, L.; Bertorelli, R.; et al. Biosafety and Biokinetics of Noble Metals: The Impact of Their Chemical Nature. *ACS Appl. Bio Mater.* **2019**, *2*, 4464–4470. [CrossRef]
32. Croissant, J.G.; Fatieiev, Y.; Khashab, N.M. Degradability and Clearance of Silicon, Organosilica, Silsesquioxane, Silica Mixed Oxide, and Mesoporous Silica Nanoparticles. *Adv. Mater.* **2017**, *29*, 1604634. [CrossRef] [PubMed]
33. Genina, N.; Hadi, B.; Löbmann, K. Hot Melt Extrusion as Solvent-Free Technique for a Continuous Manufacturing of Drug-Loaded Mesoporous Silica. *J. Pharm. Sci.* **2018**, *107*, 149–155. [CrossRef] [PubMed]
34. Rengarajan, G.T.; Enke, D.; Steinhart, M.; Beiner, M. Stabilization of the amorphous state of pharmaceuticals in nanopores. *J. Mater. Chem.* **2008**, *18*, 2537–2539. [CrossRef]

35. Knapik, J.; Wojnarowska, Z.; Grzybowska, K.; Jurkiewicz, K.; Stankiewicz, A.; Paluch, M. Stabilization of the Amorphous Ezetimibe Drug by Confining Its Dimension. *Mol. Pharm.* **2016**, *13*, 1308–1316. [CrossRef] [PubMed]
36. Laitinen, R.; Löbmann, K.; Strachan, C.J.; Grohganz, H.; Rades, T. Emerging trends in the stabilization of amorphous drugs. *Int. J. Pharm.* **2013**, *453*, 65–79. [CrossRef] [PubMed]
37. Riikonen, J.; Xu, W.; Lehto, V.P. Mesoporous systems for poorly soluble drugs—Recent trends. *Int. J. Pharm.* **2018**, *536*, 178–186. [CrossRef]
38. Bavnhøj, C.G.; Knopp, M.M.; Madsen, C.M.; Löbmann, K. The role interplay between mesoporous silica pore volume and surface area and their effect on drug loading capacity. *Int. J. Pharm. X* **2019**, *1*, 100008. [CrossRef]
39. Hempel, N.J.; Brede, K.; Olesen, N.E.; Genina, N.; Knopp, M.M.; Löbmann, K. A fast and reliable DSC-based method to determine the monomolecular loading capacity of drugs with good glass-forming ability in mesoporous silica. *Int. J. Pharm.* **2018**, *544*, 153–157. [CrossRef]
40. Mellaerts, R.; Aerts, C.A.; Van Humbeeck, J.; Augustijns, P.; Van Den Mooter, G.; Martens, J.A. Enhanced release of itraconazole from ordered mesoporous SBA-15 silica materials. *Chem. Commun.* **2007**, 1375–1377. [CrossRef]
41. Antonino, R.S.C.M.Q.; Ruggiero, M.; Song, Z.; Nascimento, T.L.; Lima, E.M.; Bohr, A.; Knopp, M.M.; Löbmann, K. Impact of drug loading in mesoporous silica-amorphous formulations on the physical stability of drugs with high recrystallization tendency. *Int. J. Pharm. X* **2019**, *1*, 100026. [CrossRef] [PubMed]
42. Kumar, D.; Sailaja Chirravuri, S.V.; Shastri, N.R. Impact of surface area of silica particles on dissolution rate and oral bioavailability of poorly water soluble drugs: A case study with aceclofenac. *Int. J. Pharm.* **2014**, *461*, 459–468. [CrossRef]
43. Yani, Y.; Chow, P.S.; Tan, R.B.H. Pore size effect on the stabilization of amorphous drug in a mesoporous material: Insights from molecular simulation. *Microporous Mesoporous Mater.* **2016**, *221*, 117–122. [CrossRef]
44. Rao, M.; Mandage, Y.; Thanki, K.; Bhise, S. Dissolution improvement of simvastatin by surface solid dispersion technology. *Dissolution Technol.* **2010**, *17*, 27–34. [CrossRef]
45. Vraníková, B.; Niederquell, A.; Ditzinger, F.; Šklubalová, Z.; Kuentz, M. Mechanistic aspects of drug loading in liquisolid systems with hydrophilic lipid-based mixtures. *Int. J. Pharm.* **2020**, *578*, 119099. [CrossRef]
46. Rao, S.; Tan, A.; Boyd, B.J.; Prestidge, C.A. Synergistic role of self-emulsifying lipids and nanostructured porous silica particles in optimizing the oral delivery of lovastatin. *Nanomedicine* **2014**, *9*, 2745–2759. [CrossRef]
47. Kremer, F.; Schonhals, A. *Broadband Dielectric Spectroscopy*; Springer: Berlin/Heidelberg, Germany, 2003; ISBN 978-3-642-62809-2.
48. Grzybowska, K.; Capaccioli, S.; Paluch, M. Recent developments in the experimental investigations of relaxations in pharmaceuticals by dielectric techniques at ambient and elevated pressure. *Adv. Drug Deliv. Rev.* **2016**, *100*, 158–182. [CrossRef]
49. Descamps, M. *Disordered Pharmaceutical Materials*; Wiley-VCH Verlag GmbH & Co. KGaA: Weinheim, Germany, 2016; ISBN 9783527652693.
50. Rams-Baron, M.; Jachowicz, R.; Boldyreva, E.; Zhou, D.; Jamroz, W.; Paluch, M. *Amorphous Drugs*; Springer International Publishing: Cham, Switzerland, 2018; ISBN 9783319720012.
51. Watson, E.S.; O'Neill, M.J.; Justin, J.; Brenner, N. A Differential Scanning Calorimeter for Quantitative Differential Thermal Analysis. *Anal. Chem.* **1964**, *36*, 1233–1238. [CrossRef]
52. Höhne, G.W.H.; Hemminger, W.F.; Flammersheim, H.-J. *Differential Scanning Calorimetry*; Springer: Berlin/Heidelberg, Germany, 2003; ISBN 9783642055935.
53. Kolodziejczyk, K.; Grzybowska, K.; Wojnarowska, Z.; Dulski, M.; Hawelek, L.; Paluch, M. Isothermal cold crystallization kinetics study of sildenafil. *Cryst. Growth Des.* **2014**, *14*, 3199–3209. [CrossRef]
54. Avramov, I.; Avramova, K.; Rüssel, C. New method to analyze data on overall crystallization kinetics. *J. Cryst. Growth* **2005**, *285*, 394–399. [CrossRef]
55. Rams-Baron, M.; Jachowicz, R.; Boldyreva, E.; Zhou, D.; Jamroz, W.; Paluch, M. *Amorphous Drugs: Benefits and Challenges*; Springer International Publishing: Cham, Switzerland, 2018; ISBN 9783319720029.
56. Dantuluri, A.K.R.; Amin, A.; Puri, V.; Bansal, A.K. Role of r-Relaxation on Crystallization of Amorphous Celecoxib above T g Probed by Dielectric Spectroscopy. *Mol. Pharm.* **2011**, *8*, 814–822. [CrossRef] [PubMed]

57. Tu, W.; Knapik-Kowalczuk, J.; Chmiel, K.; Paluch, M. Glass Transition Dynamics and Physical Stability of Amorphous Griseofulvin in Binary Mixtures with Low-T g Excipients. *Mol. Pharm.* **2019**, *16*, 3626–3635. [CrossRef] [PubMed]
58. Hargis, M.J.; Grady, B.P. Effect of sample size on isothermal crystallization measurements performed in a differential scanning calorimeter: A method to determine avrami parameters without sample thickness effects. *Thermochim. Acta* **2006**, *443*, 147–158. [CrossRef]
59. Kawakami, K. Surface effects on the crystallization of ritonavir glass. *J. Pharm. Sci.* **2015**, *104*, 276–279. [CrossRef]
60. Wu, T.; Sun, Y.; Li, N.; De Villiers, M.M.; Yu, L. Inhibiting surface crystallization of amorphous indomethacin by nanocoating. *Langmuir* **2007**, *23*, 5148–5153. [CrossRef]
61. Kawakami, K.; Harada, T.; Yoshihashi, Y.; Yonemochi, E.; Terada, K.; Moriyama, H. Correlation between Glass-Forming Ability and Fragility of Pharmaceutical Compounds. *J. Phys. Chem. B* **2015**, *119*, 4873–4880. [CrossRef]
62. Havriliak, S.; Negami, S. A complex plane representation of dielectric and mechanical relaxation processes in some polymers. *Polymer* **1967**, *8*, 161–210. [CrossRef]
63. Vogel, H. Das Temperaturabhangigkeitgesetz der Viskosität von Flüssigkeiten. *J. Phys. Z.* **1921**, *22*, 645–646.
64. Fulcher, G.S. Analysis of Recent Measurements of the Viscosity of Glasses. *J. Am. Ceram. Soc.* **1925**, *8*, 339–355. [CrossRef]
65. Tammann, G.; Hesse, W. Die Abhängigkeit der Viscosität von der Temperatur bie unterkühlten Flüssigkeiten. *Z. Anorg. Allg. Chem.* **1926**, *156*, 245–257. [CrossRef]
66. Böhmer, R.; Ngai, K.L.; Angell, C.A.; Plazek, D.J. Nonexponential relaxations in strong and fragile glass formers. *J. Chem. Phys.* **1993**, *99*, 4201–4209. [CrossRef]
67. Kawakami, K. Pharmaceutical Applications of Thermal Analysis. In *Handbook of Thermal Analysis and Calorimetry*; Elsevier: Amsterdam, The Netherlands, 2018; Volume 6, pp. 613–641, ISBN 9780444640628.
68. Knapik, J.; Wojnarowska, Z.; Grzybowska, K.; Hawelek, L.; Sawicki, W.; Wlodarski, K.; Markowski, J.; Paluch, M. Physical stability of the amorphous anticholesterol agent (Ezetimibe): The role of molecular mobility. *Mol. Pharm.* **2014**, *11*, 4280–4290. [CrossRef] [PubMed]
69. Tanaka, H. Relationship among glass-forming ability, fragility, and short-range bond ordering of liquids. *J. Non. Cryst. Solids* **2005**, *351*, 678–690. [CrossRef]
70. Williams, G.; Watts, D.C. Non-symmetrical dielectric relaxation behaviour arising from a simple empirical decay function. *Trans. Faraday Soc.* **1970**, *66*, 80. [CrossRef]
71. Shamblin, S.L.; Tang, X.; Chang, L.; Hancock, B.; Pikal, M.J. Characterization of the Time Scales of Molecular Motion in Pharmaceutically Important Glasses. *J. Phys. Chem. B* **1999**, *103*, 4113–4121. [CrossRef]
72. Paluch, M.; Knapik, J.; Wojnarowska, Z.; Grzybowski, A.; Ngai, K.L. Universal Behavior of Dielectric Responses of Glass Formers: Role of Dipole-Dipole Interactions. *Phys. Rev. Lett.* **2016**, *116*, 025702. [CrossRef]
73. Knapik-Kowalczuk, J.; Wojnarowska, Z.; Chmiel, K.; Rams-Baron, M.; Tajber, L.; Paluch, M. Can storage time improve the physical stability of amorphous pharmaceuticals with tautomerization ability exposed to compression? The case of chloramphenicol drug. *Mol. Pharm.* **2018**, *15*, 1928–1940. [CrossRef]
74. Knapik-Kowalczuk, J.; Gündüz, M.G.; Chmiel, K.; Jurkiewicz, K.; Kurek, M.; Tajber, L.; Jachowicz, R.; Paluch, M. Molecular dynamics, viscoelastic properties and physical stability studies of a new amorphous dihydropyridine derivative with T-type calcium channel blocking activity. *Eur. J. Pharm. Sci.* **2020**, *141*, 105083. [CrossRef]
75. Adrjanowicz, K.; Zakowiecki, D.; Kaminski, K.; Hawelek, L.; Grzybowska, K.; Tarnacka, M.; Paluch, M.; Cal, K. Molecular dynamics in supercooled liquid and glassy states of antibiotics: Azithromycin, clarithromycin and roxithromycin studied by dielectric spectroscopy. Advantages given by the amorphous state. *Mol. Pharm.* **2012**, *9*, 1748–1763. [CrossRef]
76. Vogel, M.; Tschirwitz, C.; Schneider, G.; Koplin, C.; Medick, P.; Rössler, E. A2H NMR and dielelectric spectroscopy study of the slow β-process in organic glass formers. *J. Non. Cryst. Solids* **2002**, *307–310*, 326–335. [CrossRef]
77. Grzybowska, K.; Paluch, M.; Wlodarczyk, P.; Grzybowski, A.; Kaminski, K.; Hawelek, L.; Zakowiecki, D.; Kasprzycka, A.; Jankowska-Sumara, I. Enhancement of amorphous celecoxib stability by mixing it with octaacetylmaltose: The molecular dynamics study. *Mol. Pharm.* **2012**, *9*, 894–904. [CrossRef] [PubMed]

78. Kolodziejczyk, K.; Paluch, M.; Grzybowska, K.; Grzybowski, A.; Wojnarowska, Z.; Hawelek, L.; Ziolo, J.D. Relaxation dynamics and crystallization study of sildenafil in the liquid and glassy states. *Mol. Pharm.* **2013**, *10*, 2270–2282. [CrossRef] [PubMed]
79. Descamps, M.; Willart, J.-F. Scaling laws and size effects for amorphous crystallization kinetics: Constraints imposed by nucleation and growth specificities. *Int. J. Pharm.* **2018**, *542*, 186–195. [CrossRef] [PubMed]
80. Delcourt, O.; Descamps, M.; Hilhorst, H.J. Size effect in a nucleation and growth transformation. *Ferroelectrics* **1991**, *124*, 109–114. [CrossRef]

Dr hab. inż. Justyna Knapik-Kowalczuk, Prof. UŚ
Instytut Fizyki
Wydział Nauk Ścisłych i Technicznych
Uniwersytet Śląski
ul. 75 Pułku Piechoty 1A, 41-500 Chorzów

Chorzów, 25.09.2024r.

OŚWIADCZENIE

Oświadczam, że w pracy:

J. Knapik-Kowalczuk, D. Kramarczyk, K. Chmiel, J. Romanova, K. Kawakami, M. Paluch, *Importance of Mesoporous Silica Particle Size in the Stabilization of Amorphous Pharmaceuticals— The Case of Simvastatin*. Pharmaceutics, 2020, 12, 384

mój udział polegał na nadzorowaniu pomiarów, kontroli przeprowadzonej analizy wyników, dyskusji wyników oraz korekcji manuskryptu.

……

Podpis

Dr Krzysztof Chmiel
Instytut Fizyki
Wydział Nauk Ścisłych i Technicznych
Uniwersytet Śląski
ul. 75 Pułku Piechoty 1A, 41-500 Chorzów

Chorzów, 25.09.2024r.

OŚWIADCZENIE

Oświadczam, że w pracy:

J. Knapik-Kowalczuk, D. Kramarczyk, K. Chmiel, J. Romanova, K. Kawakami, M. Paluch, *Importance of Mesoporous Silica Particle Size in the Stabilization of Amorphous Pharmaceuticals— The Case of Simvastatin*. Pharmaceutics, 2020, 12, 384

mój udział polegał na uczestnictwie w dyskusji wyników.

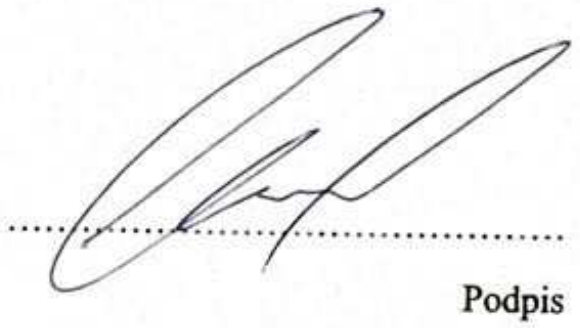

.....

Podpis

Dr. Jana Romanova
Department of Physical Chemistry,
Faculty of Chemical Technology,
University of Pardubice
Studenska 573, 532 10 Pardubice, Czech Republic

Pardubice, 25.09.2024r.

DECLARATION

I declare that in the work:

J. Knapik-Kowalczuk, D. Kramarczyk, K. Chmiel, J. Romanova, K. Kawakami, M. Paluch, *Importance of Mesoporous Silica Particle Size in the Stabilization of Amorphous Pharmaceuticals— The Case of Simvastatin*. Pharmaceutics, 2020, 12, 384

my participation consisted in partial performance of calorimetric studies.

Romanová

.....

Signature

Prof. Kohsaku Kawakami
Research Center for Macromolecules and Biomaterials,
National Institute for Materials Science,
1-1 Namiki, Tsukuba, Ibaraki 305-0044, Japan

Tsukuba, 26.09.2024r.

DECLARATION

I declare that in the work:

J. Knapik-Kowalczuk, D. Kramarczyk, K. Chmiel, J. Romanova, K. Kawakami, M. Paluch, *Importance of Mesoporous Silica Particle Size in the Stabilization of Amorphous Pharmaceuticals— The Case of Simvastatin*. Pharmaceutics, 2020, 12, 384

my contribution included supervising some of the calorimetric measurements, participating in the discussion of the obtained results and improving the manuscript.

.....

Signature

Prof. zw. dr hab. Marian Paluch
Instytut Fizyki
Wydział Nauk Ścisłych i Technicznych
Uniwersytet Śląski
ul. 75 Pułku Piechoty 1A, 41-500 Chorzów

Chorzów, 25.09.2024r.

OŚWIADCZENIE

Oświadczam, że w pracy:

J. Knapik-Kowalczuk, D. Kramarczyk, K. Chmiel, J. Romanova, K. Kawakami, M. Paluch, *Importance of Mesoporous Silica Particle Size in the Stabilization of Amorphous Pharmaceuticals— The Case of Simvastatin*. Pharmaceutics, 2020, 12, 384.

mój udział polegał na uczestnictwie w dyskusji na temat otrzymanych wyników.

.....

Podpis

3.2. A2 - D. Kramarczyk, J. Knapik-Kowalczuk, W. Smolka, M. Ferreira Monteiro, L. Tajber, M. Paluch, *Inhibition of celecoxib crystallization by mesoporous silica – Molecular dynamics studies leading to the discovery of the stabilization origin*. **2022** European Journal of Pharmaceutical Sciences 171, 106132.

Impact Factor czasopisma z roku opublikowania pracy: 4.3.
Liczba punktów ministerialnych MNiSW czasopisma z roku opublikowania pracy: 100 pkt.
DOI: 10.1016/j.ejps.2022.106132.

Udział pierwszego autora w poniżej załączonym artykule polegał na wykonaniu pomiarów kalorymetrycznych oraz dielektrycznych, analizie wszystkich otrzymanych wyników oraz przygotowaniu pierwotnej wersji manuskryptu. Wkład pozostałych współautorów, w formie oświadczeń, zamieszczono na końcu artykułu.

European Journal of Pharmaceutical Sciences 171 (2022) 106132

Contents lists available at ScienceDirect

European Journal of Pharmaceutical Sciences

journal homepage: www.elsevier.com/locate/ejps

Inhibition of celecoxib crystallization by mesoporous silica – Molecular dynamics studies leading to the discovery of the stabilization origin

Daniel Kramarczyk [a,*], Justyna Knapik-Kowalczuk [a,*], Wojciech Smolka [b], Maria Ferreira Monteiro [c], Lidia Tajber [c], Marian Paluch [a]

[a] Faculty of Science and Technology, Institute of Physics, University of Silesia in Katowice, SMCEBI, 75 Pułku Piechoty 1a, Chorzów 41-500, Poland
[b] Department of Laryngology, Medical University of Silesia, ul. Francuska 20-24, Katowice 40-027, Poland
[c] School of Pharmacy and Pharmaceutical Sciences, Trinity College Dublin, College Green, Dublin 2, Ireland

ARTICLE INFO

Keywords:
Celecoxib
Amorphous drug
Physical stability
Syloid 244FP
Molecular origin

ABSTRACT

In this article, the effect of mesoporous silica (MS) on the physical stability and molecular dynamics of the amorphous form of Celecoxib (CEL) is investigated. It has been proven that the recrystallization process of CEL slows down with increasing the MS content. Beside the elongation of stabilization time with the increase silica content leads to an increase in the amorphous drug fraction remaining after the finished crystallization. The conducted analyses show that the observed inhibition of CEL's recrystallization is associated with the formation of a monomolecular drug layer on the silica's surface. The performed non-isothermal dielectric studies of CEL + MS systems having both fully and partially amorphous CEL shows that the biggest impact of the drug's the temperature dependences of structural relaxation time $\tau_\alpha(T)$ has a crystalline fraction of the API. Silica, even in high concentration, does not modify the temperature dependence of structural relaxation of CEL.

1. Introduction

Most of the pharmaceutical products in the solid form contain a crystalline Active Pharmaceutical Ingredient (API). The principal advantage of this form is its high physical stability. However, as much as 40% of crystalline APIs are poorly soluble in water due to the presence of the crystal lattice (Fahr and Liu, 2007; Williams et al., 2013; Babu and Nangia, 2011). Moreover, it is estimated that up to 90% of drug candidates in the crystalline form may be rejected during the research and development process just for this reason (Babu and Nangia, 2011; Kalepu and Nekkanti, 2015). Taking into account that the solubility of an API is the limiting factor for its bioavailability, considerable effort is currently made to improve it (Vasconcelos et al., 2007; Cid et al., 2019).

There are number of methods developed to enhance the water solubility of poorly soluble APIs. One of them is conversion of the crystalline form of drug to its amorphous counterpart (Baird and Taylor, 2012; Hancock and Parks, 2000; Bogner et al., 2010). As opposed to the crystal, in the amorphous state, there is no long-range ordering and consequently, an amorphous material has a larger internal energy. Due to this, weakening and/or breaking the intermolecular interactions is possible after delivering a lower energy compared to the crystal, where the energy levels are much higher. It means that substance in the amorphous form dissolves quicker and to a greater degree in water, often leading to better absorption of the substance in the human body (Hancock and Zografi, 1997; Kawakami, 2012; Hu et al., 2010). However, amorphous substances are thermodynamically unstable (Kothari et al., 2014; Szklarz et al., 2017; Karmwar et al., 2011). As a consequence, they may recrystallize during storage and secondary manufacturing. The return to the crystalline form results in the loss of the beneficial properties originating from the amorphous disorder. Therefore, it is necessary to find a method to effectively improve physical stability of amorphous APIs (Knapik et al., 2015; Kawakami, 2019; Baghel et al., 2016; Knapik-Kowalczuk et al., 2018; Khanfar and Al-Nimry, 2017).

Several strategies have been tested to establish the most efficient way of improving the physical stability of amorphous pharmaceuticals (Laitinen et al., 2013; Singh et al., 2011; Shaker et al., 2020). It appears that the use of mesoporous silica (MS) materials gives promising results (Riikonen et al., 2018; Bahl and Bogner, 2006; Müller Reiner et al., 2018). MS has been shown to improve the physical stability of ibuprofen (Shen et al., 2009; Andersson et al., 2004), simvastatin (Knapik-Kowalczuk et al., 2020), ezetimibe (Knapik et al., 2016) and nifedipine

* Corresponding authors.
E-mail addresses: daniel.kramarczyk@smcebi.edu.pl (D. Kramarczyk), justyna.knapik-kowalczuk@us.edu.pl (J. Knapik-Kowalczuk).

https://doi.org/10.1016/j.ejps.2022.106132
Received 26 October 2021; Received in revised form 15 January 2022; Accepted 18 January 2022
Available online 22 January 2022

(Godec et al., 2007). In addition to being highly effective in stabilizing amorphous forms of APIs, MS reduces the drug toxicity, have adequate biosafety (lack of cytotoxicity) and might be biodegradable (Croissant et al., 2017, 2018). All these features make these materials more and more attractive from the application point of view. Two possible mechanisms are commonly discussed to explain how MS can stabilize amorphous systems. If molecules of API are loaded into pores of MS, then the impeded crystallization might be related to the pore size effect. It means that if the pore diameter is smaller than the nucleus radius, it will result in a lack of recrystallization. The second mechanism is related to the specific interactions of drug molecules with the surface of MS (Rengarajan et al., 2008; Genina et al., 2018). However, we have shown recently that none of these mechanisms can be responsible for the stabilization of simvastatin with MS (Knapik-Kowalczuk et al., 2020). As discussed in our previous work, the stabilization effect was mainly related to inhibition of the propagation of crystallization by using silica with appropriately small particle sizes. Since it has been demonstrated that a commercial grade of MS, Syloid 244FP (SYL244FP), with an average particle size of 2.5–3.7 μm and pore diameter of 23 nm gave the best stabilization result, in this work we carried out similar studies for another API, celecoxib (CEL). CEL was chosen due to its strong tendency toward recrystallization. In this context, the work of (Grzybowska et al., 2010; Dantuluri et al., 2011) are highlighted. The first paper describes in detail the dielectric response of amorphous CEL at both, supercooled liquid and glassy states. During the non-isothermal dielectric measurements performed in that work, cold crystallization with the onset at 365 K was observed. In the second paper the authors were mainly focused on investigating the isothermal crystallization of CEL from the supercooled liquid state. It has been shown that amorphous CEL at temperatures equal or higher than $T = 363$ K fully crystallized in less than 4 h. The cited works confirm that amorphous CEL is highly thermodynamically unstable, therefore, it becomes an excellent candidate for our tests.

The aim of this study is as follows. Firstly, we wanted to investigate the effect of SYL244FP on the molecular dynamics of amorphous CEL. For that purpose, systems containing CEL and 9, 18, 27, 36 and 45 wt.% of SYL244FP were subjected to non-isothermal measurements using broadband dielectric spectroscopy (BDS). Secondly, we were interested in the impact of MS in the form of SYL244FP on the physical stability of amorphous CEL. To check the effect of the silica on recrystallization of CEL, neat API and its mixtures with SYL244FP were investigated applying isothermal (at $T = 363$ K) conditions using BDS. Finally, we wanted to discover which mechanism might be responsible for the observed CEL stabilization and to check whether CEL behaves similarly to simvastatin, for which a small amount of SYL244FP was sufficient to stabilize the drug effectively.

2. Materials and methods

2.1. Materials and preparation of mixtures

The crystalline form of celecoxib (CEL) with purity 98% and molecular mass $M_w = 381$ g/mol was purchased from Polpharma (Starogard Gdański, Poland). This pharmaceutical is chemically described as 4-[5-(4-methylphenyl)-3-(trifluoromethyl) pyrazol-1-yl] benzene-sulfonamide and belongs to a class of agents that selectively inhibit cyclooxygenase-2 (COX-2) enzymes. Its chemical structure is presented in the inset of Fig. 1. Syloid 244 FP (SYL244FP) was received as a gift from Grace GmbH & CO. KG (Worms, Germany). This MS is characterized by average particle size of 2.5–3.7 μm, surface area of 314 m^2/g, pore diameter ~23 nm and the pore volume equal to 1.6 mL/g. All chemicals were used as received.

To prepare the binary mixtures containing crystalline CEL and 9, 18, 27, 36 and 45 wt.% of SYL244, the weighted amounts of ingredients were mixed in a mortar for about 10 min. Every 3 min the sample was scraped off the mortar wall with a spatula. The prepared physical mixtures and neat SYL244FP were dried at 373 K for 10 min before

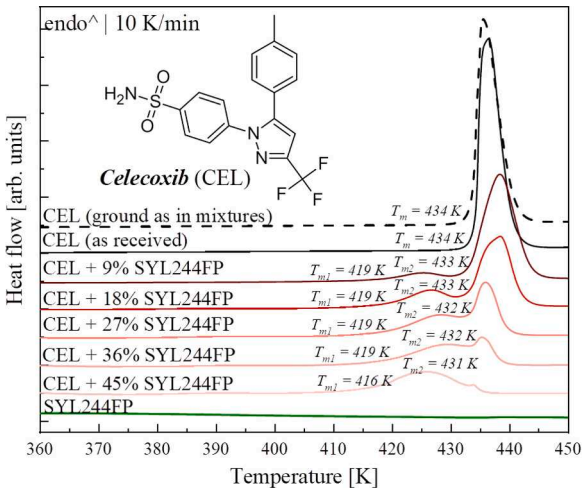

Fig. 1. DSC thermograms of neat crystalline CEL, SYL244FP, and its physical mixtures with SYL244FP.

experiments to remove water from MS, melted at $T = 434$ K and quenched directly before each experiment to obtain amorphous CEL in these mixtures. In the DSC experiments, the sample was vitrified *in situ* in the apparatus under dry nitrogen conditions, while for dielectric measurements, the melting procedure took place on the hot plate in air conditions with environmental humidity of approximately 25% RH.

2.2. Differential scanning calorimetry (DSC)

Thermal properties of neat CEL and its mixtures with SYL244FP were investigated using a Mettler−Toledo DSC 1 STAR^e System. The DSC was calibrated for temperature and enthalpy using zinc and indium standards. The instrument was equipped with an HSS8 ceramic sensor having 120 thermocouples and a liquid nitrogen cooling station. The samples were measured in aluminum crucibles (40 μL). All measurements were carried out with a heating rate of 10 K/min.

2.3. Broadband dielectric spectroscopy (BDS)

All dielectric measurements on neat CEL and its mixtures containing 9, 18, 27, 36 and 45 wt.% of SYL244FP were performed using Novo-Control GMBH Alpha dielectric spectrometer (Montabaur, Germany). The temperature in this apparatus was controlled by a Quattro temperature controller with temperature stability better than 0.1 K. Dielectric studies of fully amorphous samples were performed immediately after their vitrification by fast cooling of the melt in a parallel-plate cell made of stainless steel (diameter 15 mm and a 0.1 mm gap provided by silica spacer fibers). Dielectric experiments of partially amorphous CEL in systems with SYL244FP were performed ca. 12 h after the cessation of crystallization. During non-isothermal studies of CEL + 9, 18, 27, 36, and 45 wt.% of SYL244FP, the dielectric spectra were registered in the temperature ranging from 173 to 383 K with a step of 2 K in a broad frequency range from 10^{-1} Hz to 10^6 Hz. During the non-isothermal high frequency study of neat CEL the dielectric loss spectra were measured at temperatures from 443 to 313 K with a step of 2 K for frequencies from 10^6 Hz to 10^9 Hz. The isothermal time-dependent experiments for neat CEL and its mixtures with SYL244FP were performed at $T = 363$ K. The spectra were registered every 300 s for a period of time after which lack of changes in dielectric spectrum were observed. During the non-isothermal studies of CEL + 9, 18, and 27 wt.% of SYL244FP with partially crystalline CEL, the dielectric spectra were registered at temperatures ranging from 333 to 433 K with a step of 10 K in a broad frequency range from 10^{-1} Hz to 10^6 Hz.

3. Results and discussion

3.1. Thermal characterization of systems containing crystalline or amorphous CEL and SYL244FP

Thermal properties of neat CEL, SYL244FP, and its mixtures with 9, 18, 27, 36 and 45 wt.% of SYL244FP were investigated using DSC. Firstly, dry samples containing crystalline CEL were heated from 298 to 460 K. The heating procedure was carried out with a heating rate of 10 K/min. The obtained thermograms are presented in Fig. 1. It can be seen that the DSC trace of neat crystalline CEL is characterized by one endothermal event corresponding to the drug melting. The melting temperature (T_m), which was determined as the onset of the endothermal process, is 434 K. This value agrees well with the literature. Interestingly, CEL in the presence of SYL244FP melts in two stages, i.e., on DSC thermograms two thermal events were recorded. The first peak has an onset at lower temperatures than the pure API (T_{m1}), while the second corresponds broadly to the melting temperature of neat CEL (T_{m2}), however some shift towards lower temperature is observed with an increasing amount of MS, consistent with the presence of MS as an impurity (Knopp et al., 2015). Also, the enthalpy of the second endothermic process decreases with an increasing amount of MS. At the same time an increase in enthalpy for the first process is observed. However, the appearance of the first endothermic process is unclear. It could be related to partially filling the pores of MS by the API or interactions of the drug molecules with the surface of MS (Beiner et al., 2007; Jackson and McKenna, 1996). However, the first scenario is unlikely due to the method of preparing the mixture, which was mechanical grinding CEL with Syloid244FP in a mortar. Therefore, in this case, the observed peak could be of another polymorphic form of CEL, i.e. form IV with a melt onset at 418–421 K (Lu et al., 2006) or it may be associated with interactions of the drug molecules with the surface of MS. Infrared spectroscopy (Fig. 2) discounted the hypothesis of another polymorphic form, as all samples, included the one comprising 45 wt.% of SYL244FP and heated to 423 K, show the N—H stretching bands at the same positions, at 3335 and 3231 cm^{-1}. Lu et al. (2006) presented that CEL form IV had a different shape and position of those bands, at 3342, 3295 and 3213 cm^{-1}. Spectroscopic studies also showed that no strong interactions between the MS and CEL are present in the mixtures with no changes to the bands of the sulfonamide functional group shown as the above N—H or S=O (at 1347 and 1159 cm^{-1}) stretching vibrations. The sulfonamide would be the group most likely to be involved in interactions with the Si-O-Si moieties (visible as a broad peak at 1200–1000 cm^{-1}). Therefore, the endothermic peak at app. 419 K in thermal analysis is most likely to be an artifact created by sample preparation, a comminution process, where the two components were ground together for 5 min, creating a variation in microstructure, similar to what was observed previously for itraconazole (Kozyra et al., 2018). In addition, it appears that this intimate mixing may have generated opportunities for weaker interactions between CEL and SYL244FP, which were not discernible by infrared spectroscopy, to occur.

In the next step of calorimetric studies, the samples were quenched *in situ* in DSC to 273 K. The employed cooling rate was 20 K/min. No CEL crystallization was noted during this cooling stage. After the quenching, the samples were heated again, at 10 K/min, as used previously. The second heating thermograms presented of amorphous form of CEL (Fig. 3). In the studied temperature range, only the step-like behavior, a manifestation of glass transition, was recorded on DSC thermograms. The glass transition temperature (T_g) was determined as a midpoint of the heat capacity increment and the values are shown in Fig. 3. The presence of a single glass transition event confirms that CEL molecules do not fill the pores of SYL244FP. When the drug is incorporated inside the pores of silica, one should expect two T_gs. It is worth pointing out that the addition of SYL244FP did not change the value of CEL's glass transition temperature. This result is similar to our previous finding, where a lack of T_g modification in mixtures with SYL244FP was observed for simvastatin. With the increasing silica content one can however note a decrease in ΔC_p. Because the ΔC_p is an extensive and additive property, its value is proportional to the amorphous fraction of the system and will decrease linearly with decreasing drug content (Saunders et al., 2004). When molecules of amorphous API's fraction are absorbed to the MS surface does not contribute to any thermal event since they are "immobilized" by interactions with the functional groups of the surface of MS. Consequently, if CEL molecules do not interact with the surface of MS, the value of ΔC_p of the mixture should proportionally decrease with the silica to zeros. If some interactions between CEL molecules and MS exist, a decrease in ΔC_p values should be larger than expected since the part of the amorphous fraction is "immobilized". Therefore, as Hempel et al. showed, by measuring the ΔC_p of various concentrations of drug + MS systems, it is possible to estimate the monomolecular loading capacity of the drug on the MS surface (Hempel et al., 2018).

In order to determine the monomolecular loading capacity of CEL on the surface of SYL244FP the concentration dependence of ΔC_p for CEL + SYL244FP was prepared and is presented in Fig. 4. The experimental data were fitted to a linear function and from its extrapolation to $\Delta C_p = 0$ the monomolecular loading capacity was determined as 13.5 wt.% of CEL.

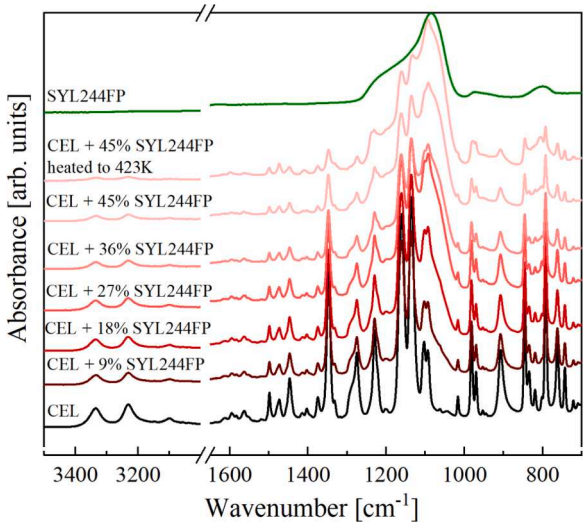

Fig. 2. Infrared analysis of crystalline CEL and its mixtures with SYL244FP.

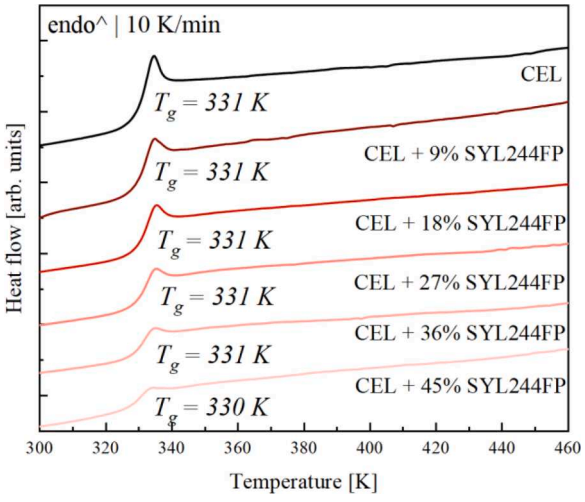

Fig. 3. DSC thermograms of amorphous CEL and its mixtures with SYL244FP.

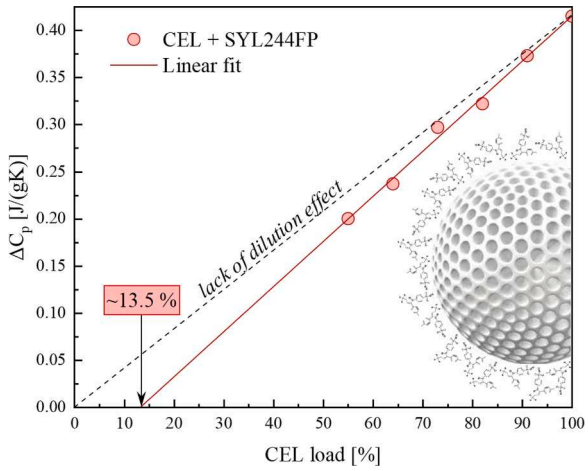

Fig. 4. Linear extrapolation of the ΔC_p values as a function of drug loading.

3.2. Molecular dynamics of CEL + SYL244FP systems

In this part of paper, the effect of MS on the molecular dynamics of CEL is investigated. The molecular dynamics studies of the quenched CEL + SYL244FP systems were performed by BDS. The non-isothermal dielectric loss spectra measurements were performed in a broad frequency (from 10^{-1} to 10^{6} Hz) and temperature range (from 173 to 383 K). Fig. 5a–e shows the representative dielectric loss spectra obtained above T_g for CEL + SYL244FP systems with different silica concentration. In the low frequency region a characteristic contribution from DC-conductivity can be identified. However, the most significant process in *ε"(ω)* is the structural (*α*) relaxation process. Increasing the temperature leads to shifting of *α*-relaxation peak towards higher frequencies, reflecting enhancement of molecular mobility. It is worth highlighting that during non-isothermal dielectric measurements, one can observe a cold crystallization process for systems at concentrations of SYL244FP of 27 wt.% or lower. The beginning of crystallization for these systems occurred at 369 K for systems with 9 and 18 wt.% of SYL244FP, and at 371 K for the system with 27 wt.% of SYL244FP. The recrystallization process is manifested by a rapid decrease in the intensity of the dielectric loss peak of *α* – process (see light-red dashed lines in Fig. 5a–e) (Grzybowska et al., 2016). The drop in the intensity of the peak is due to the fact that the population of reorienting polar molecules decreases as the crystallization progresses. Note that the intensity of the *α* –peak, $\Delta\varepsilon_\alpha$, is proportional to $N\mu$ (Williams et al., 2013), where N is a number of reorienting dipoles and μ is the value of dipole moment of molecule. For the samples containing 36 and 45 wt.% of SYL244FP, crystallization was not observed during the measurement, proving that the presence of silica improves the physical stability of CEL.

The dielectric loss spectra of all studied systems were analyzed to obtain values of the structural relaxation times (τ_α). For this purpose the dielectric loss spectra were fitted by the Havriliak-Negami (HN) function with an additional term describing the DC-conductivity contribution (Havriliak and Negami, 1967):

$$\varepsilon^*(\omega) = \varepsilon_\infty + \frac{\Delta\varepsilon}{[1+(i\omega\tau_{HN})^a]^b} + \frac{\sigma_{dc}}{\varepsilon_0 i\omega} \quad (1)$$

where ε_∞ is the high-frequency limit permittivity, ε_0 signify the permittivity of vacuum, $\Delta\varepsilon$ is dielectric strength, ω is equal to $2\pi f$, τ_{HN} is the HN relaxation time, and a and b represent symmetric and asymmetric broadening of the relaxation peak. From the fitting parameters we then determined values of τ_α using the following formula:

$$\tau_\alpha = \tau_{HN}\left[\sin\left(\frac{\pi a}{2+2b}\right)\right]^{\frac{1}{a}}\left[\sin\left(\frac{\pi ab}{2+2b}\right)\right]^{-\frac{1}{a}} \quad (2)$$

The temperature evolutions of the structural relaxation times of both neat CEL as well as its mixtures with SYL244FP are depicted in Fig. 5f. The data for neat CEL, which are marked as black filled stars, were taken from the publication of (Grzybowska et al., 2010). In order to parameterize the experimental data the Vogel-Fulcher-Tammann (VFT) equation was employed (Vogel, 1921; Fulcher, 1925; Tammann and Hesse, 1926):

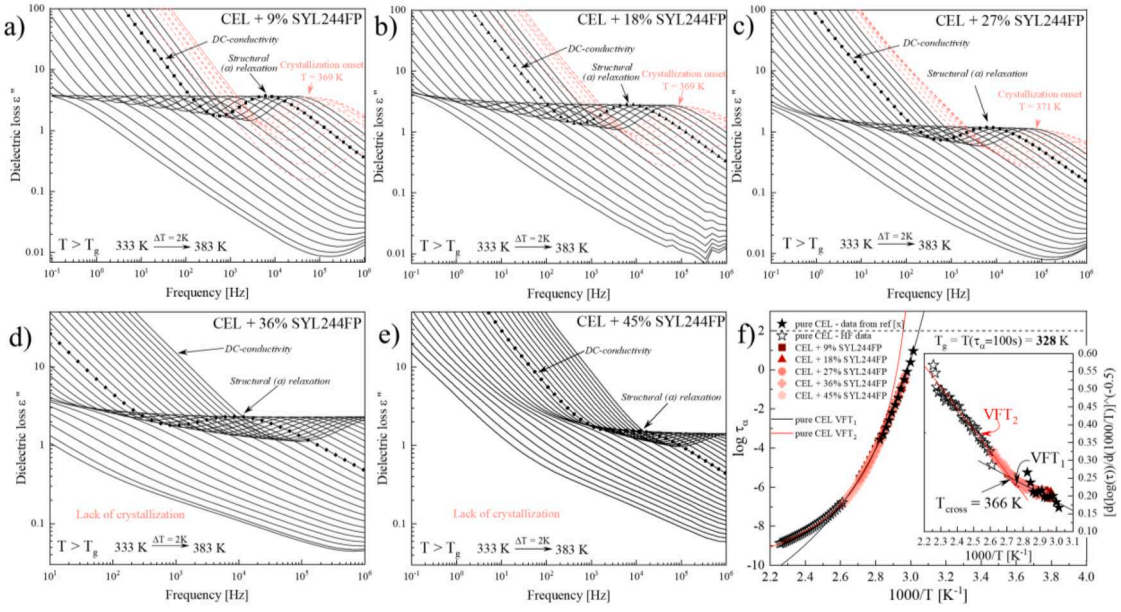

Fig. 5. Dielectric loss spectra of CEL + SYL244FP containing: (a) 9% of silica, (b) 18% of silica, (c) 27% of silica, (d) 36% of silica and (e) 45% of silica. The spectra were collected upon heating at $T > T_g$. In panel (f), the temperature dependence of τ_α for all tested systems are compared to $\tau_\alpha(T)$ of neat CEL (data from the low temperature region presented as filled stars were taken from ref. [36], while those from the high temperature region, presented as empty stars, were taken from the high frequency experiment). The inset of panel (f) shows the result of the derivative analysis focused on the validity of VFT parameterization. The intersection of the two VFT lines denotes the crossover temperature $T_{cross} = 366$ K.

$$\tau_\alpha(T) = \tau_\infty \, exp\left(\frac{DT_0}{T - T_0}\right) \quad (3)$$

where τ_∞, T_0, and D, are fitting parameters. Parameter τ_∞ is a pre-exponential factor denoting the upper limit of temperature for τ_α, and its value should be of order of around 10^{-14}s (i.e. vibrational frequency of molecule). T_0 is the Vogel temperature, which corresponds to the state with infinite relaxation time, and D denotes deviation from the Arrhenius model. During the analysis we noticed that the temperature evolution of the structural relaxation time of systems with concentrations of SYL244FP greater than 27 wt.% is not consistent over the entire experimental temperature range to fit to a single VFT equation. Therefore, the detailed analysis of the temperature dependence of τ_α were performed. For that purpose, the derivative method proposed by Stickel was employed (Stickel et al., 1996). According to this method, a plot of the values of the derivative operator $[-dlog(\tau_\alpha)/dT]^{(-0.5)}$ versus temperature should be linear for a single VFT function. Since two distinct linear regions are observed for CEL + 36% SYL244FP and CEL + 45% SYL244FP, two sets of VFT fitting parameters are required to describe the data over the entire temperature range. It is worth pointing out that in the case of neat CEL there is no information in the literature about the requirement of using two VFT. Thus, the question arises: *why in the mixtures such a behavior was noted?* There are two possible reasons. The silica used in our experiments might either modify the temperature dependence of τ_α of the drug or due to stabilization effect SYL244FP might reveal true nature of CEL $\tau_\alpha(T)$. To verify whether the silica changes or not the $\tau_\alpha(T)$ of CEL, an additional experiment was performed by means of a high frequency setup for BDS. During this experiment, to avoid recrystallization, the sample was measured on cooling from 443 to 383 K with a step of 2 K. The temperature dependence of $\tau_\alpha(T)$ for the neat API determined based on the analysis of these data is presented in Fig. 5f as the empty stars. The Stickel analysis indicated that two sets of VFT fitting parameters are required to describe the data of neat CEL over the entire temperature range. The intersection of these two VFT lines, seen in the inset of Fig. 5f, gives a crossover temperature T_{cross} = 366 K (Wu et al., 2011). This result proves that SYL244FP does not modify the temperature dependence of CEL structural relaxation time but due to the drug stabilization elongates the available for measurement frequency window. Since different mixtures of SYL244FP with CEL exhibit the same temperature dependencies as neat CEL, their glass transition temperatures are identical. To determine T_g of neat CEL and its mixtures with SYL244FP the VFT_1 functions were extrapolated to the value of $\tau_\alpha = 100$ s ($T_g = T$ ($\tau_\alpha = 100$ s) = 328 K). The T_g values determined by BDS are consistent with the data obtained from calorimetric measurements. Slight discrepancies result from the different heating rates applied during the calorimetric (HR = 10 K/min) and dielectric (HR = 0.5 K/min) measurements.

In the next step of analysis of the dielectric loss spectra, we concentrated on the shape of the α – process. Firstly, we checked if the shape of the α – process changes with temperature. In order to do this, we constructed for each composition a master plot, i.e.: the reference spectrum was selected and remaining spectra were shifted along horizontal and vertical axes to superimpose them on the reference system. The master plots for the extreme MS concentrations are presented in Fig. 6. It can be seen that, with exception of an increase in DC-conductivity with decreasing temperature, the shape of the structural relaxation process does not change in a given temperature range for the CEL + SYL244FP systems. It now becomes interesting to test if the shape of the structural relaxation peak is dependent on the concentration of SYL244FP. To perform a more quantitative analysis, we used the Kohlrausch–Williams–Watts (KWW) function to fit the α – relaxation peak. The advantage of using this fitting function is that it has only a single parameter, β_{KWW}, characterizing the shape of the relaxation curve (Williams and Watts, 1970). Its value can change from 0 to 1, with a value of 1 indicating that the alpha relaxation peak is narrow and symmetrical, which corresponds to the Debye case. As the value of β_{KWW} decreases towards 0 the peak becomes broader and asymmetric. The results of the shape analysis of the structural relaxation peak in terms of the KWW function are presented in Fig. 7. It becomes obvious that the value of the β_{KWW} parameter decreases with the increasing concentration of SYL244FP. For instance, Shamblin et al. noticed that for materials with low β_{KWW} values the tendency to crystallization is much higher (Shamblin et al., 2000). This phenomenological observation disagrees with our finding as for systems with the lowest β_{KWW} values (i.e., higher concentration of SYL244FP) crystallization was not observed during the non-isothermal dielectric measurements. Note that the similar discrepancy between the physical stability of amorphous API and its β_{KWW} value has been previously observed for other pharmaceuticals, i.e. ezetimibe and sildenafil. Furthermore, in our case, broadening the α-relaxation peak of CEL is associated with the increase of the system heterogeneity (Kolodziejczyk et al., 2013).

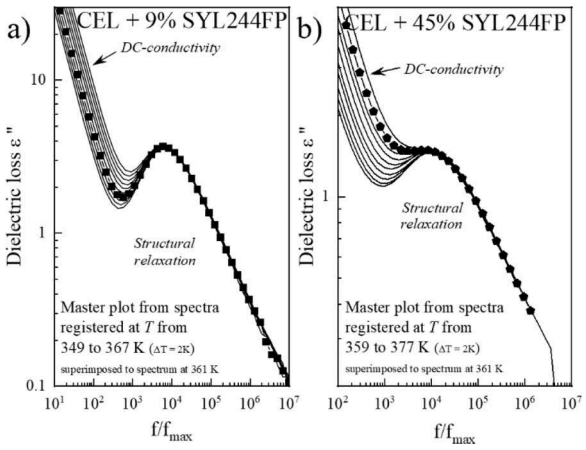

Fig. 6. The master plot from dielectric loss spectra of: (a) CEL + 9% of SYL244FP, and SVT +45% of SYL244 formed by horizontal shifting of spectra to overlap the reference system.

3.3. Studies of the effect of silica additive on the physical stability of amorphous CEL

Presented in the previous section, non-isothermal dielectric studies indicated that SYL244FP improves the physical stability of amorphous CEL. However, based on these data, it is impossible to assess the stabilization effect. Therefore, to properly evaluate the effectiveness of SYL244FP in the stabilization of the disordered form of CEL, time-dependent, isothermal dielectric studies were performed. The crystallization of both neat CEL and its mixture with SYL244FP was measured at T = 363 K (the spectra were registered every 300 s). This particular temperature was selected for two reasons. Firstly, the crystallization kinetics of neat CEL was previously investigated by (Dantuluri et al., 2011) at temperatures ranging from 363 to 378 K (ΔT = 5 K). Thus, choosing one of these temperature conditions, one can check whether the investigated by us batch of the drug behave identically as that shown in the literature. Secondly, at T = 363 K neat CEL should fully convert to its crystalline form after ca. 4 h. This period of time is on the one hand long enough to safely prepare and measure the sample avoiding partial crystallization, while on the other hand, fast enough to investigate how the silica stabilizes the drug.

Fig. 8 shows the representative (i.e., registered every 1200s), data obtained for neat CEL. It can be seen that the crystallization process can be followed directly in both the real (ε') and imaginary (ε'') parts of the complex dielectric permittivity, reflected by a decrease of the static permittivity (ε_s) and an increase in the intensity of the loss peak with time, respectively (Descamps, 2016). However, since usually the progress of crystallization is analyzed in terms of the normalized real permittivity (ε'_N), in the further part of this work we will present data

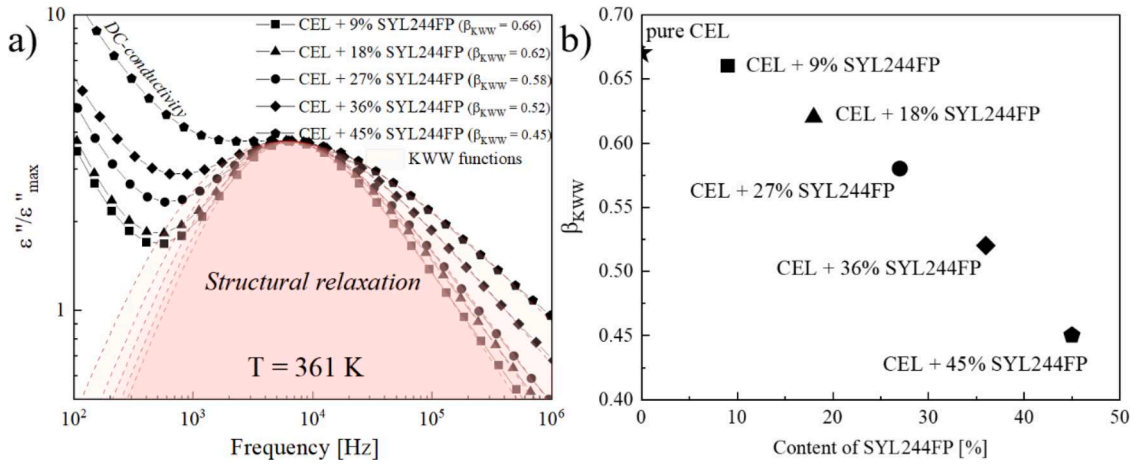

Fig. 7. (a) Comparison of the dielectric spectra of various concentrations of the CEL + SYL244FP systems recorded at $T = 361$ K. The dashed lines represent the KWW fit to the α-peak with a value of β_{KWW} given in the legend. (b) The concentration dependence of β_{KWW} for the CEL + SYL244FP systems.

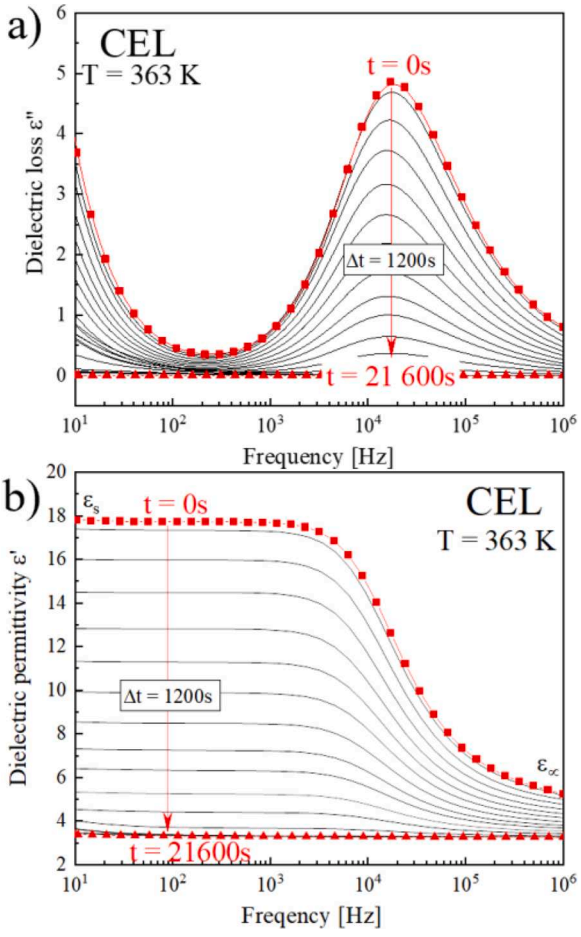

Fig. 8. Dielectric spectra of the imaginary (upper panel) and real (lower panel) parts of the complex dielectric permittivity during an isothermal crystallization of neat CEL at $T = 363$ K.

only in the dielectric permittivity representation. The aforementioned ε'_N is defined as (Kremer and Schönhals, 2003):

$$\varepsilon_N' = \frac{\varepsilon'(0) - \varepsilon'(t)}{\varepsilon'(0) - \varepsilon'(\infty)} \quad (4)$$

where $\varepsilon'(0)$ is the initial static dielectric permittivity, $\varepsilon'(\infty)$ is the long-time limiting value, and $\varepsilon'(t)$ is the value at time t. Normalized by this method data of neat CEL were compared to the crystallization kinetics of CEL obtained from digitalizing the data from the (Dantuluri et al., 2011) paper. Both time dependences are plotted together as empty and filled circles in Fig. 10a. Since the kinetics of CEL crystallization measured by us is identical as that investigated earlier, we can conclude that the sample batch has no impact on the physical stability of this API and one can investigate the effect of silica on its stabilization. For this purpose, the systems containing CEL and 9, 18, 27, 36 and 45 wt.% of SYL244FP were isothermally measured at $T = 363$ K by means of BDS ($\Delta t = 300$ s). The representative spectra obtained from these experiments (i.e., with $\Delta t = 1200$s, $\Delta t = 2400$s, and $\Delta t = 3600$s for CEL + 9% SYL244FP, CEL + 18% SYL244FP, and CEL + 27% SYL244FP, respectively) are presented in Fig. 9a–c.

Note that, since SYL244FP does not modify the temperature dependence of τ_α of neat CEL, these experiments were performed not only at fixed temperature conditions but also at constant τ_α, i.e., isothermal conditions. A drop in the static permittivity (ε_s) was observed during all experiments indicating that CEL recrystallizes from the drug-silica binary systems, even when high SYL244FP content is employed. However, crystallization observed in CEL mixtures is unfinished, and its degree decreases with the increasing amount of SYL244FP (see the green areas in Fig. 9a–c). The end of the crystallization process was considered when no further changes in the dielectric spectrum were observed. To properly analyze these data, i.e., to take into account the degree of CEL crystallization, we took the value of ε_∞ instead of $\varepsilon'(\infty)$ in Eq. (4). The comparison of all kinetic curves is presented in Fig. 10a. As can be seen by increasing the amount of the silica, the prolongation of the CEL recrystallization was noted indicating that SYL244FP improves the physical stability of amorphous CEL. It is worth pointing out that a similar partial crystallization of the drug measured by means of BDS was previously observed when API was mixed with another drug (drug-drug system) (Tu et al., 2019) or polymer (drug-polymer system) (Chmiel et al., 2017, 2019a, 2019b). In these cases, together with the reduction of $\Delta\varepsilon$, the shift in the position of the structural relaxation process was noted proving that the molecular dynamics of the system was changing. The incomplete crystallization of the drugs described in the mentioned works results from the crystallization of the excess of drug from the supersaturated system (drug-drug or drug-polymer). Thus, this allows to determine the concentration corresponding to the saturated system, which should guarantee high physical stability. However, such scenario is impossible for the CEL + SYL244FP systems since the drug cannot be dissolved in the silica.

By analyzing the kinetic curves, the crystallization half-life time ($t_{1/2}$) and the degree of CEL crystallinity were determined. The obtained

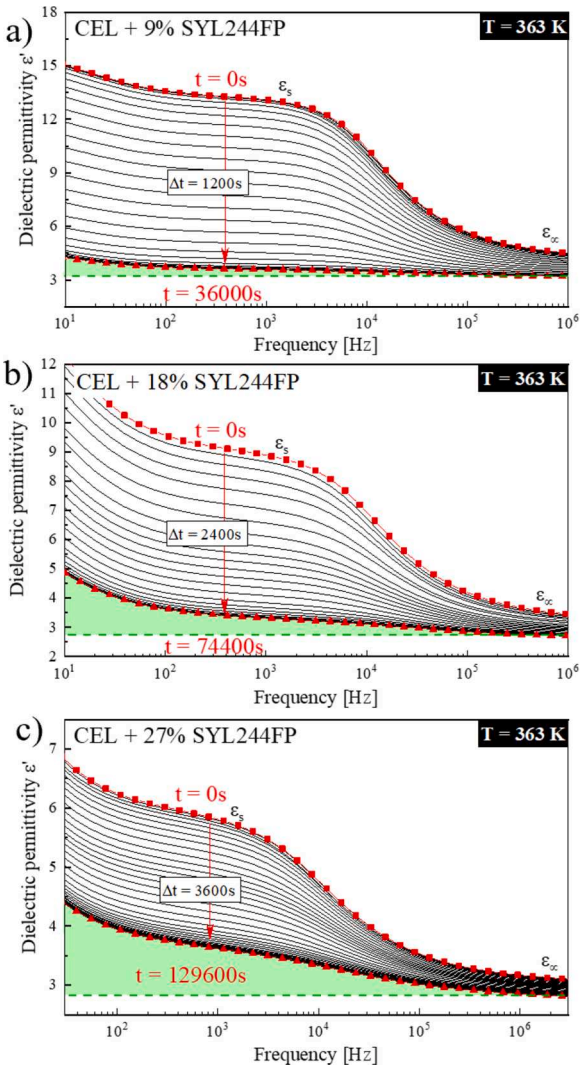

Fig. 9. Dielectric spectra of the real part of the complex dielectric permittivity during an isothermal crystallization at $T = 363$ K of (a) CEL + 9% SYL244FP, (b) CEL + 18% SYL244FP, and (c) CEL + 27% SYL244FP (For interpretation of the references to color in this figure, the reader is referred to the web version of this article.).

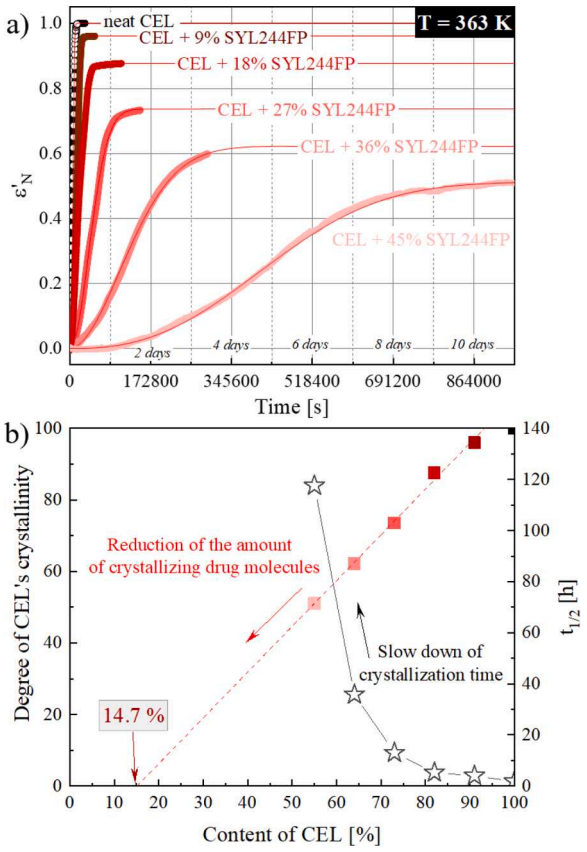

Fig. 10. Panel (a) compares the time dependences of ε_N' for neat CEL (empty circles – data from Ref. [37], filled circles – data from our experiment), and its mixtures with 9, 18, 27, 36 and 45% of SYL244FP at 363 K. Panel (b) shows presented as a squares the concentration dependence of degree of CEL crystallinity obtained after the isothermal dielectric studies and presented as a stars concentration dependence of CEL crystallization half-life time from the mixtures with SYL244FP.

values are summarized in Fig. 10b. The concentration dependence of the degree of CEL crystallinity shows a linear behavior. Therefore, by extrapolating the fitted to these data a linear function to 0% of CEL crystallinity, one can predict what concentration of the silica is needed to fully stabilize the amorphous form of the investigated drug. Based on this analysis, one can estimate that at least 85.3 wt.% of SYL244FP is needed to fully prevent crystallization of the API. Note that this concentration corresponds well (±1%) with concentration in which CEL molecules form the monomolecular layer on the silica surface (i.e., 86.5 wt.%), as determined above from the calorimetric studies. This result suggests that SYL244FP inhibits only the crystallization of CEL molecules located nearby the surface of the silica. Based on this assumption one can conclude that the observed stabilization of CEL in the systems with SYL244FP originates from the interaction of drug molecules with the surface of the silica.

3.4. Molecular dynamics of recrystallized CEL + SYL244FP systems

In the previous section, it was shown that CEL remains partially amorphous after recrystallization from the mixtures with SYL244FP. The samples obtained after the isothermal BDS experiments (where crystallization was observed) were again subjected to non-isothermal dielectric studies. These tests were performed for two reasons. On the one hand, they can prove whether or not the amorphous fraction of CEL still remains in the CEL + SYL244FP systems. While on the other hand, these experiments will show how the molecular dynamics of the investigated systems change when some part of CEL converts to the crystalline form.

The dielectric loss spectra of partially amorphous systems containing 9, 18 and 27 wt.% of SYL244FP were measured at temperatures from 333 to 433 K ($\Delta T = 10$ K). The representative dielectric loss spectra are presented in Fig. 11a and b. The investigated systems reveal two processes. One is located at higher frequencies reflecting the structural relaxation associated with the CEL glass transition dynamics, while the second i.e., slower process, is probably associated with the Maxwell-Wagner-Sillars (MWS) polarization mechanism (Ignaczak et al., 2020; Baeza et al., 2015; Gitsas et al., 2004). MWS processes reflect the trapping and accumulation of charges at the interface of the different phases of the sample. Considering that in the measured samples three different phases exists (i.e., crystalline CEL, amorphous CEL and SYL244FP) the origin of this process seems to be obvious. However, it can also originate from the dynamic of CEL molecules localized nearby the pore walls and/or the crystallite front. In order to determine the temperature evolution of the structural and "slow" processes, the dielectric loss spectra were fitted in a similar way to that used for the fully amorphous systems with two HN functions used instead of one. An exemplary fit of spectra investigated at $T = 363$ K for CEL containing 9, 18 and 27 wt.% of SYL244FP are presented in Fig. 11c. The intensity of the process

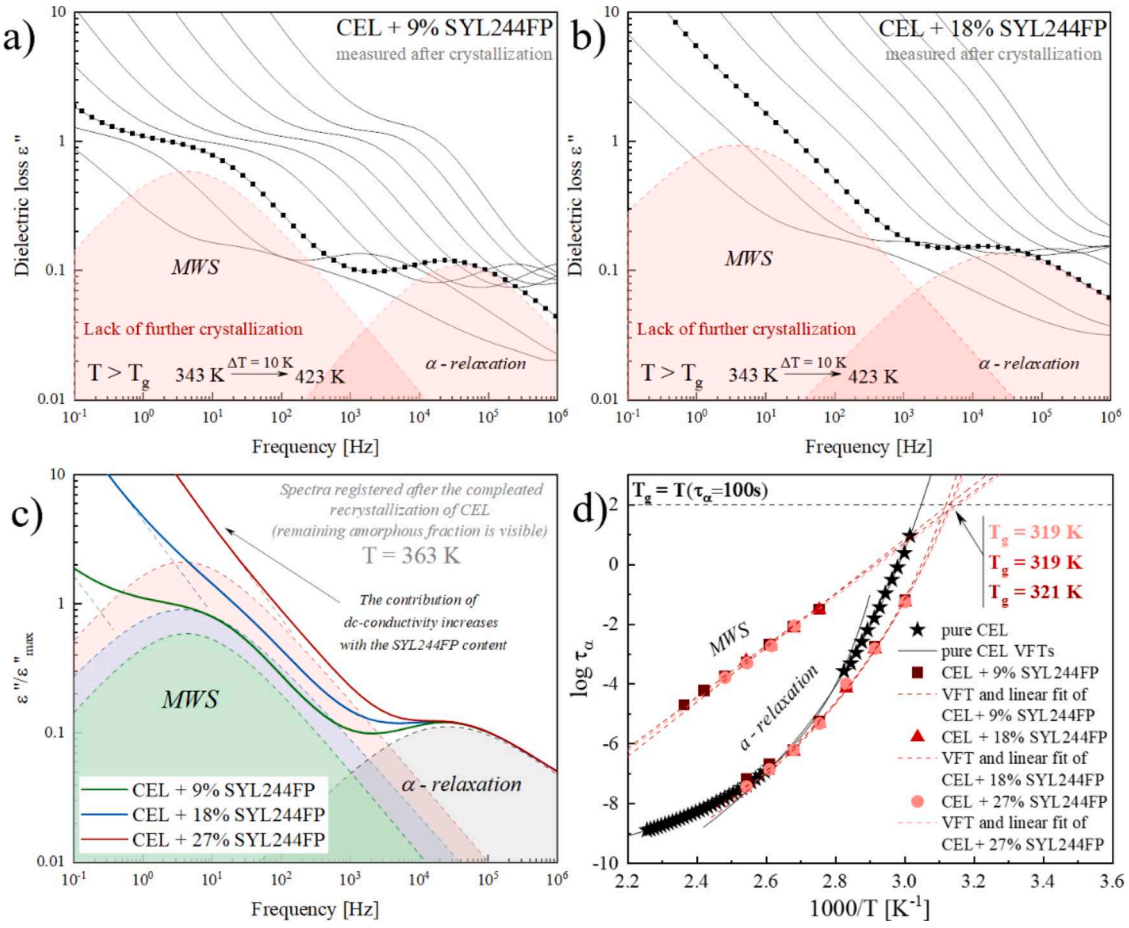

Fig. 11. Dielectric loss spectra of samples obtained after time-dependent isothermal dielectric studies which contain crystalline and amorphous fractions of CEL and (a) 9% of SYL244FP and (b) 18% of SYL244FP. Panel (c) compares the dielectric loss spectra of partially crystalline CEL + SYL244FP systems registered at $T = 363$ K. In panel (d), the temperature dependences of τ_α and τ_{MWS} of all tested systems are compared to $\tau_\alpha(T)$ of neat CEL.

located at lower frequencies increases with the increasing the silica content. This suggests that the "slower" process indeed reflects the MWS polarization. It is well known that MWS effects are more pronounced for conductive materials. This is consistent with the obtained data – as shown in Fig. 7a, conductivity of the mixture increases with the increasing SYL244FP content. If the "slower" process originated from the dynamics of the interfacial CEL molecules, a reduction of the process intensity with the increasing SYL244FP would be visible. It is because a reduction in the crystalline fraction was noted with increasing silica content consistent with a smaller surface area of the crystal.

The values of τ_α, and τ_{MWS} were determined from the obtained fitting parameters. The $\tau_\alpha(T)$, and $\tau_{MWS}(T)$ of the measured systems are compared to $\tau_\alpha(T)$ of neat CEL in Fig. 11d. The MWS process of all investigated systems reveals an Arrhenius T dependence, while the temperature dependence of CEL structural relaxation time in the partially amorphous systems follows VFT behavior. It is clear that the latter dependences differ (especially at the low temperature region) from $\tau_\alpha(T)$ of neat CEL and consequently from $\tau_\alpha(T)$ of amorphous CEL in mixtures with SYL244FP. To describe the temperature evolution of τ_α of mixtures with partially amorphous CEL, the VFT equation (Eq. (3)) was employed. The comparison of VFT fitting parameter of systems containing partially amorphous CEL and neat CEL are shown in Table 1. The glass transition temperatures of the investigated systems, which were determined from the fit extrapolation, are 321 K for CEL + 9% SYL244FP, and 319 K for CEL + 18% SYL244FP as well as CEL + 27% SYL244FP. It should be stressed that the presence of the α – relaxation process in the recorded spectra demonstrates that part of CEL indeed remains amorphous in the investigated samples.

Table 1
Comparison of the VFT_1 parameters of neat, fully amorphous CEL and partially crystalline CEL in mixtures with 9, 18 and 27% of SYL244FP.

Sample	$\log_{10}(\tau_\infty/s)$	$B = DT_0$	T_0
neat CEL	-13.97 ± 0.04	1 758.3 ± 11.6	280.2 ± 0.8
CEL + 9% SYL244FP	-14.4 ± 0.56	2044.3 ± 54.4	266.5 ± 2.1
CEL + 18% SYL244FP	-15.72 ± 0.98	2555.5 ± 48.2	256.7 ± 1.7
CEL + 27% SYL244FP	-15.87 ± 1.48	2698.0 ± 78.5	253.1 ± 3.1

4. Conclusions

In this paper we investigated the impact of MS in the form of SYL244FP on the molecular dynamics and physical stability of amorphous CEL. For that purpose, a series of calorimetric and dielectric studies of various concentrations of CEL + SYL244FP were performed. As the calorimetric data shows, the presence of SYL244FP significantly modifies the melting process of CEL resulting in the drug melting in two stages. Interestingly, SYL244FP have no impact on the glass transition temperature of the API. From the analysis of the change in specific heat capacity of glass transition temperature process of the CEL + silica systems, the monomolecular loading capacity of CEL on the silica surface was determined as 13.5 wt.%. Non-isothermal dielectric studies of systems containing fully amorphous CEL and SYL244FP show that the silica did not modify the temperature dependence of the structural relaxation time of the API. It however has an impact on the distribution of the structural relaxation peak. With the increasing amount of the silica in the system, the α – relaxation peak of CEL becomes broader.

Subsequent isothermal BDS experiments showed that the increased content of SYL244FP in CEL mixtures causes prolongation of the drug recrystallization time as well as it leads to an increase in the amount of the drug remaining stable in the amorphous form. The analysis of the degree of crystallinity of the samples in which completed crystallization was observed suggests that SYL244FP inhibits crystallization of CEL molecules located only nearby the surface of the silica. Based on this observation it can be concluded that the observed stabilization of CEL originates from interactions of drug molecules with the surface of the silica. Finally, the molecular dynamics of the systems with partially amorphous CEL were investigated. The dielectric loss spectra of the systems with only partially amorphous CEL reveals an extra process in addition to the α-relaxation peak. Due to the high inhomogeneity of these systems this process was identified as the MWS polarization. Dielectric studies of these complex systems confirmed that indeed a fraction of CEL remains amorphous in the sample and the presence of the crystalline fraction of the CEL in the system modifies the $\tau_\alpha(T)$ of the drug.

Funding

The authors D.K., J.K-K. and M.P. are grateful for the financial support received within the Project No. 2018/31/B/ST8/01327 (OPUS 16) from the National Science Centre, Poland. M.F.M. and L.T. would like to thank Science Foundation Ireland, grants 12/RC/2275_P2, 15/CDA/360 and 18/EPSRC-CDT/3587, for financial support. The studies was implemented as part of strategy of the University of Silesia - Inicjatywa Doskonałości (POB 1 - Priorytetowy Obszar Badawczy 1: Harmonijny rozwój człowieka - troska o ochronę zdrowia i jakość życia).

CRediT authorship contribution statement

Daniel Kramarczyk: Conceptualization, Investigation, Methodology, Validation, Visualization, Writing – original draft. **Justyna Knapik-Kowalczuk:** Conceptualization, Methodology, Supervision, Validation, Writing – review & editing. **Wojciech Smolka:** Investigation. **Maria Ferreira Monteiro:** Investigation. **Lidia Tajber:** Methodology, Writing – review & editing. **Marian Paluch:** Conceptualization, Funding acquisition, Supervision, Writing – review & editing.

Acknowledgments

The authors thanks Beibei Yao (University of Silesia) for carrying out additional measurements for pure celecoxib using high frequency dielectric spectroscopy.

References

Fahr, A., Liu, X., 2007. Drug delivery strategies for poorly water-soluble drugs. Expert Opin. Drug Deliv. 4 (4) https://doi.org/10.1517/17425247.4.4.403.

Williams, H.D., Trevaskis, N.L., Charman, S.A., Shanker, R.M., Charman, W.N., Pouton, C.W., Porter, C.J.H., 2013. Strategies to address low drug solubility in discovery and development. Pharmacol. Rev. 65 (1), 315–499. https://doi.org/10.1124/pr.112.005660.

Babu, N.J., Nangia, A., 2011. Solubility advantage of amorphous drugs and pharmaceutical cocrystals. Cryst. Growth Des. 11 (7), 2662–2679. https://doi.org/10.1021/cg200492w.

Kalepu, S., Nekkanti, V., 2015. Insoluble drug delivery strategies: review of recent advances and business prospects. Acta Pharm. Sin. B 5 (5), 442–453. https://doi.org/10.1016/j.apsb.2015.07.003.

Vasconcelos, T., Sarmento, B., Costa, P., 2007. Solid dispersions as strategy to improve oral bioavailability of poor water soluble drugs. Drug Discov. Today 12 (23–24), 1068–1075. https://doi.org/10.1016/j.drudis.2007.09.005.

Cid, A.G., Simonazzi, A., Palma, S.D., Bermúdez, J.M., 2019. Solid dispersion technology as a strategy to improve the bioavailability of poorly soluble drugs. Ther. Deliv. 10 (6), 363–382. https://doi.org/10.4155/tde-2019-0007.

Baird, J.A., Taylor, L.S., 2012. Evaluation of amorphous solid dispersion properties using thermal analysis techniques. Adv. Drug Deliv. Rev. 64 (5), 396–421. https://doi.org/10.1016/j.addr.2011.07.009.

Hancock, B.C.; Parks, M. What is the true solubility advantage for amorphous pharmaceuticals? 2000, 17 (4), 397–404. 10.1023/A:1007516718048.

Bogner, R.H., Murdande, S.B., Pikal, M.J., Shanker, R.M., 2010. Solubility advantage of amorphous pharmaceuticals: II. Application of quantitative thermodynamic relationships for prediction of solubility enhancement in structurally diverse insoluble pharmaceuticals. Pharm. Res. 27 (12), 2704–2714. https://doi.org/10.1007/s11095-010-0269-5.

Hancock, B.C., Zografi, G., 1997. Characteristics and significance of the amorphous state in pharmaceutical systems. J. Pharm. Sci. 86 (1), 1. https://doi.org/10.1021/js9601896.

Kawakami, K., 2012. Modification of physicochemical characteristics of active pharmaceutical ingredients and application of supersaturatable dosage forms for improving bioavailability of poorly absorbed drugs. Adv. Drug Deliv. Rev. 64 (6), 480–495. https://doi.org/10.1016/j.addr.2011.10.009.

Hu, L., Tang, X., Cui, F., 2010. Solid lipid nanoparticles (SLNs) to improve oral bioavailability of poorly soluble drugs. J. Pharm. Pharmacol. 56 (12), 1527–1535. https://doi.org/10.1211/0022357044959.

Kothari, K., Ragoonanan, V., Suryanarayanan, R., 2014. Influence of molecular mobility on the physical stability of amorphous pharmaceuticals in the supercooled and glassy states. Mol. Pharm. 11 (9), 3048–3055. https://doi.org/10.1021/mp500229d.

Szklarz, G., Adrjanowicz, K., Knapik-Kowalczuk, J., Jurkiewicz, K., Paluch, M., 2017. Crystallization of supercooled fenofibrate studied at ambient and elevated pressures. Phys. Chem. Chem. Phys. 19 (15), 9879–9888. https://doi.org/10.1039/c7cp00823f.

Karmwar, P., Graeser, K., Gordon, K.C., Strachan, C.J., Rades, T., 2011. Investigation of properties and recrystallisation behaviour of amorphous indomethacin samples prepared by different methods. Int. J. Pharm. 417 (1–2), 94–100. https://doi.org/10.1016/j.ijpharm.2010.12.019.

Knapik, J., Wojnarowska, Z., Grzybowska, K., Jurkiewicz, K., Tajber, L., Paluch, M., 2015. Molecular dynamics and physical stability of coamorphous ezetimib and indapamide mixtures. Mol. Pharm. 12 (10), 3610–3619. https://doi.org/10.1021/acs.molpharmaceut.5b00334.

Kawakami, K., 2019. Ultraslow cooling for the stabilization of pharmaceutical glasses. J. Phys. Chem. B 123 (23), 4996–5003. https://doi.org/10.1021/acs.jpcb.9b02122.

Baghel, S., Cathcart, H., O'Reilly, N.J., 2016. Polymeric amorphous solid dispersions: a review of amorphization, crystallization, stabilization, solid-state characterization, and aqueous solubilization of biopharmaceutical classification system class II drugs. J. Pharm. Sci. 105 (9), 2527–2544. https://doi.org/10.1016/j.xphs.2015.10.008.

Knapik-Kowalczuk, J., Tu, W., Chmiel, K., Rams-Baron, M., Paluch, M., 2018. Co-stabilization of amorphous pharmaceuticals - the case of nifedipine and nimodipine. Mol. Pharm. 15 (6), 2455–2465. https://doi.org/10.1021/acs.molpharmaceut.8b00308.

Khanfar, M., Al-Nimry, S., 2017. Stabilization and amorphization of lovastatin using different types of silica. AAPS PharmSciTech 18 (6), 2358–2367. https://doi.org/10.1208/s12249-017-0717-1.

Laitinen, R., Lobïmann, K., Strachan, C.J., Grohganz, H., Rades, T., 2013. Emerging trends in the stabilization of amorphous drugs. Int. J. Pharm. 453 (1), 65–79. https://doi.org/10.1016/j.ijpharm.2012.04.066.

Singh, A., Worku, Z.A., Van Den Mooter, G., 2011. Oral formulation strategies to improve solubility of poorly water-soluble drugs. Expert Opin. Drug Deliv. 8 (10), 1361–1378. https://doi.org/10.1517/17425247.2011.606808.

Shaker, M.A., Elbadawy, H.M., Shaker, M.A., 2020. Improved solubility, dissolution, and oral bioavailability for atorvastatin-pluronic® solid dispersions. Int. J. Pharm. 574, 118891 https://doi.org/10.1016/j.ijpharm.2019.118891.

Riikonen, J., Xu, W., Lehto, V.P., 2018. Mesoporous systems for poorly soluble drugs – recent trends. Int. J. Pharm. 536 (1), 178–186. https://doi.org/10.1016/j.ijpharm.2017.11.054.

Bahl, D., Bogner, R.H., 2006. Amorphization of indomethacin by co-grinding with neusilin US2: amorphization kinetics, physical stability and mechanism. Pharm. Res. 23 (10), 2317–2325. https://doi.org/10.1007/s11095-006-9062-x.

Müller Reiner, H., David, H., Nan, J., Pyo, S.M., 2018. SmartPearls – novel physically stable amorphous delivery system for poorly soluble dermal actives. Int. J. Pharm. 555, 314–321. https://doi.org/10.1016/j.ijpharm.2018.11.018.

Shen, S.C.; Ng, W.K.; Chia, L.; Dong, Y.C.; Tan, R.B.H. Stabilized amorphous state of ibuprofen by co-spray drying with mesoporous SBA-15 to enhance dissolution properties. Wiley Intersci. 2009, 99 (4), 1997–2007. 10.1002/jps.21967.

Andersson, J., Rosenholm, J., Areva, S., Lindén, M., 2004. Influences of material characteristics on ibuprofen drug loading and release profiles from ordered micro- and mesoporous silica matrices. Chem. Mater. 16 (21), 4160–4167. https://doi.org/10.1021/cm0401490.

Knapik-Kowalczuk, J., Kramarczyk, D., Chmiel, K., Romanova, J., Kawakami, K., Paluch, M., 2020. Importance of mesoporous silica particle size in the stabilization of amorphous pharmaceuticals—the case of simvastatin. Pharmaceutics 12 (4), 21–25. https://doi.org/10.3390/pharmaceutics12040384.

Knapik, J., Wojnarowska, Z., Grzybowska, K., Jurkiewicz, K., Stankiewicz, A., Paluch, M, 2016. Stabilization of the amorphous ezetimibe drug by confining its dimension. Mol. Pharm. 13 (4), 1308–1316. https://doi.org/10.1021/acs.molpharmaceut.5b00903.

Godec, A., Maver, U., Bele, M., Planinšek, O., Srčič, S., Gaberšček, M., Jamnik, J., 2007. Vitrification from solution in restricted space: formation and stabilization of amorphous nifedipine in a nanoporous silica xerogel carrier. Int. J. Pharm. 343 (1–2), 131–140. https://doi.org/10.1016/j.ijpharm.2007.05.022.

Croissant, J.G., Fatieiev, Y., Khashab, N.M., 2017. Degradability and clearance of silicon, organosilica, silsesquioxane, silica mixed oxide, and mesoporous silica nanoparticles. Adv. Mater. (9), 29. https://doi.org/10.1002/adma.201604634.

Croissant, J.G., Fatieiev, Y., Almalik, A., Khashab, N.M., 2018. Mesoporous silica and organosilica nanoparticles: physical chemistry, biosafety, delivery strategies, and

biomedical applications. Adv. Healthc. Mater 7 (4), 1–75. https://doi.org/10.1002/adhm.201700831.
Rengarajan, G.T., Enke, D., Steinhart, M., Beiner, M., 2008. Stabilization of the amorphous state of pharmaceuticals in nanopores. J. Mater. Chem. 18 (22), 2537–2539. https://doi.org/10.1039/b804266g.
Genina, N., Hadi, B., Löbmann, K., 2018. Hot melt extrusion as solvent-free technique for a continuous manufacturing of drug-loaded mesoporous silica. J. Pharm. Sci. 107 (1), 149–155. https://doi.org/10.1016/j.xphs.2017.05.039.
Grzybowska, K., Paluch, M., Grzybowski, A., Wojnarowska, Z., Hawelek, L., Kolodziejczyk, K., Ngai, K.L., 2010. Molecular dynamics and physical stability of amorphous anti-inflammatory drug: celecoxib. J. Phys. Chem. B 114 (40), 12792–12801. https://doi.org/10.1021/jp1040212.
Dantuluri, A.K.R., Amin, A., Puri, V., Bansal, A.K., 2011. Role of α-relaxation on crystallization of amorphous celecoxib above Tg probed by dielectric spectroscopy. Mol. Pharm. 8 (3), 814–822. https://doi.org/10.1021/mp100411v.
Knopp, M.M., Tajber, L., Tian, Y., Olesen, N.E., Jones, D.S., Kozyra, A., Löbmann, K., Paluch, K., Brennan, C.M., Holm, R., Healy, A.M., Andrews, G.P., Rades, T., 2015. Comparative study of different methods for the prediction of drug-polymer solubility. Mol. Pharm. 12 (9), 3408–3419. https://doi.org/10.1021/acs.molpharmaceut.5b00423.
Beiner, M., Rengarajan, G.T., Pankaj, S., Enke, D., Steinhart, M., 2007. Manipulating the crystalline state of pharmaceuticals by nanoconfinement. Nano Lett. 7 (5), 1381–1385. https://doi.org/10.1021/nl0705081.
Jackson, C.L., McKenna, G.B., 1996. Vitrification and crystallization of organic liquids confined to nanoscale pores. Chem. Mater. 8 (8), 2128–2137. https://doi.org/10.1021/cm9601188.
Lu, G.W., Hawley, M., Smith, M., Geiger, B.M., Pfund, W., 2006. Characterization of a novel polymorphic form of celecoxib. J. Pharm. Sci. 95 (2), 305–317. https://doi.org/10.1002/jps.20522.
Kozyra, A., Mugheirbi, N.A., Paluch, K.J., Garbacz, G., Tajber, L., 2018. Phase diagrams of polymer-dispersed liquid crystal systems of itraconazole/component immiscibility induced by molecular anisotropy. Mol. Pharm. 15 (11), 5192–5206. https://doi.org/10.1021/acs.molpharmaceut.8b00724.
Saunders, M., Podluii, K., Shergill, S., Buckton, G., Royall, P., 2004. The potential of high speed DSC (Hyper-DSC) for the detection and quantification of small amounts of amorphous content in predominantly crystalline samples. Int. J. Pharm. 274 (1–2), 35–40. https://doi.org/10.1016/j.ijpharm.2004.01.018.
Hempel, N.J., Brede, K., Olesen, N.E., Genina, N., Knopp, M.M., Löbmann, K., 2018. A fast and reliable DSC-based method to determine the monomolecular loading capacity of drugs with good glass-forming ability in mesoporous silica. Int. J. Pharm. 544 (1), 153–157. https://doi.org/10.1016/j.ijpharm.2018.04.035.
Grzybowska, K., Capaccioli, S., Paluch, M., 2016. Recent developments in the experimental investigations of relaxations in pharmaceuticals by dielectric techniques at ambient and elevated pressure. Adv. Drug Deliv. Rev. 100, 158–182. https://doi.org/10.1016/j.addr.2015.12.008.
Havriliak, S., Negami, S., 1967. A complex plane representation of dielectric and mechanical relaxation processes in some polymers. Polymer 8 (C), 161–210. https://doi.org/10.1016/0032-3861(67)90021-3 (Guildf).
Vogel, H., 1921. Das Temperaturabhangigkeitgesetz Der Viskosität von Flüssigkeiten. J. Phys. Z. 22, 645–646.
Fulcher, G.S., 1925. Analysis of recent measurements of the viscosity of glasses. J. Am. Ceram. Soc. 8 (6), 339–355. https://doi.org/10.1111/j.1151-2916.1925.tb16731.x.
Tammann, G., Hesse, W., 1926. Die abhängigkeit der viscosität von der temperatur bie unterkühlten flüssigkeiten. Z. für Anorg. und Allg. Chem. 156 (1), 245–257. https://doi.org/10.1002/zaac.19261560121.
Stickel, F., Fischer, E.W., Richert, R., 1996. Dynamics of glass-forming liquids. II. Detailed comparison of dielectric relaxation, de-conductivity, and viscosity data. J. Chem. Phys. 104 (5), 2043–2055. https://doi.org/10.1063/1.470961.
Wu, X., Wang, H., Liu, C., Zhu, Z., 2011. Longer-scale segmental dynamics of amorphous poly(ethylene oxide)/poly(vinyl acetate) blends in the softening dispersion. Soft Matter 7 (2), 579–586. https://doi.org/10.1039/c0sm00633e.
Williams, G., Watts, D.C., 1970. Non-symmetrical dielectric relaxation behaviour arising from a simple empirical decay function. Trans. Faraday Soc. 66 (1), 80–85. https://doi.org/10.1039/TF9706600080.
Shamblin, S.L., Hancock, B.C., Dupuis, Y., Pikal, M.J., 2000. Interpretation of relaxation time constants for amorphous pharmaceutical systems. J. Pharm. Sci. 89 (3), 417–427. https://doi.org/10.1002/(SICI)1520-6017(200003)89:3<417::AID-JPS12>3.0.CO;2-V.
Kolodziejczyk, K., Paluch, M., Grzybowska, K., Grzybowski, A., Wojnarowska, Z., Hawelek, L., Ziolo, J.D., 2013. Relaxation dynamics and crystallization study of sildenafil in the liquid and glassy states. Mol. Pharm. 10 (6), 2270–2282. https://doi.org/10.1021/mp300479r.
Descamps, M., 2016. Disordered Pharmaceutical Materials. Wiley-VCH Verlag GmbH & Co. KGaA, Weinheim, Germany.
Kremer, F., Schönhals, A., 2003. Local dielectric relaxation by solvation dynamics. Broadband Dielectric Spectroscopy. Springer-Verlag, Berlin Heidelberg, Germany.
Tu, W., Knapik-Kowalczuk, J., Chmiel, K., Paluch, M., 2019. Glass transition dynamics and physical stability of amorphous griseofulvin in binary mixtures with low- Tg excipients. Mol. Pharm. 16 (8), 3626–3635. https://doi.org/10.1021/acs.molpharmaceut.9b00476.
Chmiel, K., Knapik-Kowalczuk, J., Jurkiewicz, K., Sawicki, W., Jachowicz, R., Paluch, M., 2017. A new method to identify physically stable concentration of amorphous solid dispersions (I): case of flutamide + kollidon VA64. Mol. Pharm. 14 (10), 3370–3380. https://doi.org/10.1021/acs.molpharmaceut.7b00382.
Chmiel, K., Knapik-Kowalczuk, J., Paluch, M., 2019a. How does the high pressure affects the solubility of the drug within the polymer matrix in solid dispersion systems. Eur. J. Pharm. Biopharm. 143 (April), 8–17. https://doi.org/10.1016/j.ejpb.2019.08.003.
Chmiel, K., Knapik-Kowalczuk, J., Jachowicz, R., Paluch, M., 2019b. Broadband dielectric spectroscopy as an experimental alternative to calorimetric determination of the solubility of drugs into polymer matrix: case of flutamide and various polymeric matrixes. Eur. J. Pharm. Biopharm. 136 (July 2018), 231–239. https://doi.org/10.1016/j.ejpb.2019.01.025.
Ignaczak, W., Skov, A.L., El Fray, M., 2020. Interfacial polarization in thermoplastic basalt fiber-reinforced composites. Polymers 12 (7), 1–16. https://doi.org/10.3390/polym12071486 (Basel).
Baeza, G.P., Oberdisse, J., Alegria, A., Couty, M., Genix, A.C., 2015. A high-temperature dielectric process as a probe of large-scale silica filler structure in simplified industrial nanocomposites. Phys. Chem. Chem. Phys. 17 (3), 1660–1666. https://doi.org/10.1039/c4cp04597a.
Gitsas, A., Floudas, G., Wegner, G., 2004. Effects of temperature and pressure on the stability and mobility of phases in rigid rod poly [Formula Presented]-Phenylenes. Phys. Rev. E 69 (4), 8. https://doi.org/10.1103/PhysRevE.69.041802. Stat. Phys. Plasmas Fluids Relat. Interdiscip. Top.

Dr hab. inż. Justyna Knapik-Kowalczuk, Prof. UŚ
Instytut Fizyki
Wydział Nauk Ścisłych i Technicznych
Uniwersytet Śląski
ul. 75 Pułku Piechoty 1A, 41-500 Chorzów

Chorzów, 25.09.2024r.

OŚWIADCZENIE

Oświadczam, że w pracy:

D. Kramarczyk, J. Knapik-Kowalczuk, W. Smolka, M. Ferreira Monteiro, L. Tajber, M. Paluch, *Inhibition of celecoxib crystallization by mesoporous silica – Molecular dynamics studies leading to the discovery of the stabilization origin*. European Journal of Pharmaceutical Sciences, 2022, 171, 106132.

mój udział polegał na uczestnictwie w dyskusji wyników oraz korekcji manuskryptu.

……

Podpis

Maria Ferreira Monteiro
School of Pharmacy and Pharmaceutical Sciences,
Trinity College Dublin,
College Green,
Dublin 2, Ireland

Dublin, 26.09.2024r.

DECLARATION

I declare that in the work:

D. Kramarczyk, J. Knapik-Kowalczuk, W. Smolka, M. Ferreira Monteiro, L. Tajber, M. Paluch, *Inhibition of celecoxib crystallization by mesoporous silica – Molecular dynamics studies leading to the discovery of the stabilization origin*. European Journal of Pharmaceutical Sciences, 2022, 171, 106132.

my participation consisted of performing FTIR studies.

Maria F Monteiro

Signature

Prof. Lidia Tajber
School of Pharmacy and Pharmaceutical Sciences,
Trinity College Dublin,
College Green,
Dublin 2, Ireland

Dublin, 26.09.2024r.

OŚWIADCZENIE

Oświadczam, że w pracy:

D. Kramarczyk, J. Knapik-Kowalczuk, W. Smolka, M. Ferreira Monteiro, L. Tajber, M. Paluch, *Inhibition of celecoxib crystallization by mesoporous silica – Molecular dynamics studies leading to the discovery of the stabilization origin*. European Journal of Pharmaceutical Sciences, 2022, 171, 106132.

mój udział polegał na nadzorowaniu pomiarów FTIR, uczestnictwie w dyskusji na temat otrzymanych wyników oraz poprawie manuskryptu.

.....
(PROF. LIDIA TAJBER) Podpis

Prof. zw. dr hab. Marian Paluch
Instytut Fizyki
Wydział Nauk Ścisłych i Technicznych
Uniwersytet Śląski
ul. 75 Pułku Piechoty 1A, 41-500 Chorzów

Chorzów, 25.09.2024r.

OŚWIADCZENIE

Oświadczam, że w pracy:

D. Kramarczyk, J. Knapik-Kowalczuk, W. Smolka, M. Ferreira Monteiro, L. Tajber, M. Paluch, *Inhibition of celecoxib crystallization by mesoporous silica – Molecular dynamics studies leading to the discovery of the stabilization origin*. European Journal of Pharmaceutical Sciences, 2022, 171, 106132.

mój udział polegał na uczestnictwie w dyskusji na temat otrzymanych wyników.

.....

Podpis

Wojciech Smółka
Katedra i Klinika Laryngologii
Śląski Uniwersytet Medyczny w Katowicach

Katowice, 25.09.2024r.

OŚWIADCZENIE

Oświadczam, że w pracy:

D. Kramarczyk, J. Knapik-Kowalczuk, W. Smolka, M. Ferreira Monteiro, L. Tajber, M. Paluch, *Inhibition of celecoxib crystallization by mesoporous silica – Molecular dynamics studies leading to the discovery of the stabilization origin*. European Journal of Pharmaceutical Sciences, 2022, 171, 106132.

mój udział polegał na uczestnictwie w dyskusji na temat otrzymanych wyników.

Wojciech Smółka

Podpis

3.3. A3 - A3 D. Kramarczyk*, J. Knapik-Kowalczuk, J. Klimontko, M. Kurek, R. Jachowicz, M. Paluch, *Tuning the Physical State of Aripiprazole by Mesoporous Silica*. **2024** Mol. Pharmaceutics 21, 5, 2315–2326.

Impact Factor czasopisma z roku opublikowania pracy: 4.6.
Liczba punktów ministerialnych MNiSW czasopisma z roku opublikowania pracy: 140 pkt.
DOI: 10.1021/acs.molpharmaceut.3c01095.

Udział pierwszego autora w poniżej załączonym artykule polegał na wykonaniu pomiarów kalorymetrycznych oraz dielektrycznych, analizie wszystkich otrzymanych wyników oraz przygotowaniu pierwotnej wersji manuskryptu. Wkład pozostałych współautorów, w formie oświadczeń, zamieszczono na końcu artykułu.

molecular pharmaceutics

pubs.acs.org/molecularpharmaceutics

Article

Tuning the Physical State of Aripiprazole by Mesoporous Silica

Daniel Kramarczyk,* Justyna Knapik-Kowalczuk,* Joanna Klimontko, Mateusz Kurek, Renata Jachowicz, and Marian Paluch

Cite This: *Mol. Pharmaceutics* 2024, 21, 2315−2326

Read Online

ACCESS | Metrics & More | Article Recommendations

ABSTRACT: The main purpose of our studies is to demonstrate that commercially available mesoporous silica (MS) can be used to control the physical state of aripiprazole (ARP). The investigations performed utilizing differential scanning calorimetry and broadband dielectric spectroscopy reveal that silica can play different roles depending on its concentration in the system with amorphous ARP. At low MS content, it activates recrystallization of the active pharmaceutical ingredient and supports forming the III polymorphic form of ARP. At intermediate MS content (between ca. 27 and 65 wt %), MS works as a recrystallization inhibitor of ARP. At these concentrations, the formation of III polymorphic form is no longer favorable; therefore, it is possible to use this additive to obtain ARP in either IV or X polymorphic form. At the same time, employing MS in concentrations >65 wt % amorphous form of ARP with high physical stability can be obtained. Finally, regardless of the polymorphic form it crystallizes into, each composite is characterized by the same temperature dependence of relaxation times in the supercooled and glassy states.

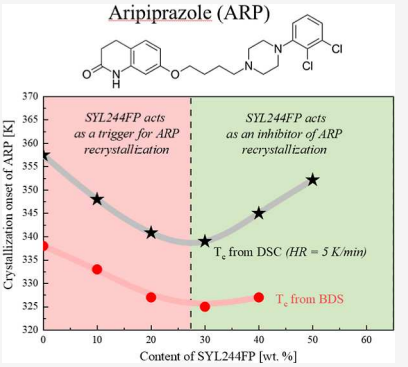

KEYWORDS: *aripiprazole, amorphous, physical stability, polymorphism, silica materials*

1. INTRODUCTION

The manipulation of the physical state of active pharmaceutical ingredients (APIs) is an important and innovative field of pharmaceutical science. This is because by altering the physical form of API, one can improve, among others, the dissolution properties of drug compounds, ultimately increasing their bioavailability and therapeutic efficacy.[1−4] It is crucial, especially because approximately 40% of marketed drugs reveal poor aqueous solubility.[5−8] Furthermore, it is anticipated that up to 90% of new chemical entities will encounter this issue and thus might be rejected from the research and development pipeline.[5,9] The recalled statistics highlight the significance of developing effective strategies to improve the solubility of drugs and thus enhance their therapeutic efficacy and patient outcomes. In the literature, many reports prove that API's aqueous solubility, bioavailability, and dissolution rate can be improved even a dozen times when it is converted to an amorphous or metastable polymorphic form.[10−15]

In general, the improved solubility of pharmaceuticals after conversion to metastable polymorph is associated with differences in molecular packing and surface area in their crystal structure.[12,16] For example, the packing of molecules in the metastable form may be less dense, which can increase the free energy of the system and enhance the solubility. Unlike any polymorphic form of crystalline material, amorphous material does not have a regular arrangement of atoms in a repeating pattern. The lack of long-range molecular order and associated high Gibbs free energy are reasons for its unique properties, including increased solubility and bioavailability compared with their crystalline counterparts. In both described approaches (i.e., a conversion of API having solubility-limited bioavailability to its metastable polymorph or amorphous form), the advantages come at the cost of the material's physical stability. Due to its disordered nature associated with that highest internal energy, an amorphous form reveals the most prominent tendency toward recrystallization.[17−21] In comparison, the metastable polymorph reveals better physical stability than its amorphous counterparts but might also possess a lower solubility. Usually, developing a selective, fully controlled, and reproducible technology for obtaining a specific metastable polymorph of a drug is not easy. It requires a lot of work and time and, frequently, it turns out that the conditions needed for its formation may be difficult to repeat, resulting in problems in manufacturing procedures.[22,23]

In this paper, the impact of mesoporous silica (MS) on the physical state of aripiprazole (ARP) will be presented. The use of ARP, an atypical antipsychotic employed in treating various mood and psychotic disorders, as a model drug was essential.

Received: November 19, 2023
Revised: April 1, 2024
Accepted: April 2, 2024
Published: April 22, 2024

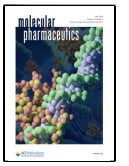

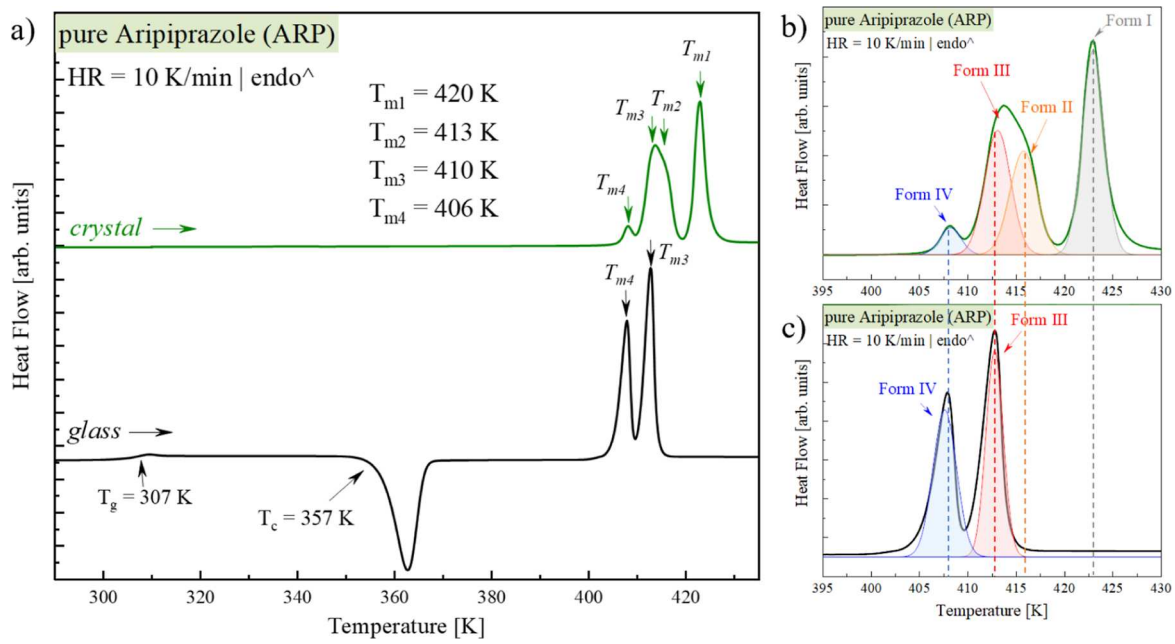

Figure 1. In panel (a), DSC thermograms of crystalline and amorphous ARP are presented. Panels (b,c) present the zoomed areas of meltings.

On the one hand, according to the classification system introduced in 2010 by Baird et al.,[24,25] ARP belongs to the second group of glass-forming substances. This classification divides organic molecules into three classes and links the glass-forming ability of the material with its crystallization tendency from the melt when treated in a particular way (N_2 atmosphere; heating rate 10 K/min; cooling rate 20 K/min; reheating rate 10 K/min). The first class includes nonglass-formers, i.e., compounds that crystallize on cooling the melt at a temperature lower than the melting temperature. Glass formers, which crystallize on heating the melt-quenched material (above its glass transition temperature (T_g)), such as ARP, were defined as class two compounds. At the same time, the third class contains compounds that show no sign of crystallization on heating after the melt-quenching. Consequently, using ARP as a model system, it is possible to investigate, in a relatively quick time, whether the employed MS will effectively improve the physical stability of the amorphous form of ARP. On the other hand, this particular API is characterized by unique structural flexibility, allowing different structural conformations and resulting in nine different polymorphs.[26−29] This makes ARP one of the most polymorphically rich organic crystals discovered so far. Therefore, it will be interesting to check how the employed MS affects the recrystallization tendency of ARP and which polymorphic form is preferred in the ARP−MS composite. The effect of the MS concentration on the formation of different ARP polymorphic forms will also be examined. Consequently, our experiments will assess the mechanism of ARP's stabilization by the MS.[30−36]

To solve all the above issues, this paper uses the neat APR and systems containing ARP and 10, 20, 30, 40, and 50 wt % of Syloid 244FP (SYL244FP). All composites were thoroughly investigated by differential scanning chromatography (DSC) and broadband dielectric spectroscopy (BDS). The results obtained indicated that the chosen MS at low concentrations works as a trigger for ARP's recrystallization, but after reaching a certain content, it starts to play a role as a stabilizer. We show that the observed changes in the stabilization of the ARP amorphous form are associated with the inhibition of nucleation of its III polymorphic form. Consequently, our studies have shown that employing an appropriate amount of MS can control the ARP's physical state.

2. MATERIALS AND METHODS

2.1. Materials. ARP with purity ≥99.0% and molecular mass M_w = 448,4 g/mol was purchased from HyperChem (Zhejiang, China); ARP is chemically described as 7-[4-[4-(2,3-dichlorophenyl)piperazin-1-yl]butoxy]-3,4-dihydro-1*H*-quinolin-2-one. Syloid 244FP (SYL244FP) was received as a gift from Grace GmbH & CO. KG (Worms, Germany). This MS is characterized by an average particle size of 2.5−3.7 μm, a surface area of 314 m^2/g, a pore diameter ∼23 nm, and the pore volume equal to 1.6 mL/g. All chemicals were used as received.

2.2. Sample Preparation. Binary mixtures containing ARP and 10, 20, 30, 40, 50, and 65 wt % of SYL244FP, respectively, were prepared by physically mixing in a mortar. The procedure consisted of about 3 min of mixing, and then the sample was scraped off the mortar wall with a spatula. The mixing procedure was repeated three times. Before each experiment, pure ARP and systems were dried at 373 K for 10 min to remove water contribution. In the BDS experiments, the samples were placed in a parallel-plate cell made of stainless steel (diameter 15 mm and a 0.1 mm gap provided by silica spacer fibers) and then melted in the hot plate at 421 K and quenched on a copper plate. The melting procedure occurred under air conditions with an environmental humidity of approximately 25% RH. In the DSC experiments, the samples were placed in aluminum crucibles (40 μL) and vitrified in situ in the apparatus under dry nitrogen conditions.

2.3. Differential Scanning Calorimetry. Thermal properties of pure ARP and its mixtures with SYL244FP were investigated using a Mettler-Toledo DSC 1 STARe System. The DSC was calibrated for temperature and enthalpy using zinc and indium standards. The instrument had an HSS8

https://doi.org/10.1021/acs.molpharmaceut.3c01095
Mol. Pharmaceutics 2024, 21, 2315−2326

ceramic sensor with 120 thermocouples and a liquid nitrogen cooling station. The measurements were carried out with a heating rate of 10 or 5 K/min. The obtained DSC thermograms were analyzed in Origin (OriginLab Corporation, Northampton, MA, USA) using Multiple Peak Fit analysis based on the Gaussian model. The available tools allowed for a detailed analysis of the melting processes, which was shown in the DSC analysis of pure ARP.

2.4. Broadband Dielectric Spectroscopy. The dielectric measurements of pure ARP and its mixtures containing 10, 20, 30, 40, and 50 wt % of SYL244FP were performed using a Novo-Control GMBH Alpha dielectric spectrometer (Montabaur, Germany). The temperature in this apparatus was controlled by a Quattro temperature controller with temperature stability better than 0.1 K. Nonisothermal studies of ARP + 10, 20, 30, 40, and 50 wt % of SYL244FP were performed in the temperature range from 153 to 308 K with a step of 5 K and from 310 to 342 K with a step of 2 K in a broad frequency range from 10^{-1} to 10^{6} Hz.

2.5. X-ray Diffraction. The X-ray diffraction (XRD) studies of powdered samples (ARP + 10% SYL244FP, ARP + 30% SYL244FP, and ARP + 50% SYL244FP) were performed with a Malvern Panalytical Empyrean diffractometer (Malvern Panalytical Ltd., Malvern, UK) using a nickel filtered Cu K$\alpha_{1,2}$ source (λ = 1.5406 Å) and equipped with a PIXcell^{3D} ultrafast solid-state hybrid detector. Measurements were carried out at room T condition, in reflection mode in the Bragg–Brentano geometry, within the scattering angle 2θ range of 5–70°. Prior to the XRD experiment, the samples (i.e., physical mixtures) were quench cooled, then annealed at 313 K for 20 h, and recrystallized at 353 K for 48 h.

3. RESULTS AND DISCUSSION

3.1. Thermal Properties of Neat ARP. The thermal properties of pure ARP were investigated using DSC. First, crystalline ARP was heated from 280 to 433 K with a heating rate (HR) of 10 K/min. Further, the sample was vitrified in DSC and subsequently reheated with the same temperature range and HR. As presented in Figure 1, the crystalline ARP is characterized by four endothermic peaks, which indicate four different polymorphic forms in the examined sample. These processes are labeled from the right to the left. Consequently, the process with the highest melting temperature has been called form I, and the others have been consistently labeled as form II, III, and IV. The melting points were determined at the onset of the process at temperatures equal to $T_{m\,I}$ = 421 K, $T_{m\,II}$ = 414 K, $T_{m\,III}$ = 410 K, and $T_{m\,IV}$ = 406 K. It is worth noting that peaks characterizing form II and form III overlap, therefore to determine their onsets and peak temperatures, the Multiple Peak Fit analysis in the Origin software was performed. The results are summarized in Table 1, supplemented by the literature data.

Returning to Figure 1, a step-like behavior was revealed during the heating of the amorphous form of ARP, reflecting the glass transition at T_g = 307 K. Further heating of the sample showed a single exothermic process corresponding to a recrystallization that begins at T_c = 357 K, followed by the three endothermic processes reflecting sample melting. As can be seen, the initial crystal of ARP has a different melting characteristic in comparison to the sample after vitrification and recrystallization. The ARP's crystal obtained from devitrification does not form I and II polymorphic forms (which are dominant in the starting material). Instead, it combines III and IV polymorphs.

Table 1. Comparison of the Melting Point Values at the Place of the Beginning and the Maximum for the Obtained Forms During DSC Measurements[a]

form	onset temperature (K)		peak temperature (K)	
I	420.5	422.3[b]	423.0	422.7[c]
II	414.4	416.3[b]	416.5	417.8[c]
III	410.3	412.4[b]	413.8	412.7[c]
IV	406.3	408.1[b]	408.1	408.9[c]

[a]Table also includes literature values. [b]Values taken from Braun et al. (2009).[26] [c]Data digitalized from Braun et al. (2009).[26]

3.2. Molecular Dynamics of Neat Amorphous ARP. As mentioned in the previous section, the main limitation of using amorphous APIs in the pharmaceutical industry is their poor physical stability. Many factors may cause disordered materials to recrystallize; however, the material's molecular mobility is often considered crucial.[37−45]

The dielectric loss spectra were measured using the BDS technique to investigate the molecular dynamics of neat ARP in both glassy and supercooled liquid states. In this experiment, the temperature was increased from 153 to 308 K in the 5 K step (i.e., in the glassy state) and from 310 to 342 K in the 2 K step (i.e., in the supercooled liquid state). The representative spectra are shown in Figure 2. For better visualization, the data are divided into two panels presenting spectra collected at temperatures above and below the glass transition temperature of APR. As can be seen, three main features characterize the spectra of ARP collected at $T > T_g$ (panel a). On the low-frequency side, the DC conductivity associated with the translational motion of residual ion impurities can be distinguished. Next, looking toward higher frequencies, two relaxation processes are visible: (i) very well-pronounced structural (α) relaxation, which reflects the cooperative motions of entire molecules, and (ii) the barely seen secondary (β) process. As can be seen, the α-relaxation peak is shifted toward higher frequencies with increasing temperature. Note that at 338 K, a drastic drop in the α-relaxation peak intensity was registered. Such behavior is a manifestation of sample recrystallization. This is a consequence of the reduction in the total number (N) of actively reorienting dipoles (μ), which contribute to the structural relaxation process once the fraction of the amorphous phase decreases ($N\mu^2 \sim \varepsilon_s - \varepsilon_\infty = \Delta\varepsilon = \frac{2}{\pi}\int_0^\infty \varepsilon''(\omega)\mathrm{d}\ln\omega$).[46]

Since the secondary relaxation processes originate from the local (intra- or intermolecular) motions of the molecules, they are much faster than the structural relaxation. These relaxation processes are usually better visible on the dielectric loss spectra collected at temperatures below the material's T_g (i.e., in a glassy state). As shown in Figure 2b, ARP is characterized by two secondary relaxation processes. The nature of both of these secondary relaxations will be discussed later in this paper.

To check whether or not the shape of the α-relaxation peak remains constant in the whole examined temperature range, a so-called masterplot has been constructed (see Figure 3a) by the horizontal shifting of dielectric spectra taken at temperatures from 302 to 326 K to superimpose on the reference spectrum at 312 K. Next, the Kohlrausch–Williams–Watts (KWW) function[47] has been used to describe the shape of dielectric loss spectra (see the red lines in Figure 3a). The

https://doi.org/10.1021/acs.molpharmaceut.3c01095
Mol. Pharmaceutics 2024, 21, 2315−2326

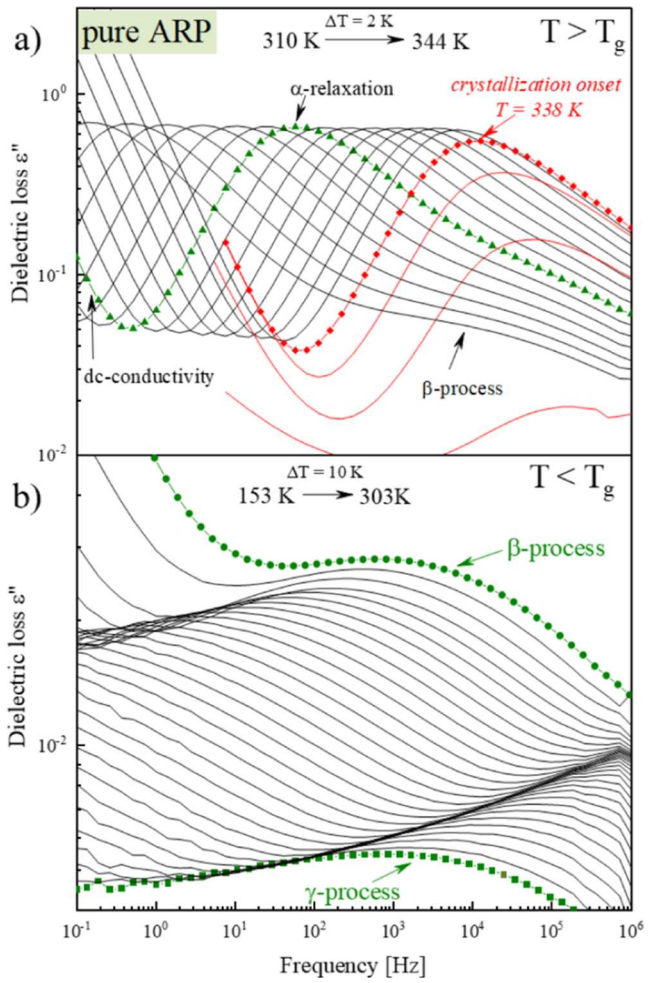

Figure 2. Dielectric spectra of amorphous ARP obtained (a) above T_g and (b) below T_g.

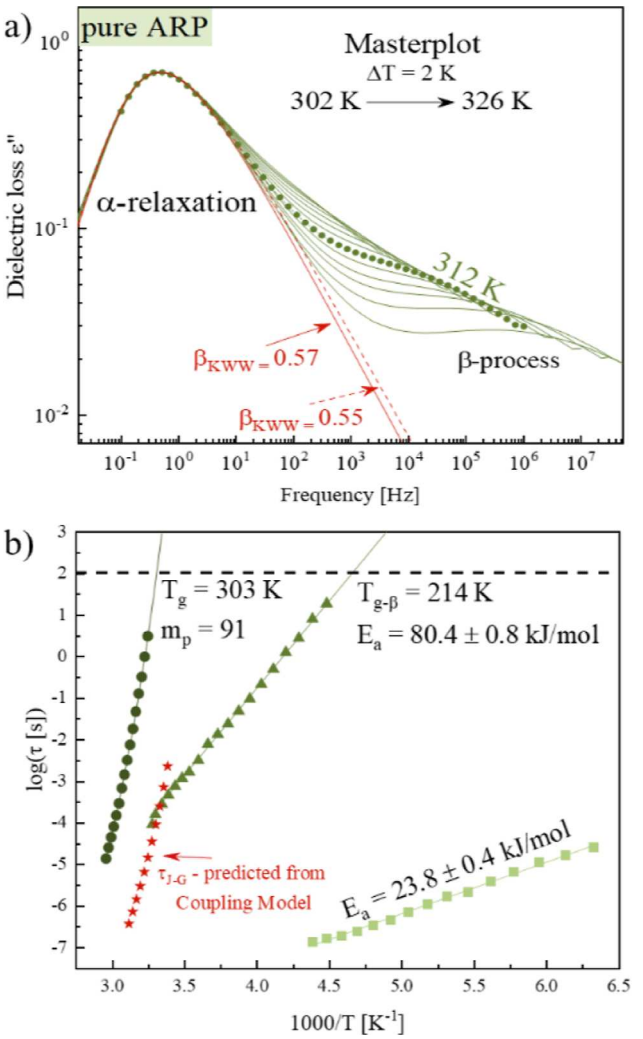

Figure 3. Panel (a) presents the analysis of the widening of the structural relaxation process and (b) presents the analysis of relaxation times of ARP.

stretch exponent in the KWW function, β_{KWW}, takes values from 0 to 1. The value of 1 represents the narrow and symmetrical peak. When the β_{KWW} value decreases, the α-peak widens and becomes increasingly asymmetric. In the case of ARP, an increase in the temperature causes a slight broadening of the α-peak. For the lowest presented temperature, the β_{KWW} parameter is 0.57, while for the temperature higher by 24 K, β_{KWW} is 0.55. In this case, the α-peak broadening phenomenon is due to the presence of a secondary β-process on the right-side wing of the α-process that widens the structural relaxation peak.

From further analysis of ARP's dielectric loss spectra, the temperature dependences of the relaxation times of the α-, β-, and γ-relaxation processes were obtained (see Figure 3b). For this purpose, the asymmetric structural relaxation process as well as symmetric secondary relaxation processes have been fitted using the Havriliak–Negami (HN) and the Cole–Cole (CC) functions, respectively. The empirical HN is defined as follows[48]

$$\varepsilon^*(\omega) = \varepsilon_\infty + \frac{\Delta\varepsilon}{[1 + (i\omega\tau_{HN})^a]^b} \quad (1)$$

where ε_∞ is the high-frequency limit permittivity, ε_0 denotes the permittivity of vacuum, $\Delta\varepsilon$ is dielectric strength, ω is equal to $2\pi f$, τ_{HN} is the HN relaxation time, and a and b represent symmetric and asymmetric broadening of the relaxation peak.

When the b parameter is equal to 1, the HN function becomes the CC function, which was used to fit the secondary relaxations of ARP. The obtained fit parameters were then used to calculate the τ_α, τ_β, and τ_γ in accordance with the equation

$$\tau_{\alpha/\beta/\gamma} = \tau_{HN}\left[\sin\left(\frac{\pi a}{2 + 2b}\right)\right]^{1/a}\left[\sin\left(\frac{\pi ab}{2 + 2b}\right)\right]^{-1/a} \quad (2)$$

As can be seen in Figure 3b, in the supercooled liquid region, the temperature evolution of the structural (α) relaxation time of ARP (represented as a circle points) can be well described by the Vogel–Fulcher–Tammann (VFT) equation[49−51]

$$\tau_\alpha(T) = \tau_\infty \exp\left(\frac{DT_0}{T - T_0}\right) \quad (3)$$

with corresponding fitting parameters equal to $\log_{10}(\tau_\infty) = 15.73 \pm 0.78$, $T_0 = 248.0 \pm 0.3$ K, and $D = 2257 \pm 11$. To estimate the kinetic glass transition temperature of the investigated API, the commonly known definition of $T_g = T(\tau_\alpha = 100\ s)$ was employed. The extrapolation of $\tau_\alpha(T)$ dependence to $\tau_\alpha = 100$ s gives the value of the glass transition

https://doi.org/10.1021/acs.molpharmaceut.3c01095
Mol. Pharmaceutics 2024, 21, 2315−2326

temperature equal to T_g = 303 K. It is worth noting that this value corresponds well with that obtained from DSC experiments. A slight difference in these values results from the differences in the heating rates employed in BDS and DSC experiments. Based on VFT fits, one can also calculate the steepness index (m_p), also called the fragility parameter, which is defined as follows[52]

$$m_p = \left.\frac{\mathrm{d}\log_{10}\tau_\alpha}{\mathrm{d}(T_g/T)}\right|_{T=T_g} \quad (4)$$

The typical values of the steepness index for various materials vary between 16 and 200. The determined fragility parameter of ARP is equal to m_p = 91.

Now, we return to the discussion on the molecular origin of the ARP's secondary relaxations. As can be seen in Figure 3b, in the glassy state, the temperature evolutions of both τ_β and τ_γ exhibit a linear behavior. Thus, these dependencies can be well parametrized by the Arrhenius equation, defined as follows

$$\tau_{\beta/\gamma}(T) = \tau_\infty \exp\left(\frac{E_a}{RT}\right) \quad (5)$$

where τ_∞ is the pre-exponential factor, E_a is the energy barrier, and R is the gas constant. The resulting fit parameters of ARP's secondary processes are collected in Table 2.

Table 2. Fit Parameters are for Secondary Relaxation Processes[a]

secondary relaxation	log τ_∞	E_a [kJ/mol]	type/origin
β	−17.57 ± 0.01	80.4 ± 0.8	JG/intramolecular
γ	−12.39 ± 0.11	23.8 ± 0.4	non-JG/intermolecular

[a]The table also shows the type and the origin of the process.

Secondary relaxations might be of two types: intra- or intermolecular secondary relaxations. The intramolecular secondary relaxations, also known as non-Johari−Goldstein (non-JG) processes, originate from motions that involve only a subset of the entire molecule. Meanwhile, the intermolecular secondary relaxations, called Johari−Goldstein (JG) processes, come from the local motions of the whole molecule.[53] Taking into account that the latter are believed to be precursors of structural relaxation, it can be responsible for the recrystallization process of amorphous APIs. Consequently, from the point of view of physical stability, it is important to identify the molecular origin of the secondary relaxations of ARP. For this purpose, we applied the coupling model according to which τ_{JG} is related to the α-relaxation time (τ_α) as follows

$$\tau_{JG} \approx \tau_0 = (t_c)^{1-\beta_{KWW}}(\tau_\alpha)^{\beta_{KWW}} \quad (6)$$

herein, τ_0 is the primitive relaxation time, while t_c is the onset time of intermolecular coupling, which for small molecules (such as ARP) is equal to 2 ps. The values of τ_{JG} determined based on the recalled approach for several temperatures above T_g of ARP are shown as red stars in Figure 3b. Since the temperature dependence of τ_{JG} appears to be the continuation of the experimentally obtained $\tau_\beta(T)$ one can classify the β-relaxation of ARP as the JG process. At the same time, γ-relaxation is a non-JG processes. The observed complex molecular mobility of amorphous ARP (including the presence of the JG process−the precursor of structural relaxation) well reflects the limited physical stability of this material, which was revealed during both nonisothermal BDS and DSC experiments.

3.3. Influence of MS on the Thermal Properties of Supercooled ARP. To investigate the influence of MS on the thermal properties of supercooled ARP, the systems containing ARP and 10, 20, 30, 40, and 50 wt % of SYL244FP have been measured nonisothermally using the DSC. Samples were vitrified in DSC and subsequently reheated from 280 to 433 K with an HR of 5 K/min. Each experiment was performed in triplicate, while the representative DSC traces are presented in Figure 4a.

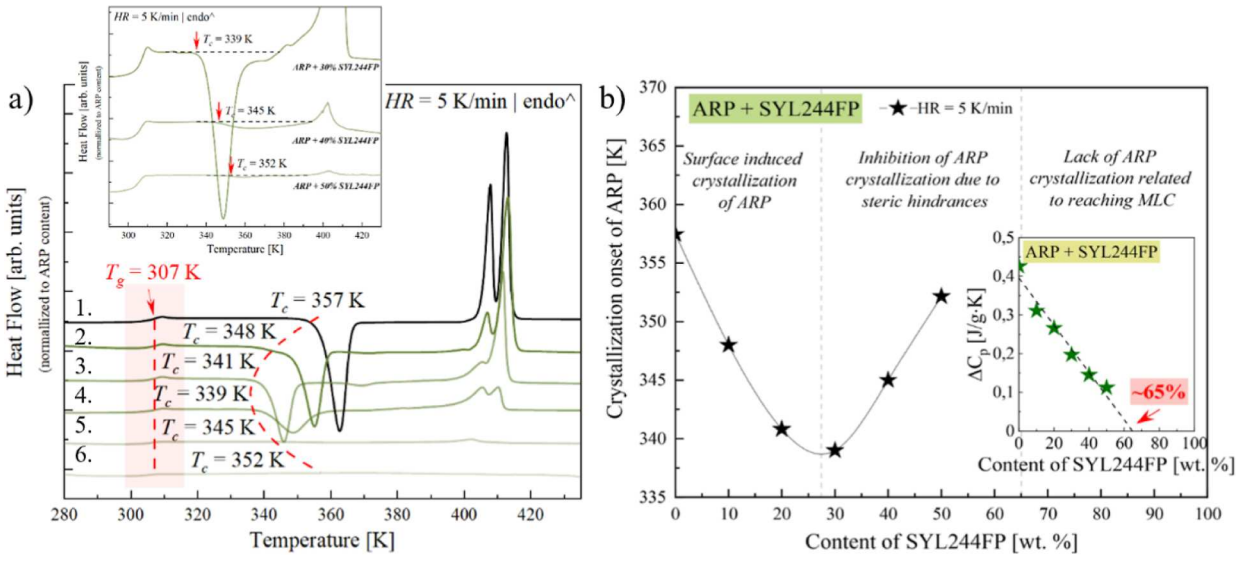

Figure 4. Panel (a) presents DSC thermograms of vitrified ARP and the systems ARP with SYL244FP; inset presents the zoomed area of the panel (a). Panel (b) presents the dependence of the crystallization temperature on the concentration of the tested systems. Inset presents the ΔC_p dependence on the content of SYL 244FP [wt %].

https://doi.org/10.1021/acs.molpharmaceut.3c01095
Mol. Pharmaceutics 2024, 21, 2315−2326

As can be seen, the employed MS has no impact on the glass transition temperature of ARP. All systems are characterized by the same value of T_g equal to 307 K. A similar pattern of behavior has been previously found in the cases of simvastatin and celecoxib. However, with increasing SYL244FP, one can observe the decrease in ΔC_p at the glass transition temperature (T_g). This behavior results from the extensive and additive properties of ΔC_p. The value of ΔC_p is proportional to the amorphous fraction of API and decreases linearly with decreasing drug content. If drug molecules are absorbed on the surface of MS, they are not contributing to any thermal event since they are "immobilized" through interactions with the functional groups of the MS surface. Consequently, by determining the ΔC_p value and extrapolation to zero, one can evaluate the monomolecular loading capacity (MLC) of the drug in the MS. The described approach has been introduced by Hempel et al. Based on this method,[54] the MLC of ARP molecules on the surface of SYL244FP was determined. For that purpose, the ΔC_p of ARP-SYL244FP was plotted as a function of MS concentration (see the green stars in the inset of Figure 4b). Subsequently, the experimentally determined dependence was parametrized by a linear function. From the fit extrapolation to $\Delta C_p = 0$, the SYL244FP content, which guarantees enough space to form MLC of ARP on the silica surface, was determined to be 65% (see the dashed line in the inset of Figure 4b). Herein, it is worth pointing out that the composition corresponding to the MLC of the drug molecules on the silica surface is believed to provide a high physical stability of the API. This is connected with the "immobilization" of the drug molecules on the silica surface that finally blocks the drug recrystallization.

To recognize how the employed silica modifies the physical stability of ARP, we analyzed the exothermal processes associated with the recrystallization of ARP from the systems containing different SYL244FP concentrations. As can be seen on the thermograms presented in Figure 4a, for low concentrations of SYL244FP (up to ca. 30 wt %), the additive facilitates ARP's recrystallization, which is reflected in the significant shift of the onset of the API crystallization process to the lower temperature. After reaching some critical concentration (attributed to ARP + 27.3 wt % SYL244FP), the onset of ARP's recrystallization shifts toward higher temperatures with increasing SYL244FP content. From that moment, the stabilizing effect dominates until it reaches a concentration that provides the MLC of the drug molecules on the silica surface, for which crystallization should not occur. Thus, for higher silica concentrations (>30 wt %), the excipient becomes the stabilizer of the API. The described behavior, i.e., modification of recrystallization onset of ARP in the presence of the MS, has been graphically shown in Figure 4b.

To answer the question of why, at low concentrations, MS triggers ARP's recrystallization, while at higher concentrations, it works as a stabilizer, it is worth analyzing the melting endotherms of ARP obtained after heating the ARP + SYL244FP systems. For comparative analysis, the obtained heating curves were normalized to the amount of ARP present in a given sample since silica does not contribute to the melting process (Figure 5a). Based on this analysis, one can notice that first (i.e., up to a concentration containing 20 wt % of SYL244FP), form III dominates over the other polymorphic forms of ARP (i.e., form IV). For concentrations equal to 30 wt % of SYL244FP, the contribution of other crystalline fractions (for instance, no IV) becomes more pronounced. Consequently, form III is no longer dominant over the other ARP's polymorphs. Further increasing the SYL244FP content leads to a substantial decrease in the API's tendency to recrystallize. Furthermore, during the devitrification, some other polymorph appeared.

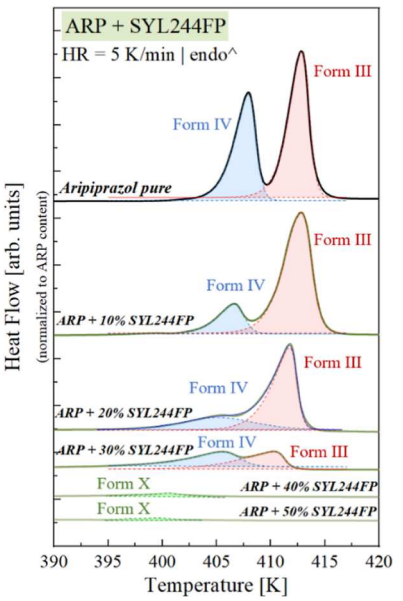

Figure 5. DSC thermograms of vitrified ARP and the systems ARP with SYL244FP that have been normalized to the amount of ARP in the system.

Considering all of the above, it has been hypothesized that SYL244FP modifies the recrystallization behavior of ARP by affecting its nucleation. To verify this hypothesis, one should first investigate the impact of the employed MS on the molecular dynamics of ARP. As mentioned in Section 3.2, molecular dynamics is believed to be the critical factor governing the physical stability of amorphous materials. Until now, we have discovered that the employed silica does not plasticize or antiplasticize ARP (has no impact on the API T_g). Further studies have been performed to investigate whether SYL244FP affects the temperature evolution of structural and/or secondary relaxation times, as well as the shape of these processes.

3.4. Influence of MS on the Molecular Dynamics of Both Glassy and Supercooled ARP. To provide a complete picture of how the employed MS impacts the ARP's molecular dynamics, the binary systems containing ARP and 10, 20, 30, 40, and 50% of SYL244FP were investigated using the BDS. The dielectric loss spectra were measured on heating at temperatures ranging from 173 to 303 K in step of 10 K, and from 305 to 363 K in step of 2 K. The representative spectra, i.e., for systems containing 10, 30, and 50% of SYL244FP, are shown in Figure 6. Gray lines represent spectra collected at $T < T_g$, and black at $T > T_g$, dashed black lines indicate spectra measured during the recrystallization process, while spectra marked as red lines were measured after the recrystallization. With increasing SYL244FP content, a decrease in the dielectric response is noted, which is obviously connected with the reduction of the ARP fraction in the system (silica does not contribute to the dielectric response). Regardless of the amount of silica used in the composite, the dielectric loss spectra of ARP recorded at $T < T_g$ are characterized by two secondary relaxation processes—β and γ, whose peaks shift

https://doi.org/10.1021/acs.molpharmaceut.3c01095
Mol. Pharmaceutics 2024, 21, 2315−2326

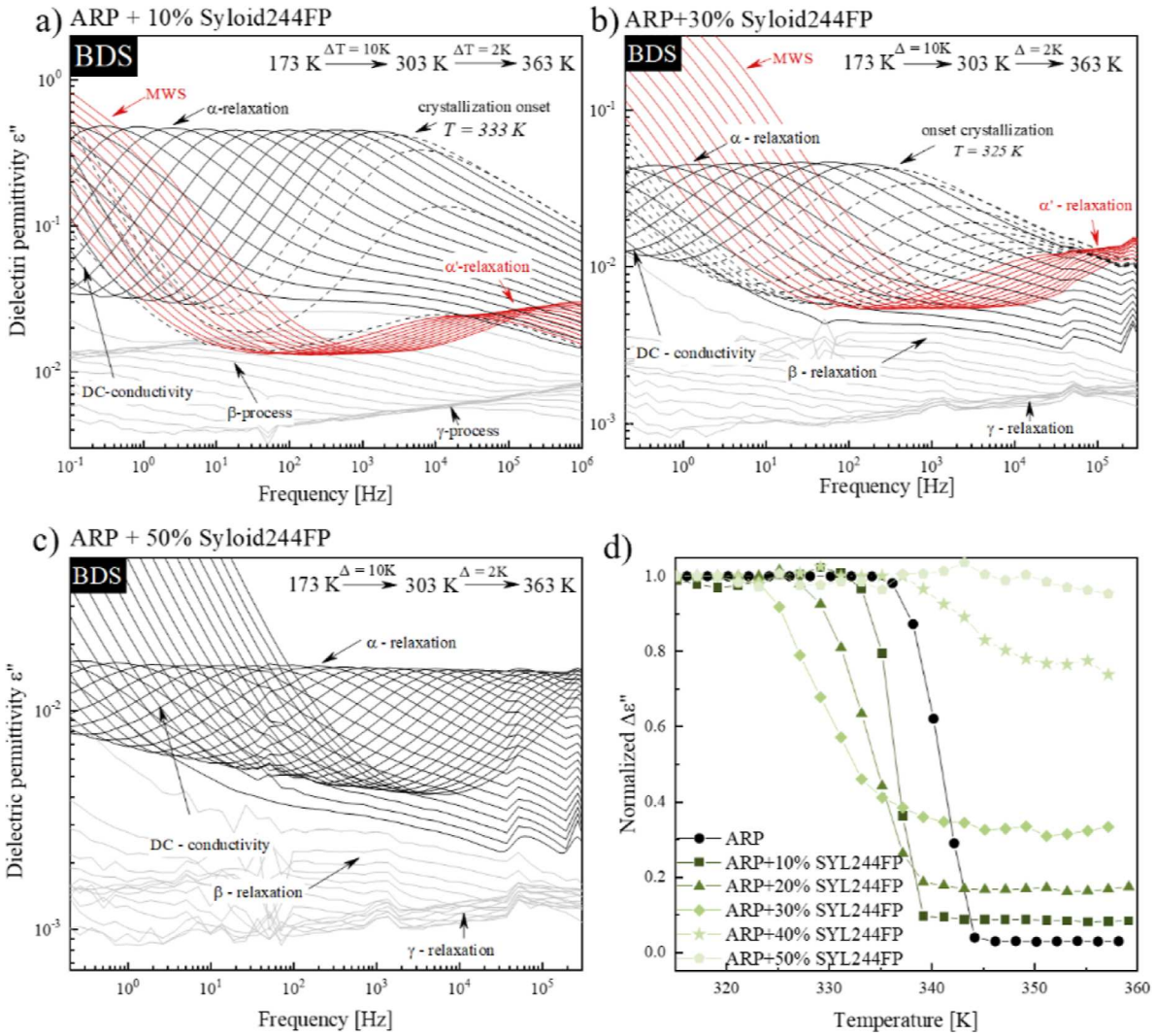

Figure 6. Dielectric loss spectra of ARP + SYL244FP containing (a) 10, (b) 30, and (c) 50% of silica. Panel d presents the normalized value of $\Delta\varepsilon$.

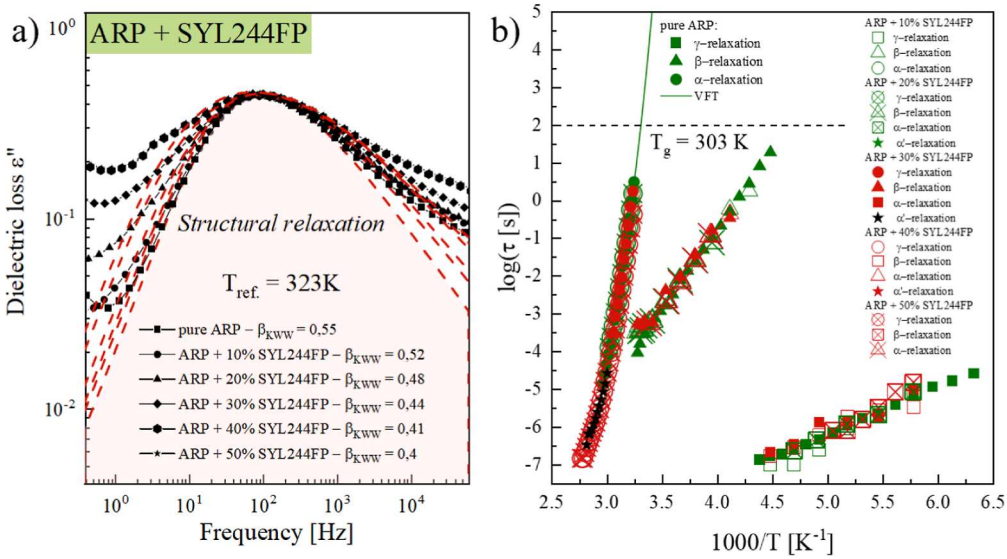

Figure 7. Panel (a) presents a comparison of the dielectric spectra of various concentrations of the ARP + SYL244FP systems recorded at T = 313 K. The dashed red lines represent the KWW fit to the α-peak with a value of β_{KWW} given in the legend. Panel b presents the relaxation map of studied systems ARP + SYL244FP. The VFT equation was applied to describe structural relaxation times.

https://doi.org/10.1021/acs.molpharmaceut.3c01095
Mol. Pharmaceutics 2024, 21, 2315−2326

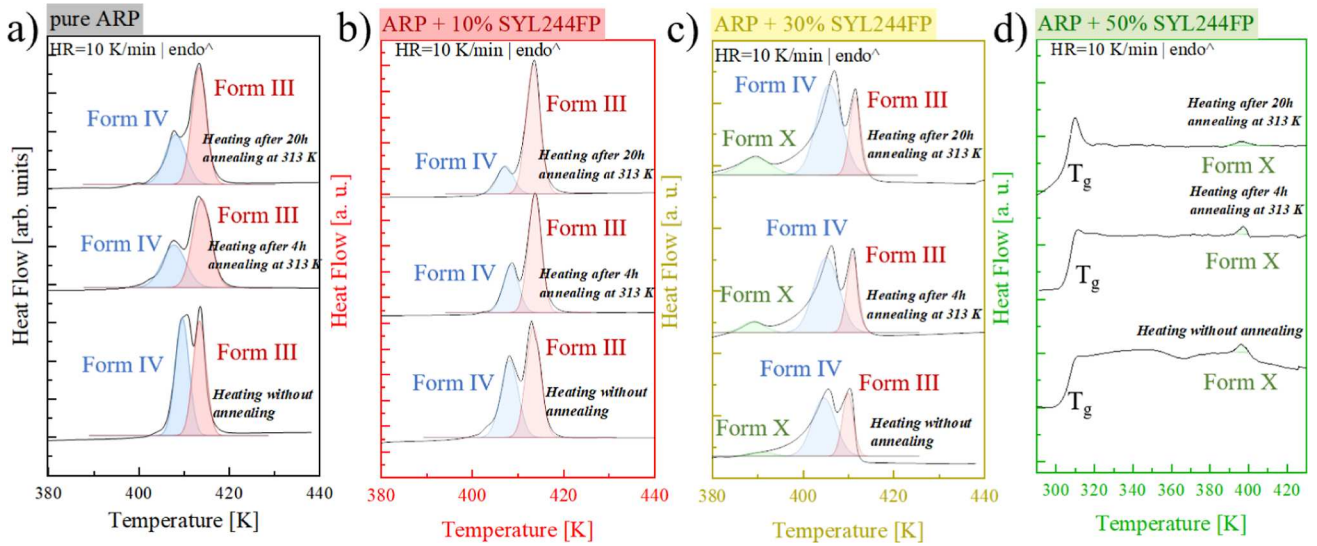

Figure 8. DSC thermograms obtained for quenched samples and after the finished isothermal measurements for (a) pure ARP, (b) ARP + 10% SYL244FP, (c) ARP + 30% SYL244FP and (d) ARP + 50% SYL244FP.

toward higher frequencies with increasing temperature. On the other hand, at $T > T_g$, three main features can be noted on the ARP's spectra. On the low-frequency side, the DC conductivity can be distinguished. Next, the very well-pronounced α—relaxation and secondary β—process are visible.

It should be noted that for concentrations from 10 to 40% of SYL244FP, the recrystallization of ARP from the system was observed as a drastic drop in the intensity of the α-relaxation peak. The onset of recrystallization was registered at 333, 327, 325, and 337 K for systems containing 10, 20, 30, and 40% SYL244FP, respectively. Consequently, the dielectric and calorimetric studies reveal similar recrystallization behaviors of ARP in MS composites. For a low silica content, the additive accelerates API recrystallization. However, after reaching a concentration of 30%, the silica material suppressed ARP's recrystallization and became its stabilizer. For example, there is no recrystallization during the nonisothermal dielectric measurement of the sample containing 50% of SYL244FP (see Figure 6c). At this point, it is worth noting that ARP's recrystallization is always incomplete in the SYL244FP composite (i.e., even for the lowest employed concentration −10% of SYL244FP). In other words, some fraction of ARP remains amorphous after the recrystallization process. The dielectric signature of uncompleted recrystallization of ARP is the presence of the residual α'-relaxation process in the dielectric loss spectra (see red spectra in Figure 6a,b). The higher the content of SYL244FP, the greater the extent to which the API fraction remains amorphous after recrystallization. To compare the recrystallization tendency of ARP in silica composites, the normalized values of $\Delta\varepsilon_N$ are plotted as a function of temperature in Figure 6d. The normalization has been performed as follows: $\Delta\varepsilon_N = \Delta\varepsilon(T)/\Delta\varepsilon(T = 312\ \mathrm{K})$.

Next, we compared the spectra registered at a reference temperature of 323 K for samples characterized by various silica content. As shown in Figure 7, with increasing the amount of SYL244FP, the α-relaxation peak of ARP becomes broader, which is reflected by a smaller β_{KWW} parameter, i.e., β_{KWW} of pure ARP oscillates around 0.55, and it drops down to 0.4 for a sample containing 50% of SYL244FP. Such behavior is associated with an increase in heterogeneity in the sample.[55,56]

The next step of the dielectric loss spectra analysis is to investigate how silica affects the temperature dependences of the α-, β-, and γ-relaxation times. For this purpose, a similar analysis as that presented in Section 3.2 was performed. The asymmetric α-relaxation as well as the symmetric β- and γ-relaxation processes were fitted using the HN and the CC functions, respectively. The obtained fit parameters were subsequently employed to calculate the τ_α, τ_β, and τ_γ following eq 2. Determined by this approach, the temperature evolutions of α-, β-, and γ-relaxation times of ARP-SYL244FP composites are plotted in Figure 7b. As noted, the employed silica does not significantly impact the temperature dependencies for both structural or secondary relaxation times of ARP. No significant changes in the molecular dynamics of the tested API in MS composites suggest that the silica modifies the physical stability of ARP by affecting its nucleation. The performed analysis also proved that the α'-relaxation process visible after recrystallization is associated with the structural α-relaxation of the nonrecrystallized fraction of ARP. This conclusion was drawn from the continuation of the temperature evolution of τ_α by $\tau_{\alpha'}$ visible in Figure 7b.

3.5. Effect of Annealing on the Formation of Different Polymorphs of ARP from the Systems Containing SYL244FP. So far, our research has demonstrated that the primary mechanism behind the enhanced physical stability of ARP in MS composites is suppressed nucleation. Therefore, it would be interesting to see whether the nucleation time affects the polymorph characteristics of ARP. For this reason, a series of calorimetric studies have been performed on samples containing 0, 10, 30, and 50% SYL244FP. Each sample was subjected to three types of tests. During these experiments, the most important was the annealing step conducted at a temperature 6 K higher than ARP's T_g—the temperature at which the maximum nucleation was noted (data not shown).

In all types of experiments, the first step includes heating the sample at a rate of 10 K/min from 298 to 433 K followed by quick (with a rate of 20 K/min) cooling to 298 K. This step aimed to melt and quench the ARP. After that, in the first type of experiment, the sample was reheated to 438 K with 10 K/min (experiment without annealing). In the second and third

https://doi.org/10.1021/acs.molpharmaceut.3c01095
Mol. Pharmaceutics 2024, 21, 2315−2326

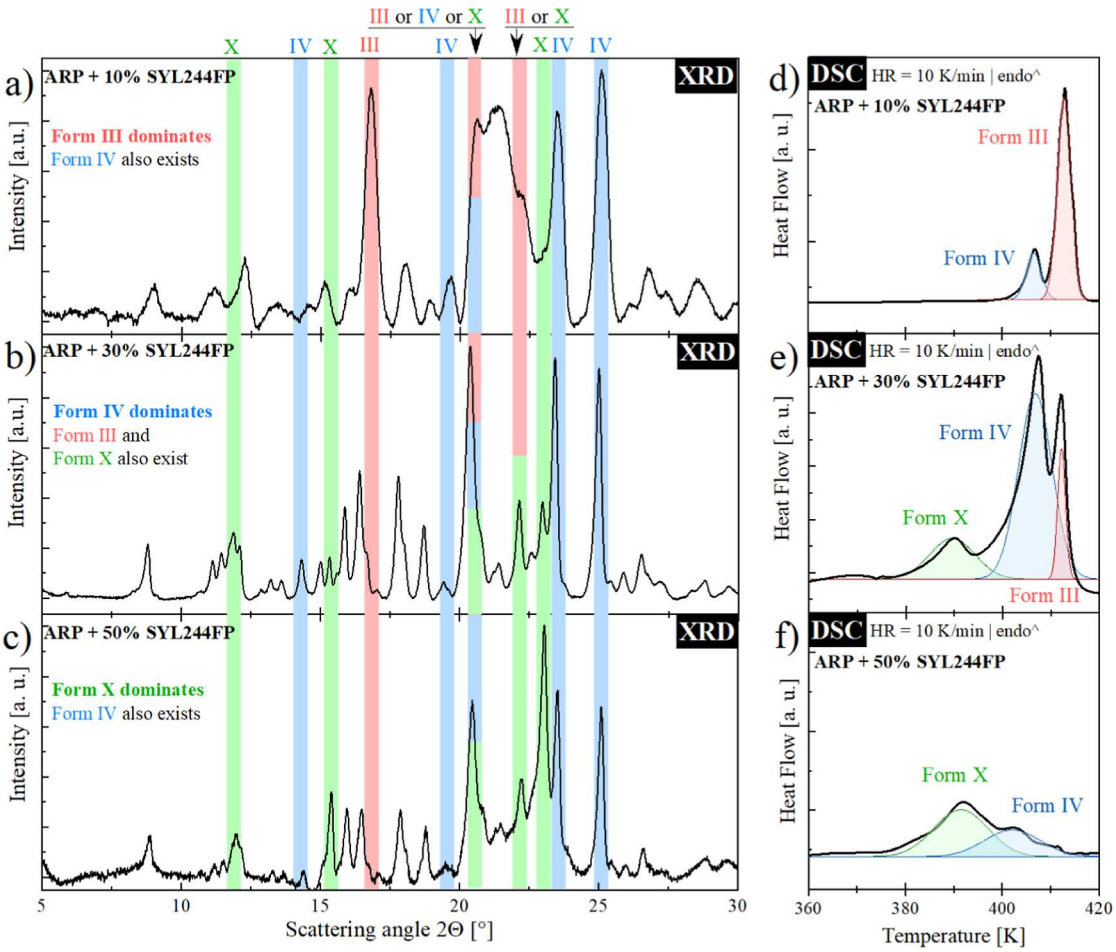

Figure 9. (a–c) XRD patterns and (d–f) DSC thermograms of ARP + MS composites.

types of experiments, the reheating step was interrupted by an additional isothermal step at 313 K. The annealing time was set to 4 or 20 h, for the second and third types of experiments, respectively. After this step, the reheating run was continued to 438 K at a 10 K/min rate. The chosen annealing temperature corresponds to the maximum of the ARP's nucleation curve. Thus, any modification in the melting behavior of the annealed ARP in the composite should indicate the role of MS in ARP nucleation.

The obtained results are summarized in Figure 8. Panel a of this figure refers to a neat ARP and its behavior during the annealing procedure. The significant increase of fraction III over those of other polymorphic forms can be noted by elongating the annealing time. When the small concentration of MS is considered (i.e., up to 27% that speeds up the recrystallization of the API), one can observe an increase of fraction III over polymorphic form IV. On the other hand, for a composite containing 30 wt % of SYL244FP, a drastic change in the melting behavior of the recrystallized sample is observed. Now, form IV dominates; however, some substantial contribution of other, so far undefined polymorph, appears. Furthermore, the annealing brings more nuclei of IV and undefined polymorphs. It is reflected in the more pronounced melting peaks at 385 and 403 K compared to the nearly unchanged melting of form III. A further increase in the MS loading leads to the vanishing of the III ARP polymorphic form. Instead, a slight crystallization to some other polymorph takes place. This is visualized in Figure 8d, where the DSC thermograms of ARP + 50 wt % of SYL244FP are summarized.

Herein, it would be interesting to identify the ARP polymorph existing in compositions containing 30 and 50% wt MS. For this purpose, the XRD measurements have been performed. As shown in Figure 9, recrystallization of ARP from 10 wt % composition indeed brings III and IV polymorphs, while the significant contribution of the former one is observed. However, when the MS loading is increased to 30 wt %, three polymorphs exist in the sample: III, IV, and form X, discovered for the first time in ref 26. Further increase in MS concentration results in crystallization to form X. At the same time, XRD signals from form IV are also observed, while the formation of III polymorph is entirely suppressed.

The results presented in this section indicate that the visible modifications in the ARP's physical stability after the employment of MS are associated with the modifications in the API nucleation.

4. CONCLUSIONS

This paper investigated the impact of commercially available MS material, SYL244FP—on the physical stability of supercooled ARP. Our studies revealed unusual recrystallization of API for various content of MS. It has been shown that depending on the concentration of SYL244FP, this additive can trigger, delay, or even block the API recrystallization. Low silica content accelerates the recrystallization of ARP. Using the intermediate content of the MS (i.e., between 27 and 65 wt

https://doi.org/10.1021/acs.molpharmaceut.3c01095
Mol. Pharmaceutics 2024, 21, 2315−2326

%), one can inhibit the recrystallization of API. At the same time, high silica concentrations (i.e., >65 wt %) guarantee high physical stability of the drug. A series of calorimetric and dielectric studies were performed to determine the molecular origin of these results. Dielectric and calorimetric experiments indicated that the examined silica material (in any measured concentration) does not modify either the glass transition temperature of ARP or the temperature evolution of its structural (α) or secondary (β and γ) relaxation times. Consequently, the effect of additives on the molecular dynamics of ARP has been excluded from the factors governing the physical stability of ARP. Instead, two other molecular sources of the observed effects can be considered. One is the "immobilization" of the drug molecules on the surface of the silica. The visible effect of this mechanism is an increasing fraction of amorphous API after recrystallization from composites of higher MS content. On the other hand, it has been shown that the silica material affects ARP nucleation. At low concentrations, the MS supports forming the III polymorphic form of ARP. However, when the amount of SYL244FP is $\geq$ 27 wt %, the formation of the III polymorphic form is no longer favorable. This is because the nuclei of forms IV and X are preferred. Moreover, the crystal growth of forms IV and X takes longer in comparison to that of form III. Additionally, a significant modification in the recrystallization tendency of amorphous ARP was observed when various silica contents were employed. The presented finding demonstrates that by changing the MS loading and controlling the experiment conditions, one can tune the physical state of the ARP.

AUTHOR INFORMATION

Corresponding Authors

Daniel Kramarczyk − *Faculty of Science and Technology, Institute of Physics, University of Silesia in Katowice, SMCEBI, 41-500 Chorzów, Poland;* orcid.org/0000-0003-0783-0122; Email: daniel.kramarczyk@smcebi.edu.pl

Justyna Knapik-Kowalczuk − *Faculty of Science and Technology, Institute of Physics, University of Silesia in Katowice, SMCEBI, 41-500 Chorzów, Poland;* orcid.org/0000-0003-3736-8098; Email: justyna.knapik-kowalczuk@us.edu.pl

Authors

Joanna Klimontko − *Faculty of Science and Technology, Institute of Physics, University of Silesia in Katowice, SMCEBI, 41-500 Chorzów, Poland*

Mateusz Kurek − *Department of Pharmaceutical Technology and Biopharmaceutics, Faculty of Pharmacy, Jagiellonian University, 30-688 Kraków, Poland*

Renata Jachowicz − *Department of Pharmaceutical Technology and Biopharmaceutics, Faculty of Pharmacy, Jagiellonian University, 30-688 Kraków, Poland*

Marian Paluch − *Faculty of Science and Technology, Institute of Physics, University of Silesia in Katowice, SMCEBI, 41-500 Chorzów, Poland;* orcid.org/0000-0002-7280-8557

Complete contact information is available at: https://pubs.acs.org/10.1021/acs.molpharmaceut.3c01095

Notes

The authors declare no competing financial interest.

ACKNOWLEDGMENTS

The authors are grateful for the financial support received within Project no. 2018/31/B/ST8/01327 (OPUS 16) from the National Science Centre, Poland. The studies were implemented as part of the strategy of the University of Silesia—Inicjatywa Doskonałości (POB 1—Priorytetowy Obszar Badawczy 1: Harmonijny rozwój człowieka—troska o ochronę zdrowia i jakość życia). The authors wish to express their thanks for the materials received as a gift from Grace GmbH & CO. KG (Worms, Germany).

REFERENCES

(1) Patra, J. K.; Das, G.; Fraceto, L. F.; Campos, E. V. R.; Rodriguez-Torres, M. D. P.; Acosta-Torres, L. S.; Diaz-Torres, L. A.; Grillo, R.; Swamy, M. K.; Sharma, S.; et al. Nano Based Drug Delivery Systems: Recent Developments and Future Prospects. *J. Nanobiotechnol.* **2018**, *16* (1), 71.

(2) Sahoo, S. K.; Labhasetwar, V. Nanotech Approaches to Drug Delivery and Imaging. *Drug Discovery Today* **2003**, *8* (24), 1112−1120.

(3) Bharti, C.; Gulati, N.; Nagaich, U.; Pal, A. Mesoporous Silica Nanoparticles in Target Drug Delivery System: A Review. *Int. J. Pharm. Investig.* **2015**, *5* (3), 124.

(4) Trzeciak, K.; Chotera-ouda, A.; Bak-sypien, I. I.; Potrzebowski, M. J. Mesoporous Silica Particles as Drug Delivery Systems—the State of the Art in Loading Methods and the Recent Progress in Analytical Techniques for Monitoring These Processes. *Pharmaceutics* **2021**, *13* (7), 950.

(5) Andersson, J.; Rosenholm, J.; Areva, S.; Lindén, M. Influences of Material Characteristics on Ibuprofen Drug Loading and Release Profiles from Ordered Micro- and Mesoporous Silica Matrices. *Chem. Mater.* **2004**, *16* (21), 4160−4167.

(6) Hashim Ali, K.; Mohsin Ansari, M.; Ali Shah, F.; Ud Din, F.; Abdul Basit, M.; Kim, J. K.; Zeb, A. Enhanced Dissolution of Valsartan-Vanillin Binary Co-Amorphous System Loaded in Mesoporous Silica Particles. *J. Microencapsul.* **2019**, *36* (1), 10−20.

(7) Ren, X.; Cheng, S.; Liang, Y.; Yu, X.; Sheng, J.; Wan, Y.; Li, Y.; Wan, J.; Luo, Z.; Yang, X. Mesoporous Silica Nanospheres as Nanocarriers for Poorly Soluble Drug Itraconazole with High Loading Capacity and Enhanced Bioavailability. *Microporous Mesoporous Mater.* **2020**, *305* (June), 110389−110398.

(8) Zhang, Y.; Wang, J.; Bai, X.; Jiang, T.; Zhang, Q.; Wang, S. Mesoporous Silica Nanoparticles for Increasing the Oral Bioavailability and Permeation of Poorly Water Soluble Drugs. *Mol. Pharm.* **2012**, *9* (3), 505−513.

(9) Slowing, I. I.; Vivero-Escoto, J. L.; Wu, C.-W.; Lin, V. S. Y. Mesoporous Silica Nanoparticles as Controlled Release Drug Delivery and Gene Transfection Carriers. *Adv. Drug Delivery Rev.* **2008**, *60* (11), 1278−1288.

(10) Mekaru, H.; Lu, J.; Tamanoi, F. Development of Mesoporous Silica-Based Nanoparticles with Controlled Release Capability for Cancer Therapy. *Adv. Drug Delivery Rev.* **2015**, *95*, 40−49.

(11) Planinšek, O.; Kovačič, B.; Vrečer, F. Carvedilol Dissolution Improvement by Preparation of Solid Dispersions with Porous Silica. *Int. J. Pharm.* **2011**, *406* (1−2), 41−48.

(12) Kankala, R. K.; Han, Y. H.; Na, J.; Lee, C. H.; Sun, Z.; Wang, S. B.; Kimura, T.; Ok, Y. S.; Yamauchi, Y.; Chen, A. Z.; et al. Nanoarchitectured Structure and Surface Biofunctionality of Mesoporous Silica Nanoparticles. *Adv. Mater.* **2020**, *32* (23), 1907035.

(13) Asefa, T.; Tao, Z. Biocompatibility of Mesoporous Silica Nanoparticles. *Chem. Res. Toxicol.* **2012**, *25* (11), 2265−2284.

(14) Zhang, W.; Zheng, N.; Chen, L.; Xie, L.; Cui, M.; Li, S.; Xu, L. Effect of Shape on Mesoporous Silica Nanoparticles for Oral Delivery of Indomethacin. *Pharmaceutics* **2018**, *11* (1), 4.

(15) Mohamed, F.; Oo, M. K.; Chatterjee, B.; Alallam, B. Biocompatible Supramolecular Mesoporous Silica Nanoparticles as

the Next-Generation Drug Delivery System. *Front. Pharmacol* **2022**, *13*, 1−7.
(16) Riikonen, J.; Xu, W.; Lehto, V. P. Mesoporous Systems for Poorly Soluble Drugs - Recent Trends. *Int. J. Pharm.* **2018**, *536* (1), 178−186.
(17) Knapik-Kowalczuk, J.; Wojnarowska, Z.; Rams-Baron, M.; Jurkiewicz, K.; Cielecka-Piontek, J.; Ngai, K. L.; Paluch, M. Atorvastatin as a Promising Crystallization Inhibitor of Amorphous Probucol: Dielectric Studies at Ambient and Elevated Pressure. *Mol. Pharm.* **2017**, *14* (8), 2670−2680.
(18) Knapik-Kowalczuk, J.; Rams-Baron, M.; Paluch, M. Current Research Trends in Dielectric Relaxation Studies of Amorphous Pharmaceuticals: Physical Stability, Tautomerism, and the Role of Hydrogen Bonding. *TrAC, Trends Anal. Chem.* **2021**, *134*, 116097.
(19) Bahl, D.; Bogner, R. H. Amorphization of Indomethacin by Co-Grinding with Neusilin US2: Amorphization Kinetics, Physical Stability and Mechanism. *Pharm. Res.* **2006**, *23* (10), 2317−2325.
(20) Müller, R. H.; David, H.; Nan, J.; Pyo, S. M. SmartPearls - Novel Physically Stable Amorphous Delivery System for Poorly Soluble Dermal Actives. *Int. J. Pharm.* **2018**, *555*, 314−321.
(21) Shen, S.-C.; Ng, W. K.; Chia, L.; Dong, Y.-C.; Tan, R. B. H. Stabilized Amorphous State of Ibuprofen by Co-Spray Drying With Mesoporous SBA-15 to Enhance Dissolution Properties. *J. Pharm. Sci.* **2010**, *99* (4), 1997−2007.
(22) Godec, A.; Maver, U.; Bele, M.; Planinsek, O.; Srcic, S.; Gaberscek, M.; Jamnik, J. Vitrification from Solution in Restricted Space: Formation and Stabilization of Amorphous Nifedipine in a Nanoporous Silica Xerogel Carrier. *Int. J. Pharm.* **2007**, *343* (1−2), 131−140.
(23) Ditzinger, F.; Price, D. J.; Nair, A.; Becker-Baldus, J.; Glaubitz, C.; Dressman, J. B.; Saal, C.; Kuentz, M. Opportunities for Successful Stabilization of Poor Glass-Forming Drugs: A Stability-Based Comparison of Mesoporous Silica versus Hot Melt Extrusion Technologies. *Pharmaceutics* **2019**, *11* (11), 577−615.
(24) Baird, J. A.; Van Eerdenbrugh, B.; Taylor, L. S. A Classification System to Assess the Crystallization Tendency of Organic Molecules from Undercooled Melts. *J. Pharm. Sci.* **2010**, *99* (9), 3787−3806.
(25) Alhalaweh, A.; Alzghoul, A.; Kaialy, W.; Mahlin, D.; Bergström, C. A. S. Computational Predictions of Glass-Forming Ability and Crystallization Tendency of Drug Molecules. *Mol. Pharm.* **2014**, *11* (9), 3123−3132.
(26) Braun, D. E.; Gelbrich, T.; Kahlenberg, V.; Tessadri, R.; Wieser, J.; Griesser, U. J. Conformational Polymorphism in Aripiprazole: Preparation, Stability and Structure of Five Modifications. *J. Pharm. Sci.* **2009**, *98* (6), 2010−2026.
(27) Braun, D. E.; Gelbrich, T.; Kahlenberg, V.; Tessadri, R.; Wieser, J.; Griesser, U. J. Stability of Solvates and Packing Systematics of Nine Crystal Forms of the Antipsychotic Drug Aripiprazole. *Cryst. Growth Des.* **2009**, *9* (2), 1054−1065.
(28) Genina, N.; Hadi, B.; Löbmann, K. Hot Melt Extrusion as Solvent-Free Technique for a Continuous Manufacturing of Drug-Loaded Mesoporous Silica. *J. Pharm. Sci.* **2018**, *107* (1), 149−155.
(29) Takeuchi, H.; Nagira, S.; Yamamoto, H.; Kawashima, Y. Solid Dispersion Particles of Amorphous Indomethacin with Fine Porous Silica Particles by Using Spray-Drying Method. *Int. J. Pharm.* **2005**, *293* (1−2), 155−164.
(30) Knapik-Kowalczuk, J.; Kramarczyk, D.; Chmiel, K.; Romanova, J.; Kawakami, K.; Paluch, M. Importance of Mesoporous Silica Particle Size in the Stabilization of Amorphous Pharmaceuticals—The Case of Simvastatin. *Pharmaceutics* **2020**, *12* (4), 384.
(31) Antonino, R. S. C. M. Q.; Ruggiero, M.; Song, Z.; Nascimento, T. L.; Lima, E. M.; Bohr, A.; Knopp, M. M.; Löbmann, K. Impact of Drug Loading in Mesoporous Silica-Amorphous Formulations on the Physical Stability of Drugs with High Recrystallization Tendency. *Int. J. Pharm. X* **2019**, *1* (July), 100026.
(32) Knapik, J.; Wojnarowska, Z.; Grzybowska, K.; Jurkiewicz, K.; Stankiewicz, A.; Paluch, M. Stabilization of the Amorphous Ezetimibe Drug by Confining Its Dimension. *Mol. Pharm.* **2016**, *13* (4), 1308−1316.
(33) Rengarajan, G. T.; Enke, D.; Steinhart, M.; Beiner, M. Stabilization of the Amorphous State of Pharmaceuticals in Nanopores. *J. Mater. Chem.* **2008**, *18* (22), 2537−2539.
(34) Vraníková, B.; Niederquell, A.; Šklubalová, Z.; Kuentz, M. Relevance of the Theoretical Critical Pore Radius in Mesoporous Silica for Fast Crystallizing Drugs. *Int. J. Pharm.* **2020**, *591*, 120019.
(35) Kovačič, B.; Vrečer, F.; Planinšek, O. Solid Dispersions of Carvedilol with Porous Silica. *Chem. Pharm. Bull.* **2011**, *59* (4), 427−433.
(36) Cordeiro, T.; Castineira, C.; Mendes, D.; Danède, F.; Sotomayor, J.; Fonseca, I. M.; Gomes Da Silva, M.; Paiva, A.; Barreiros, S.; Cardoso, M. M.; et al. Stabilizing Unstable Amorphous Menthol through Inclusion in Mesoporous Silica Hosts. *Mol. Pharm.* **2017**, *14* (9), 3164−3177.
(37) Knapik, J.; Wojnarowska, Z.; Grzybowska, K.; Tajber, L.; Mesallati, H.; Paluch, K. J.; Paluch, M. Molecular Dynamics and Physical Stability of Amorphous Nimesulide Drug and Its Binary Drug-Polymer Systems. *Mol. Pharm.* **2016**, *13* (6), 1937−1946.
(38) Bhardwaj, S. P.; Suryanarayanan, R. Molecular Mobility as an Effective Predictor of the Physical Stability of Amorphous Trehalose. *Mol. Pharm.* **2012**, *9* (11), 3209−3217.
(39) Bhardwaj, S. P.; Arora, K. K.; Kwong, E.; Templeton, A.; Clas, S. D.; Suryanarayanan, R. Correlation between Molecular Mobility and Physical Stability of Amorphous Itraconazole. *Mol. Pharm.* **2013**, *10* (2), 694−700.
(40) Hancock, B. C.; Shamblin, S. L.; Zografi, G. Molecular Mobility of Amorphous Pharmaceutical Solids Below Their Glass Transition Temperatures. *Pharm. Res.* **1995**, *12* (6), 799−806.
(41) Yoshioka, S.; Aso, Y. Correlations between Molecular Mobility and Chemical Stability During Storage of Amorphous Pharmaceuticals. *J. Pharm. Sci.* **2007**, *96* (5), 960−981.
(42) Shamblin, S. L.; Tang, X.; Chang, L.; Hancock, B. C.; Pikal, M. J. Characterization of the Time Scales of Molecular Motion in Pharmaceutically Important Glasses. *J. Phys. Chem. B* **1999**, *103* (20), 4113−4121.
(43) Láng, P.; Kiss, V.; Ambrus, R.; Farkas, G.; Szabó-Révész, P.; Aigner, Z.; Várkonyi, E. Polymorph Screening of an Active Material. *J. Pharm. Biomed. Anal.* **2013**, *84*, 177−183.
(44) Beiner, M.; Rengarajan, G. T.; Pankaj, S.; Enke, D.; Steinhart, M. Manipulating the Crystalline State of Pharmaceuticals by Nanoconfinement. *Nano Lett.* **2007**, *7* (5), 1381−1385.
(45) Ha, J. M.; Wolf, J. H.; Hillmyer, M. A.; Ward, M. D. Polymorph Selectivity under Nanoscopic Confinement. *J. Am. Chem. Soc.* **2004**, *126* (11), 3382−3383.
(46) Williams, H. D.; Trevaskis, N. L.; Charman, S. A.; Shanker, R. M.; Charman, W. N.; Pouton, C. W.; Porter, C. J. H. Strategies to Address Low Drug Solubility in Discovery and Development. *Pharmacol. Rev.* **2013**, *65* (1), 315−499.
(47) Williams, G.; Watts, D. C. Non-Symmetrical Dielectric Relaxation Behaviour Arising from a Simple Empirical Decay Function. *Trans. Faraday Soc.* **1970**, *66* (0), 80−85.
(48) Havriliak, S.; Negami, S. A Complex Plane Representation of Dielectric and Mechanical Relaxation Processes in Some Polymers. *Polymer* **1967**, *8* (C), 161−210.
(49) Vogel, H. Das Temperaturabhangigkeitgesetz Der Viskosität von Flüssigkeiten. *J. Phys. Z.* **1921**, *22*, 645−646.
(50) Fulcher, G. S. ANALYSIS OF RECENT MEASUREMENTS OF THE VISCOSITY OF GLASSES. *J. Am. Ceram. Soc.* **1925**, *8* (6), 339−355.
(51) Tammann, G.; Hesse, W. Die Abhängigkeit Der Viscosität von Der Temperatur Bie Unterkühlten Flüssigkeiten. *Z. Anorg. Allg. Chem.* **1926**, *156* (1), 245−257.
(52) Böhmer, R.; Ngai, K. L.; Angell, C. A.; Plazek, D. J. Nonexponential Relaxations in Strong and Fragile Glass Formers. *J. Chem. Phys.* **1993**, *99* (5), 4201−4209.
(53) Ngai, K. L.; Paluch, M. Classification of Secondary Relaxation in Glass-Formers Based on Dynamic Properties. *J. Chem. Phys.* **2004**, *120* (2), 857−873.

(54) Hempel, N. J.; Brede, K.; Olesen, N. E.; Genina, N.; Knopp, M. M.; Löbmann, K. A Fast and Reliable DSC-Based Method to Determine the Monomolecular Loading Capacity of Drugs with Good Glass-Forming Ability in Mesoporous Silica. *Int. J. Pharm.* **2018**, *544* (1), 153−157.
(55) Kolodziejczyk, K.; Paluch, M.; Grzybowska, K.; Grzybowski, A.; Wojnarowska, Z.; Hawelek, L.; Ziolo, J. D. Relaxation Dynamics and Crystallization Study of Sildenafil in the Liquid and Glassy States. *Mol. Pharm.* **2013**, *10* (6), 2270−2282.
(56) Kramarczyk, D.; Knapik-Kowalczuk, J.; Smolka, W.; Monteiro, M. F.; Tajber, L.; Paluch, M. Inhibition of Celecoxib Crystallization by Mesoporous Silica - Molecular Dynamics Studies Leading to the Discovery of the Stabilization Origin. *Eur. J. Pharm. Sci.* **2022**, *171*, 106132.

https://doi.org/10.1021/acs.molpharmaceut.3c01095
Mol. Pharmaceutics 2024, 21, 2315−2326

Dr hab. inż. Justyna Knapik-Kowalczuk, Prof. UŚ
Instytut Fizyki
Wydział Nauk Ścisłych i Technicznych
Uniwersytet Śląski
ul. 75 Pułku Piechoty 1A, 41-500 Chorzów

Chorzów, 25.09.2024r.

OŚWIADCZENIE

Oświadczam, że w pracy:

D. Kramarczyk, J. Knapik-Kowalczuk, J. Klimontko, M. Kurek, R. Jachowicz, M. Paluch, *Tuning the Physical State of Aripiprazole by Mesoporous Silica.* Mol. Pharmaceuticals 2024, 21, 5, 2315–2326

mój udział polegał na uczestnictwie w dyskusji wyników oraz korekcji manuskryptu.

……

Podpis

Dr Joanna Klimontko
Instytut Fizyki
Wydział Nauk Ścisłych i Technicznych
Uniwersytet Śląski
ul. 75 Pułku Piechoty 1A, 41-500 Chorzów

Chorzów, 25.09.2024r.

OŚWIADCZENIE

Oświadczam, że w pracy:

D. Kramarczyk, J. Knapik-Kowalczuk, J. Klimontko, M. Kurek, R. Jachowicz, M. Paluch, *Tuning the Physical State of Aripiprazole by Mesoporous Silica.* Mol. Pharmaceuticals 2024, 21, 5, 2315–2326

mój udział polegał na wykonaniu pomiarów XRD.

.....

Podpis

Dr n. farm. Mateusz Kurek
Katedra Technologii Postaci Leku i Biofarmacji
Wydział Farmaceutyczny
Uniwersytet Jagielloński – Collegium Medicum
ul. Medyczna 9, 30-688 Kraków

Kraków, 25.09.2024r.

OŚWIADCZENIE

Oświadczam, że w pracy:

D. Kramarczyk, J. Knapik-Kowalczuk, J. Klimontko, M. Kurek, R. Jachowicz, M. Paluch, *Tuning the Physical State of Aripiprazole by Mesoporous Silica.* Mol. Pharmaceuticals 2024, 21, 5, 2315–2326

mój udział polegał na dostarczeniu materiału do badań (aripiprazolu) oraz uczestnictwie w dyskusji na temat otrzymanych wyników.

dr n. farm.
.....Mateusz Kurek.....

Podpis

Prof. zw. dr hab. Marian Paluch
Instytut Fizyki
Wydział Nauk Ścisłych i Technicznych
Uniwersytet Śląski
ul. 75 Pułku Piechoty 1A, 41-500 Chorzów

Chorzów, 25.09.2024r.

OŚWIADCZENIE

Oświadczam, że w pracy:

D. Kramarczyk, J. Knapik-Kowalczuk, J. Klimontko, M. Kurek, R. Jachowicz, M. Paluch, *Tuning the Physical State of Aripiprazole by Mesoporous Silica.* Mol. Pharmaceuticals 2024, 21, 5, 2315–2326

mój udział polegał na uczestnictwie w dyskusji na temat otrzymanych wyników.

.....

Podpis

Prof. dr hab. Renata Jachowicz
Katedra Technologii Postaci Leku i Biofarmacji
Wydział Farmaceutyczny
Uniwersytet Jagielloński – Collegium Medicum
ul. Medyczna 9, 30-688 Kraków

Kraków, 25.09.2024r.

OŚWIADCZENIE

Oświadczam, że w pracy:

D. Kramarczyk, J. Knapik-Kowalczuk, J. Klimontko, M. Kurek, R. Jachowicz, M. Paluch, *Tuning the Physical State of Aripiprazole by Mesoporous Silica.* Mol. Pharmaceuticals 2024, 21, 5, 2315–2326

mój udział polegał uczestnictwie w dyskusji na temat otrzymanych wyników oraz kierowaniem projektem badawczym, z którego finansowane były przeprowadzone w pracy badania.

Renata Jachowicz
.....
Podpis

4. PODSUMOWANIE

Niniejszą rozprawę doktorską stanowi seria trzech artykułów naukowych dotyczących badania wpływu NMK na fizyczną stabilność amorficznych farmaceutyków (symwastatyny, celekoksybu oraz aripiprazolu). Motywacja dla przeprowadzonych eksperymentów była dwojaka. Z jednej strony planowano wykazać, że NMK są wartościowymi stabilizatorami amorficznych substancji leczniczych i warto rozważać ich częstsze stosowanie w tym celu. Z drugiej strony chciano poznać i zrozumieć mechanizmy molekularne odgrywające kluczową rolę w modyfikacji tendencji do rekrystalizacji amorficznych farmaceutyków po zastosowaniu materiału krzemionkowego. Aby można było ocenić wpływ zastosowanych NMK na fizyczną stabilność badanych amorficznych substancji leczniczych, w pierwszej kolejności prowadzone badania skupiono na scharakteryzowaniu oraz ocenie tendencji do rekrystalizacji czystych amorficznych farmaceutyków. W kolejnych etapach prac badawczych: (i) przygotowane zostały binarne układy zawierające lek oraz krzemionkowy materiał, (ii) zbadano właściwości termiczne oraz dynamikę molekularną tych kompozycji oraz (iii) przeprowadzono badania mające na celu ocenić fizyczną stabilność amorficznych farmaceutyków w układach binarnych.

Przeprowadzone badania wykazały, że w przypadku wszystkich badanych materiałów leczniczych, zastosowany dodatek (NMK) nie wpływa istotnie na T_g badanych farmaceutyków oraz ich temperaturową zależność czasów pierwszorzędowej ($\tau_\alpha(T)$) oraz drugorzędowych relaksacji ($\tau_{\beta,\gamma,\delta}(T)$). Wykazano, że materiał krzemionkowy ma natomiast ogromy wpływ na fizyczną stabilność badanych materiałów leczniczych.

W A1 dowiedziono, że na hamowanie propagacji rekrystalizacji amorficznej formy symwastatyny istotny wpływ ma wielkość zastosowanych cząstek NMK. Wykazano, że powodem zarejestrowanych różnic w stabilizacji tego farmaceutyku po zastosowaniu dwóch odmiennych NMK, jest tworzenie się różnej wielkości przestrzeni, którą wypełnia amorficzny lek. Innymi słowy, za wzrost fizycznej stabilności amorficznej symwastatyny w obecności NMK, odpowiada większa ilość zawad sterycznych utrudniających wzrost kryształu farmaceutyku. Dane zaprezentowane w artykule A2 wykazały, że podobny efekt (tj. spowolnienie procesu rekrystalizacji amorficznego leku przez zwiększenie ilości zawad sterycznych wywieranych przez NMK) można uzyskać nie tylko zmniejszając rozmiar cząstek NMK, ale również zwiększając jego ilość. Co ważniejsze badając wpływ koncentracji NMK na fizyczną stabilność amorficznej formy celekoksybu wykazano, że za hamowanie jego rekrystalizacji odpowiadają dwa odrębne mechanizmy. Pierwszym z nich jest wyżej opisany efekt zawad sterycznych, natomiast drugi związany jest z oddziaływaniem cząsteczek leku z

powierzchnią NMK. Badania przedstawione w artykule A3 potwierdziły obecność oraz ważność opisanych wyżej mechanizmów w modyfikacji fizycznej stabilności amorficznych leków równocześnie pokazując, że efektywność NMK w hamowaniu rekrystalizacji zależy od stabilizowanego materiału amorficznego. W przypadku aripiprazolu wykazującego wysoki potencjał do formowania wielu odmian polimorficznych zawady steryczne wywierane przez NMK wpływają na typ powstających zarodków krystalizacji. Ponieważ różne odmiany polimorficzne aripiprazolu rekrystalizują w różnym tempie, przy koncentracjach NMK < 30% w układach binarnych lek + NMK zaobserwowano przyspieszenie rekrystalizacji tego farmaceutyku z układu binarnego w porównaniu do czystego amorficznego aripiprazolu. Natomiast stosując koncentracje NMK >30% obserwuje się zmianę opisanego trendu i wzrost fizycznej stabilności aripiprazolu.

5. BIBLIOGRAFIA

(1) Rodriguez-Aller, M.; Guillarme, D.; Veuthey, J. L.; Gurny, R. Strategies for Formulating and Delivering Poorly Water-Soluble Drugs. *J. Drug Deliv. Sci. Technol.* **2015**, *30*, 342–351. https://doi.org/10.1016/J.JDDST.2015.05.009.

(2) Awad, A.; Trenfield, S. J.; Basit, A. W. Solid Oral Dosage Forms. In *Remington: The Science and Practice of Pharmacy*; Academic Press, 2020; pp 333–358. https://doi.org/10.1016/B978-0-12-820007-0.00019-2.

(3) Liu, X.; Fahr, A. Drug Delivery Strategies for Poorly Water-Soluble Drugs. *Expert Opin. Drug Deliv.* **2007**, *4* (4), 403–416. https://doi.org/10.1517/17425247.2011.614228.

(4) Williams, H. D.; Trevaskis, N. L.; Charman, S. A.; Shanker, R. M.; Charman, W. N.; Pouton, C. W.; Porter, C. J. H. Strategies to Address Low Drug Solubility in Discovery and Development. *Pharmacol. Rev.* **2013**, *65* (1), 315–499. https://doi.org/10.1124/pr.112.005660.

(5) Ting, J. M.; Porter, W. W.; Mecca, J. M.; Bates, F. S.; Reineke, T. M. Advances in Polymer Design for Enhancing Oral Drug Solubility and Delivery. *Bioconjugate Chemistry*. American Chemical Society April 18, 2018, pp 939–952. https://doi.org/10.1021/acs.bioconjchem.7b00646.

(6) Iyer, R.; Jovanovska, V. P.; Berginc, K.; Jaklič, M.; Fabiani, F.; Harlacher, C.; Huzjak, T.; Sanchez-Felix, M. V. Amorphous Solid Dispersions (ASDs): The Influence of Material Properties, Manufacturing Processes and Analytical Technologies in Drug Product Development. *Pharmaceutics* **2021**, *13* (10). https://doi.org/10.3390/pharmaceutics13101682.

(7) Löbmann, K.; Grohganz, H.; Laitinen, R.; Strachan, C.; Rades, T. Amino Acids as Co-Amorphous Stabilizers for Poorly Water Soluble Drugs - Part 1: Preparation, Stability and Dissolution Enhancement. *Eur. J. Pharm. Biopharm.* **2013**, *85* (3 PART B), 873–881. https://doi.org/10.1016/j.ejpb.2013.03.014.

(8) Vasconcelos, T.; Sarmento, B.; Costa, P. Solid Dispersions as Strategy to Improve Oral Bioavailability of Poor Water Soluble Drugs. *Drug Discov. Today* **2007**, *12* (23–24), 1068–1075. https://doi.org/10.1016/j.drudis.2007.09.005.

(9) Knapik-Kowalczuk, J.; Rams-Baron, M.; Paluch, M. Current Research Trends in Dielectric Relaxation Studies of Amorphous Pharmaceuticals: Physical Stability, Tautomerism, and the Role of Hydrogen Bonding. *TrAC Trends Anal. Chem.* **2021**, *134*, 116097. https://doi.org/10.1016/J.TRAC.2020.116097.

(10) Willart, J. F.; Descamps, M. Solid State Amorphization of Pharmaceuticals. *Mol. Pharm.* **2008**, *5* (6), 905–920. https://doi.org/10.1021/mp800092t.

(11) Bogner, R. H.; Murdande, S. B.; Pikal, M. J.; Shanker, R. M. Solubility Advantage of Amorphous Pharmaceuticals: II. Application of Quantitative Thermodynamic Relationships for Prediction of Solubility Enhancement in Structurally Diverse Insoluble Pharmaceuticals. *Pharm. Res.* **2010**, *27* (12), 2704–2714. https://doi.org/10.1007/s11095-010-0269-5.

(12) Paradkar, A. R.; Chauhan, B.; Yamamura, S.; Pawar, A. P. Preparation and Characterization of Glassy Celecoxib. *Drug Dev. Ind. Pharm.* **2003**, *29* (7), 739–744. https://doi.org/10.1081/DDC-120021773.

(13) Chmiel, K.; Knapik-Kowalczuk, J.; Jurkiewicz, K.; Sawicki, W.; Jachowicz, R.; Paluch, M. A New Method to Identify Physically Stable Concentration of Amorphous Solid Dispersions (I): Case of Flutamide + Kollidon VA64. *Mol. Pharm.* **2017**, *14* (10), 3370–3380. https://doi.org/10.1021/acs.molpharmaceut.7b00382.

(14) Rams-Baron, M.; Jachowicz, R.; Boldyreva, E.; Zhou, D.; Jamroz, W.; Paluch, M. Amorphous Drugs: Benefits and Challenges. *Amorph. Drugs Benefits Challenges* **2018**, 1–230. https://doi.org/10.1007/978-3-319-72002-9.

(15) Szklarz, G.; Adrjanowicz, K.; Knapik-Kowalczuk, J.; Jurkiewicz, K.; Paluch, M. Crystallization of Supercooled Fenofibrate Studied at Ambient and Elevated Pressures. *Phys. Chem. Chem. Phys.* **2017**, *19* (15), 9879–9888. https://doi.org/10.1039/C7CP00823F.

(16) Knapik-Kowalczuk, J.; Wojnarowska, Z.; Rams-Baron, M.; Jurkiewicz, K.; Cielecka-Piontek, J.; Ngai, K. L.; Paluch, M. Atorvastatin as a Promising Crystallization Inhibitor of Amorphous Probucol: Dielectric Studies at Ambient and Elevated Pressure. *Mol. Pharm.* **2017**, *14* (8), 2670–2680. https://doi.org/10.1021/acs.molpharmaceut.7b00152.

(17) Gupta, P.; Thilagavathi, R.; Chakraborti, A. K.; Bansal, A. K. Role of Molecular Interaction in Stability of Celecoxib-PVP Amorphous Systems. *Mol. Pharm.* **2005**, *2* (5), 384–391. https://doi.org/10.1021/mp050004g.

(18) Bhugra, C.; Pikal, M. J. Role of Thermodynamic, Molecular, and Kinetic Factors in Crystallization from the Amorphous State. *J. Pharm. Sci.* **2008**, *97* (4), 1329–1349. https://doi.org/10.1002/JPS.21138.

(19) Laitinen, R.; Lo̊bmann, K.; Strachan, C. J.; Grohganz, H.; Rades, T. Emerging Trends in the Stabilization of Amorphous Drugs. *Int. J. Pharm.* **2013**, *453* (1), 65–79. https://doi.org/10.1016/j.ijpharm.2012.04.066.

(20) Van Eerdenbrugh, B.; Taylor, L. S. Small Scale Screening to Determine the Ability of Different Polymers to Inhibit Drug Crystallization upon Rapid Solvent Evaporation. *Mol. Pharm.* **2010**, *7* (4), 1328–1337. https://doi.org/10.1021/mp1001153.

(21) Priemel, P. A.; Laitinen, R.; Barthold, S.; Grohganz, H.; Lehto, V. P.; Rades, T.; Strachan, C. J. Inhibition of Surface Crystallisation of Amorphous Indomethacin Particles in Physical Drug-Polymer Mixtures. *Int. J. Pharm.* **2013**, *456* (2), 301–306. https://doi.org/10.1016/j.ijpharm.2013.08.046.

(22) Serajuddln, A. T. M. Solid Dispersion of Poorly Water-Soluble Drugs: Early Promises, Subsequent Problems, and Recent Breakthroughs. *J. Pharm. Sci.* **1999**, *88* (10), 1058–1066. https://doi.org/10.1021/js980403l.

(23) Kothari, K.; Ragoonanan, V.; Suryanarayanan, R. The Role of Drug-Polymer Hydrogen Bonding Interactions on the Molecular Mobility and Physical Stability of Nifedipine Solid Dispersions. *Mol. Pharm.* **2015**, *12* (1), 162–170. https://doi.org/10.1021/mp5005146.

(24) Knapik, J.; Wojnarowska, Z.; Grzybowska, K.; Hawelek, L.; Sawicki, W.; Wlodarski, K.; Markowski, J.; Paluch, M. Physical Stability of the Amorphous Anticholesterol Agent (Ezetimibe): The Role of Molecular Mobility. *Mol. Pharm.* **2014**, *11* (11). https://doi.org/10.1021/mp500498e.

(25) Knapik-Kowalczuk, J.; Chmiel, K.; Jurkiewicz, K.; Wojnarowska, Z.; Kurek, M.; Jachowicz, R.; Paluch, M. Influence of Polymeric Additive on the Physical Stability and Viscoelastic Properties of Aripiprazole. *Mol. Pharm.* **2019**, *16* (4). https://doi.org/10.1021/acs.molpharmaceut.9b00084.

(26) Shi, Q.; Zhang, C.; Su, Y.; Zhang, J.; Zhou, D.; Cai, T. Acceleration of Crystal Growth of Amorphous Griseofulvin by Low-Concentration Poly(Ethylene Oxide): Aspects of Crystallization Kinetics and Molecular Mobility. *Mol. Pharm.* **2017**, *14* (7), 2262–2272. https://doi.org/10.1021/acs.molpharmaceut.7b00097.

(27) Tu, W.; Knapik-Kowalczuk, J.; Chmiel, K.; Paluch, M. Glass Transition Dynamics and Physical Stability of Amorphous Griseofulvin in Binary Mixtures with Low-T<inf>g</Inf> Excipients. *Mol. Pharm.* **2019**, *16* (8). https://doi.org/10.1021/acs.molpharmaceut.9b00476.

(28) Li, B.; Luo, X.; Deng, B.; Wang, J.; McComb, D. W.; Shi, Y.; Gaensler, K. M. L.; Tan, X.; Dunn, A. L.; Kerlin, B. A.; et al. An Orthogonal Array Optimization of Lipid-like Nanoparticles for MRNA Delivery in Vivo. *Nano Lett.* **2015**, *15* (12), 8099–8107. https://doi.org/10.1021/ACS.NANOLETT.5B03528/SUPPL_FILE/NL5B03528_SI_00

1.PDF.

(29) Moreno, E.; Schwartz, J.; Larrea, E.; Conde, I.; Font, M.; Sanmartín, C.; Irache, J. M.; Espuelas, S. Assessment of β-Lapachone Loaded in Lecithin-Chitosan Nanoparticles for the Topical Treatment of Cutaneous Leishmaniasis in L. Major Infected BALB/c Mice. *Nanomedicine Nanotechnology, Biol. Med.* **2015**, *11* (8), 2003–2012. https://doi.org/10.1016/J.NANO.2015.07.011.

(30) Rocha, J.; Carlos, L. D.; Paz, F. A. A.; Ananias, D. Luminescent Multifunctional Lanthanides-Based Metal–Organic Frameworks. *Chem. Soc. Rev.* **2011**, *40* (2), 926–940. https://doi.org/10.1039/C0CS00130A.

(31) Piao, Y.; Burns, A.; Kim, J.; Wiesner, U.; Hyeon, T. Designed Fabrication of Silica-Based Nanostructured Particle Systems for Nanomedicine Applications. *Adv. Funct. Mater.* **2008**, *18* (23), 3745–3758. https://doi.org/10.1002/ADFM.200800731.

(32) Vallet-Regi, M.; Rámila, A.; Del Real, R. P.; Pérez-Pariente, J. A New Property of MCM-41: Drug Delivery System. *Chem. Mater.* **2000**, *13* (2), 308–311. https://doi.org/10.1021/CM0011559.

(33) Nunes, C. D.; Vaz, P. D.; Fernandes, A. C.; Ferreira, P.; Romão, C. C.; Calhorda, M. J. Loading and Delivery of Sertraline Using Inorganic Micro and Mesoporous Materials. *Eur. J. Pharm. Biopharm.* **2007**, *66* (3), 357–365. https://doi.org/10.1016/J.EJPB.2006.11.023.

(34) Qu, F.; Zhu, G.; Huang, S.; Li, S.; Sun, J.; Zhang, D.; Qiu, S. Controlled Release of Captopril by Regulating the Pore Size and Morphology of Ordered Mesoporous Silica. *Microporous Mesoporous Mater.* **2006**, *92* (1–3), 1–9. https://doi.org/10.1016/J.MICROMESO.2005.12.004.

(35) Semete, B.; Booysen, L.; Lemmer, Y.; Kalombo, L.; Katata, L.; Verschoor, J.; Swai, H. S. In Vivo Evaluation of the Biodistribution and Safety of PLGA Nanoparticles as Drug Delivery Systems. *Nanomedicine Nanotechnology, Biol. Med.* **2010**, *6* (5), 662–671. https://doi.org/10.1016/J.NANO.2010.02.002.

(36) Wang, Y.; Zhao, Q.; Han, N.; Bai, L.; Li, J.; Liu, J.; Che, E.; Hu, L.; Zhang, Q.; Jiang, T.; et al. Mesoporous Silica Nanoparticles in Drug Delivery and Biomedical Applications. *Nanomedicine Nanotechnology, Biol. Med.* **2015**, *11* (2), 313–327. https://doi.org/10.1016/J.NANO.2014.09.014.

(37) Knapik, J.; Wojnarowska, Z.; Grzybowska, K.; Jurkiewicz, K.; Tajber, L.; Paluch, M. Molecular Dynamics and Physical Stability of Coamorphous Ezetimib and Indapamide Mixtures. *Mol. Pharm.* **2015**, *12* (10), 3610–3619.

https://doi.org/10.1021/acs.molpharmaceut.5b00334.

(38) Bhugra, C.; Shmeis, R.; Krill, S. L.; Pikal, M. J. Prediction of Onset of Crystallization from Experimental Relaxation Times. II. Comparison between Predicted and Experimental Onset Times. *J. Pharm. Sci.* **2008**, *97* (1), 455–472. https://doi.org/10.1002/jps.21162.

(39) Grzybowska, K.; Paluch, M.; Wlodarczyk, P.; Grzybowski, A.; Kaminski, K.; Hawelek, L.; Zakowiecki, D.; Kasprzycka, A.; Jankowska-Sumara, I. Enhancement of Amorphous Celecoxib Stability by Mixing It with Octaacetylmaltose: The Molecular Dynamics Study. *Mol. Pharm.* **2012**, *9* (4), 894–904. https://doi.org/10.1021/mp200436q.

(40) Gupta, P.; Chawla, G.; Bansal, A. K. Physical Stability and Solubility Advantage from Amorphous Celecoxib: The Role of Thermodynamic Quantities and Molecular Mobility. *Mol. Pharm.* **2004**, *1* (2), 406–413. https://doi.org/10.1021/mp049938f.

(41) Grzybowska, K.; Paluch, M.; Grzybowski, a; Wojnarowska, Z.; Hawelek, L.; Kolodziejczyk, K.; Ngai, K. L. Molecular Dynamics and Physical Stability of Amorphous Anti-Inflammatory Drug: Celecoxib. *J. Phys. Chem. B* **2010**, *114* (40), 12792–12801. https://doi.org/10.1021/jp1040212.